2013

Optimal Control of Power Quality in Microgrids Using Particle Swarm Optimisation

Waleed Abood Baddai Al-Saedi
Edith Cowan University

Edith Cowan University

Copyright Warning

Optimal Control of Power Quality in Microgrids Using Particle Swarm Optimisation

by

Waleed Abood Baddai AL-SAEDI

This thesis is presented in fulfilment of the requirements for the degree of

Doctor of Philosophy

SCHOOL OF ENGINEERING

FACULTY OF HEALTH, ENGINEERING AND SCIENCE

EDITH COWAN UNIVERSITY

September 15, 2013

USE OF THESIS

The Use of Thesis statement is not included in this version of the thesis.

ABSTRACT

Driven by environmental protection, economic factors, conservation of energy resources, and technical challenges, the microgrid has emerged as an innovative small-scale power generation network. Microgrids consist of a cluster of Distributed Generation units that encompass a portion of an electric power distribution system and may rely on different energy sources. Functionally, the microgrid is required to provide adequate levels and quality of power to meet load demands. The issue of power quality is significant as it directly affects the characteristics of the microgrid's operation. This problem can be defined as an occurrence of short to long periods of inadequate or unstable power outputs by the microgrid. In a stand-alone operation mode, the system voltage and frequency must be established by the microgrid, otherwise the system will collapse due to the variety in the microgrid component characteristics. The harmonic distortion of the output power waveforms is also a serious problem that often occurs because of the high speed operation of the converter switches. The long transient period is a critical issue that is usually caused by changing the operation mode or the load demand. Power sharing among the Distributed Generation units is also an important matter for sharing the load appropriately, particularly given that some renewable energy resources are not available continuously. In a utility connected microgrid, the reliable power quality mainly depends on the regulation of both active and reactive power, because the microgrid's behaviour is mostly dominated by the bulk power system. Therefore, an optimal power control strategy is proposed in this thesis to improve the quality of the power supply in a microgrid scenario. This controller comprises an inner current control loop and an outer power control loop based on a synchronous reference frame and conventional PI regulators. The power control loop can operate in two modes: voltage-frequency power control mode and active-reactive power control mode. Particle Swarm Optimisation is an intelligent searching algorithm that is applied here for real-time self-tuning of the power control parameters. The voltage-frequency power controller is proposed for an inverter-based Distributed Generation unit in an autonomous operation mode. The results show satisfactory system voltage and frequency,

high dynamic response, and an acceptable harmonic distortion level. The active-reactive power controller is adopted for an inverter-based Distributed Generation unit in a utility operation mode. This controller provides excellent regulation of the active and reactive power, in particular when load power has to be shared equally between the microgrid and utility. The voltage-frequency and active-reactive power control modes are used for a microgrid configured from two DG units in an autonomous operation mode. The proposed control strategy maintains the system voltage and frequency within acceptable limits, and injects sustained output power from one DG unit during a load change. The reliability of the system's operation is investigated through developing a small-signal dynamic model for the microgrid. The results prove that the system was stable for the given operating point and under the proposed power controller. Consequently, this research reveals that the microgrid can successfully operate as a controllable power generation unit to support the utility, thus reducing the dependency on the bulk power system and increasing the market penetration of the micro-sources.

DECLARATION

I certify that this thesis does not, to the best of my knowledge and belief:

(i) incorporate without acknowledgement any material previously submitted for a degree or diploma in any institution of higher education;

(ii) contain any material previously published or written by another person except where due reference is made in the text; or

(iii) contain any defamatory material.

I also grant permission for the Library at Edith Cowan University to make duplicate copies of my thesis as required.

Signed:

Date: .....15 / 09 / 2013.....

ACKNOWLEDGMENT

I would like to gratefully acknowledge the enthusiastic supervision of Dr Stefan W. Lachowicz whom I was fortunate to have as my mentor. His wide knowledge and his logical way of thinking have been of great value for me. In particular I have appreciated his valuable suggestions, critical reviews and our intellectual exchanges. Dr Lachowicz's experience has been most helpful in ensuring the quality of this work. I would also like to thank Prof Daryoush Habibi and Dr Octavian Bass for sharing abundant sources of information throughout my journey.

I would like to express my profound gratitude to my wife for her understanding, endless patience and encouragement when it was most required during difficult times. Also, special thanks to my sons and my daughter, Zaid, Mohammed and Reema, who have always removed my fatigue with their smiles. I would also like to thank my family and friends from Iraq for their unconditional love and support.

Finally, I am grateful to all my friends in Australia, including those who are from the School of Engineering, Edith Cowan University, for being my surrogate family during the many years that I stayed there, and also for their continued moral support.

Contents

List of Tables

List of Figures

LIST OF SYMBOLS

V_{abc}	Voltages of phases a, b and c
V_{dq}	Voltages vectors in dq synchronous reference frame
$V_{\alpha\beta}$	Voltages vectors in $\alpha\beta$ stationary reference frame
i_{abc}	Currents of phases a, b and c
i_{dq}	Currents vectors in dq synchronous reference frame
i^*	Reference vector of current
V^*	Reference voltage
V	System voltage
f^*	Reference frequency
f	System frequency
P^*	Reference active power
P	Active power
Q^*	Reference reactive power
Q	Reactive power
R_s	Line resistance of source
L_s	Line inductance of source
R_f	Filter resistance
L_f	Filter inductance
C_f	Filter capacitance

ω	Angular frequency
θ	Synchronous rotating angle
K_p, K_i	Proportional and integral gain constants
$[\,]^T$	Transpose matrix
p	Participation factor
X_{gbest}	Global best position
X_{pbest}	Local best position
c_1, c_2	Cognitive coefficients

LIST OF ACRONYMS

MG	Microgrid
MGCC	Microgrid Control Centre
DG	Distributed Generation Unit
DER	Distributed Energy Resources
PCC	Point of Common Coupling
PV	Photovoltaic
PE	Power Electronics
VSI	Voltage Source Inverter
IGBT	Insulated Gate Bipolar Transistor
PWM	Pulse Width Modulation
SVPWM	Space Vector Pulse Width Modulation
PLL	Phase Locked Loop
THD	Total Harmonic Distortion
LPF	Low Pass Filter
AI	Artificial Intelligence
PSO	Particle Swarm Optimisation
IAE	Integral Absolute Error
ISE	Integral Square Error
ITSE	Integral Time Square Error
ITAE	Integral Time Absolute Error

Chapter 1

INTRODUCTION

Concerns over climate change are now moving the energy sector into a new era of modern power grids, in which rapid increases in the load demand can be met through widespread power generation units called Distributed Generation (DG) units. These units can be operated in either parallel to the main grid (grid-connected mode) or as an autonomous group (microgrid mode). The load demand in the latter is handled by a several DG units that connect to the distribution network, in order to maintain a reliable power supply to meet the load demand, when the grid is not available or cost-effective, due to a network fault or a market decision, respectively.

Accordingly, a microgrid can be defined as a recent innovation for a small-scale power generation network that aggregates a cluster of DG units using power electronic devices such as the Voltage Source Inverter (VSI) system. This scenario can represent a complementary infrastructure to the utility grid to deal with a rapid change in the load demand. The high market penetration of micro-sources such as wind, photovoltaic, hydro, and fuel cells, has created alternatives which provide green energy and a flexible extension to the utility grid [1]. These sources are usually connected to the power system by Pulse-Width-Modulation (PWM)-VSI systems which have the nonlinear voltage-current characteristics of semiconductor components, and produce high switching frequency, both of which affect the quality of the power supply for the end user [2].

Moreover, there are three main factors that affect the characteristics of the microgrid's operation. First, the type of connected DG units; these can be classified into three power sources, namely; variable frequency, high frequency, and direct energy conversion, the last of which produces dc voltage and current. Second, the type of DC/AC PWM-VSI system; these are typically used to interface the major types of DG units either to the utility grid or directly to the customer load and affect the microgrid's operation through lack of physical inertia, production of harmonic distortion, increase the system dynamics band,

and limits on the overload capability. Third, the control loop that is used for the DC/AC PWM-VSI system; the microgrid's operation is mostly dominated by the VSI system, so an efficient control loop is necessary for reliable operation [3]. The interaction between all these components yields temporal changes in the characteristics of the power supplied to the customers. The power quality mainly depends on the occurrence of short to long periods of abnormality or outages in the output power characteristics [4].

The serious problems that affect power quality can be categorised based on the microgrid's operation mode. In a microgrid mode, the voltage and frequency profiles have to be established by the microgrid, otherwise the system will collapse due to the sensitivity of the connected DG units and the power converter applications [5]. The harmonic distortion of the output power waveforms is a critical problem that is often caused by the high speed operation of the inverter switches. The long transient period can affect all system equipment regardless of whether it occurs in the islanding operation mode or during a load change [6]. The load sharing mechanism among the DG units must be appropriate for sharing the load [7]. A microgrid in grid-connected mode also faces issues that can substantially influence the power supply quality. For example, the behaviour of the microgrid is mostly dictated by the bulk power system, so regulating the flows of both active and reactive power is an essential control objective for managing the microgrid's output power [8].

The aforementioned issues necessitate a power control strategy that guarantees high performance operation to meet power quality requirements. In a synthetic control scheme, the current control loop of the PWM-VSI system is a particularly important characteristic of modern electronic power converters which allow the DG unit to be connected to the microgrid. This controller forces the inverter to operate as a current source amplifier, thus improving the inverter output current. An additional power controller can play a key role in ensuring stable, high quality power injection by regulating the system's voltage and frequency in microgrid mode or controlling the active and reactive power flows in the grid-connected mode. If the above features can be optimised, the microgrid can be successfully installed as a supportive power generation unit, to the utility grid, that reduces dependency on the grid, and also facilitates high market penetration of the micro-sources without causing power quality problems.

1.1 Research Motivations

In a microgrid, the problems of the power quality challenge the reliability and stability of the system operation. Disturbances to the supplied power, which are related to the voltage, frequency, active power, reactive power, harmonic distortion, and dynamic response, can impact performance for both microgrid operation modes: islanding and grid-connected. Recently, researchers have focussed on improving power quality by investigating optimal microgrid designs and optimal locations for the connected DG units. This work proposes a new power control strategy, based on a real-time Particle Swarm Optimisation technique, to improve the quality of the power supply in a microgrid. Therefore, the benefits of this work can be summarised as follows.

1. Enhancing the market penetration of micro-sources.
2. Protecting sensitive systems from the detrimental effects of power quality and reliability problems.
3. Reducing the capital cost, in particular when the microgrid is designed for Peak Shaving application.
4. Ensuring best utilisation of the microgrid's output power .
5. Providing stable and reliable operation of the microgrid in response to the load demand.

1.2 Aims of this Thesis

The main aim of this thesis is to improve the quality of the power supply in a microgrid scenario through new power control strategy based on the Particle Swarm Optimisation technique. In both microgrid operation modes: islanding and grid-connected, there are many types of disturbances that impact power quality. Therefore, pursuing following specific objectives should help achieve the main aim of this thesis.

1. Implementing an optimisation technique for a real-time self-tuning method for the proposed power controller.
2. Controlling the microgrid voltage and frequency in the islanding operation mode.
3. Regulating the active and reactive power flows in the grid-connected operation mode, in order to halve the load between the microgrid and utility.

4. Achieving an appropriate power sharing among the DG units in the islanding operation mode, in addition to ensuring appropriate voltage and frequency regulation.

5. Investigating the system's stability under the proposed power controller, and also examining sensitivity to the control parameters, in order to validate the proposed power controller.

1.3 Thesis Contributions

Based the above objectives, the contributions of this thesis should be:

1. The power controller is proposed for the voltage and frequency regulation based DG unit in a microgrid operation mode. This controller is designed in voltage-frequency mode and a Particle Swarm Optimisation algorithm is incorporated for real-time self-tuning method.

2. The proposed power controller should regulate active and reactive power in grid-connected operation mode. This controller is designed in active-reactive power mode, and a Particle Swarm Optimisation algorithm is also incorporated for real-time self-tuning, to support sharing of the load equally between the microgrid and utility.

3. The voltage-frequency control mode and active-reactive control mode are presented for a microgrid configured from two DG units in an autonomous microgrid operation mode. To regulate the system voltage and frequency, both DG units adopt the voltage-frequency mode when the microgrid is transferred to the islanding operation mode, while one of them used in active-reactive power mode during load change to sustain the injected output power. A Particle Swarm Optimisation algorithm is also incorporated for each DG unit to implement real-time self-tuning. It should be applicable when more than two DG units are configured in the microgrid.

4. The Particle Swarm Optimisation algorithm is an intelligent technique that is implemented for a real-time self-tuning of the proposed power controllers. This algorithm is a part of the swarm intelligence family that can be used efficiently to solve the optimisation problems. It is employed in this research to find the best power control parameters that satisfy the control objectives.

5. A linearised small-signal dynamic model is developed for an autonomous microgrid. This model is constructed in a way that can be used even when the system is complex

and contains any number of DG units. The model is used for the eigenvalue analysis to examine system stability for the given operating point and under the proposed power controller. This also can be used for sensitivity analyse.

1.4 Publications from this Research

1. **W. Al-Saedi**, S. W. Lachowicz, D. Habibi, and O. Bass, "*Power quality enhancement in autonomous microgrid operation using particle swarm optimization*", International Journal of Electrical Power and Energy Systems, Elsevier, Vol. 42, No. 1, Pages 139–149, 2012.

2. **W. Al-Saedi**, S. W. Lachowicz, D. Habibi, and O. Bass, "*Power flow control in grid-connected microgrid operation using particle swarm optimization under variable load conditions*", International Journal of Electrical Power and Energy Systems, Elsevier, Vol. 49, Pages 76–85, 2013.

3. **W. Al-Saedi**, S. W. Lachowicz, D. Habibi, and O. Bass, "*Voltage and frequency regulation based DG unit in an autonomous microgrid operation using particle swarm optimization*", International Journal of Electrical Power and Energy Systems, Elsevier, Vol. 53, Pages 742–751, 2013.

4. **W. Al-Saedi**, S. W. Lachowicz, D. Habibi, and O. Bass, "*Stability analysis of parallel DG units in an autonomous microgrid*", Submitted to International Transactions on Electrical Energy Systems, Wiley.

5. **W. Al-Saedi**, S. W. Lachowicz, and D. Habibi, "*An optimal current control strategy for a three-phase grid-connected photovoltaic system using particle swarm optimization*", in Power Engineering and Automation Conference (PEAM), 2011 IEEE, Vol. 1, Pages 286–290.

6. **W. Al-Saedi**, S. Lachowicz, D. Habibi, and O. Bass, "*Power quality improvement in autonomous microgrid operation using particle swarm optimization*", in Innovative Smart Grid Technologies Asia (ISGT), 2011 IEEE PES, Pages 1–6.

7. **W. Al-Saedi**, S. Lachowicz, D. Habibi, and O. Bass, "*Stability analysis of an autonomous microgrid operation based on particle swarm optimization*", in International Conference on Power Systems Technology (POWERCON), 2012 IEEE PES, Pages 1-6.

1.5 Thesis Outline

The thesis has been organised as eight chapters. This chapter introduces the concept of the microgrid and the motivations for the research. The rest of the thesis is outlined below.

- **Chapter 2** reviews the relevant literature and provides the background for undertaking research on improving the quality of the power supply in microgrids.
- **Chapter 3** describes the Particle Swarm Optimisation algorithm that is applied in this research. This algorithm is employed to solve the optimisation problem related to improving power supply quality in a microgrid.
- **Chapter 4** explores the voltage and frequency power control mode that is adopted for the inverter-based DG unit in an autonomous microgrid mode. The Particle Swarm Optimisation technique is embedded in this controller. The proposed controller scheme regulates the system voltage and frequency and provides high current quality with fast dynamic response.
- **Chapter 5** profiles the active and reactive power control mode that is considered for the inverter-based DG unit in grid-connected microgrid mode. The Particle Swarm Optimisation technique is embedded in this controller. The proposed controller scheme regulates both active and reactive power with the aim of halving the load demand between the utility and the microgrid.
- **Chapter 6** explores the control method for an autonomous microgrid mode that is configured from two DG units. This method addresses the voltage and frequency power control mode, and the active and reactive power control mode. The Particle Swarm Optimisation algorithm is used for each DG unit. The proposed control method regulates the system voltage and frequency and ensures sustained output power from the second DG unit during load change.
- **Chapter 7** characterises the small-signal state-space model for the microgrid. This model is developed to investigate the system stability through eigenvalue analysis. The sensitivity to the power control parameters is also considered to examine the validity of the proposed control method.
- **Chapter 8** provides the general conclusions, highlights any limitations, and explores the scope for future related research.

Chapter 2

BACKGROUND AND LITERATURE SURVEY

A microgrid is a modern electrical distribution system that has complicated aggregations of several components and numerous supply sources. Thus, the interactions between them or with the power utility yield temporal variations in the characteristics of the power supplied to the customer. Therefore, the quality of the power supply in a microgrid scenario is the main focus of this research. This problem often occurs in such systems and for both operation modes: grid-connected and islanding. It is important to note that improving the quality of the power supply implies interest in many different subjects such as voltage and frequency regulation, power flow control, power sharing, harmonic distortion, dynamic response, and system stability. For example, power quality disturbances arise due to issues like type of DG units, Power Electronics (PE) applications, switching between two operation modes, power system faults, and load change. The power flow also needs to be regulated to optimise use of the connected DG units. Therefore, it is important to propose a control concept for both microgrid operation modes; to provide high quality and reliable energy supply to the load and thus greater utilisation of increasingly popular DG units, but not cause power quality problems in the distribution network.

This chapter presents a literature review and background theory relevant to the work presented in this thesis and is divided into five main sections. Section 2.1 describes the common types of DG units utilised as energy sources in microgrids. The concept of the inverter-based distributed generation unit is introduced in Section 2.2. Then, Section 2.3 addresses microgrid control to explain the most efficient power control strategies that can be used to improve power supply quality. In Section 2.4, stability analysis is investigated for the microgrid model under different types of control strategies. Finally, the conclusions are outlined in Section 2.5.

2.1 Distributed Generation

Smaller energy sources in a microgrid are usually called Distributed Generation (DG) units, and form part of the Distributed Energy Resources (DER), which can also include any energy storage systems. DG units are rated up to 10 MW and can be directly connected to the distribution network through a power electronic converter to form a microgrid scenario. A microgrid is a recent innovation, in small-scale power generation networks, that can represent a complementary infrastructure to the utility grid to help cope with a rapid increase of the load demand [4]. Figure 2.1 categorises the common types of DG units, and the following subsections introduce their salient features.

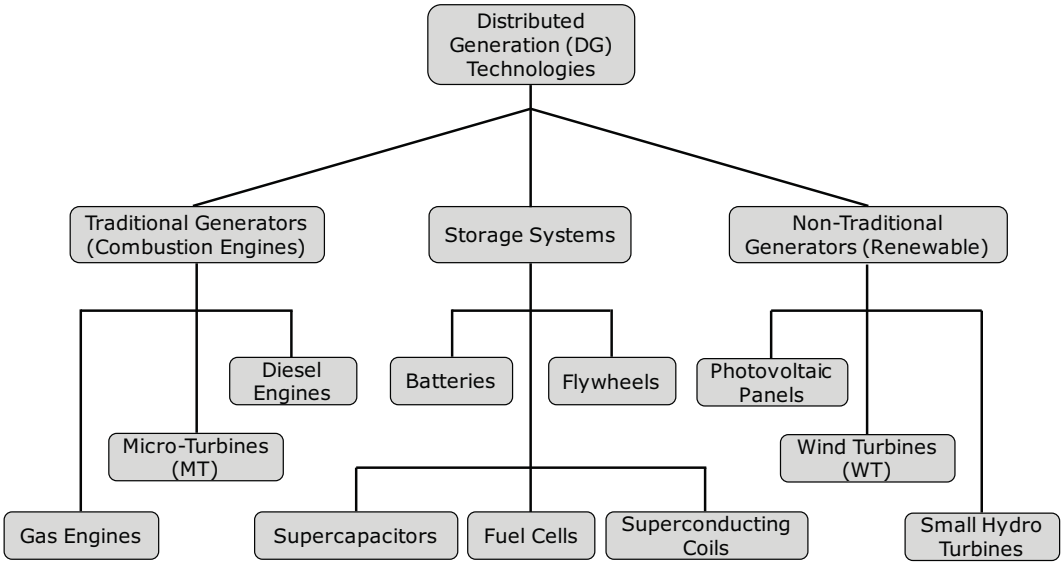

Figure 2.1: Types and technologies of the DG units

2.1.1 Micro-turbines

Micro-turbines are small traditional generators that use combustion turbines, as prime mover technology, that may use gas, propane, gasoline, or other liquid or gaseous fuels. Micro-turbines generally comprise a generator, small turbine, compressor, combustor, and recuperator; importantly, their rating and volume are mostly limited to 20-500 kW and 0.4-1.0 m^3, respectively. Moreover, micro-turbine is designed to operate without gearbox; at lower temperature and pressure; and at higher speed than traditional combustion turbines [9, 10, 11]. Therefore, this technology has emerged as a promising energy system due to the low price of its fuel sources, low emissions, and low maintenance and installation costs.

A power electronic converter, such as a voltage source inverter system is usually required

to interface this unit to the grid or load. Thus, a reliable operation can be obtained when a proper control strategy is proposed to make the micro-turbine able to respond to the temporal command signals.

2.1.2 Fuel Cells

Fuel cell technology is well suited for use in DG units as it employs chemical energy to generate electric and thermal energy through an electrochemical process. As long as the fuel is provided, the fuel cell behaves the same as a battery by converting chemical energy to electric energy; however charging is not needed while the electrochemical process continues. The hydrogen-rich fuels that can be used include natural gas, biogas, gasoline, and propane. Thus, relatively clean power and heat can be provided. Fuel cells are made in portable and stationary designs, with ratings ranging from 1 kW to a few MW. They can also operate in a wide range of atmospheric pressures and temperatures [12, 13, 14].

The voltage source inverter system is also required to connect this unit to the grid or load. Thus, this unit can be operated as a dispatchable source without causing intermittent generation problems.

2.1.3 Wind Turbines

Wind energy has been used for decades in electrical power production and, as it uses only wind, it generates power with zero emissions. A wind turbine consists of a rotor, generator, turbine blades, coupling device and a shaft, as well as a nacelle, which contains the gearbox and generator drive. Therefore, based on wind forecast, two or three turbine blades are used in a design that ensures high efficiency generation. Wind turbine efficiency is usually in the range of 20-40 per cent, and the size is between 0.3 kW to 5 MW [15, 16, 17].

Wind turbines can be classified into two types based on their connection to the grid or load. The first is connected through a rotary machine, usually an induction generator, while the second employs a full-scale voltage source inverter [18]. Wind power plants have been installed in many countries because of their efficiency and contribution to ameliorating man-made global warming. These plants provide supported power to the main utility without causing negative impacts on the performance of the power system. The wind turbines have been investigated by many researchers in terms of; impacts on system operation [15], power quality [19], stability [16], market and pricing [20], and planning and reliability [17].

2.1.4 Photovoltaic (PV) Systems

This system largely relies on sunlight for power generation and a cell made from a doped silicon crystal is the key component. A group of cells can form a module or panel and several of these can be configured as an array in a photovoltaic system. Driven by green energy policies, photovoltaic farms are being adopted, thus increasing the penetration of photovoltaic arrays. This scenario was uneconomic solution because of the high installation cost and a relatively low power generation. Therefore, small scale distributed PV generation, with ratings ranging from 1 to 100 kW, has been viewed as a more economical solution for reliable power generation [21].

The rating of the photovoltaic array is mostly in the range of 0.3 kW to a few MW. For the purpose of supporting green electricity, using PV arrays faces two main limits. First is land costs as 0.25 ha is required to generate 150 kW of electrical energy. Second is climate as reliable operation is only obtained in sunny weather. The voltage fluctuations and harmonic distortion are usually associated with PV systems; however, these can be mitigated through internal controlled-reactive power sources [22]. Therefore, many PV system researchers focus on control strategies to track maximum power for better power generation [23], and developing cell technology with higher efficiency and lower costs [24].

In conclusion, awareness of climate change increasingly makes renewable energy sources a priority. Therefore, wind and PV power plants can be represented as efficient power support for the utility, provided that these plants connect at the substations or transmission levels. Moreover when the stiffness of the utility is high, thus their impacts are certainly less. Conversely, flawed results are obtained when wind and PV power farms are considered as distribution systems.

2.1.5 Energy Storage Devices

Efficient energy storage devices commonly involve batteries, flywheels, super-conducting coils, or super-capacitors [25]. When connected as distributed generation units, they offer fast load pick-up, reliability enhancement, and an improved generated power profile for non-dispatchable sources.

2.1.6 Hybrid Systems

Hybrid system can increase the performance efficiency of the microgrid, and thus improve generation characteristics, for example, a gas micro-turbine and a fuel cell can be integrated to form a full cycle power plant that exceeds 70 per cent efficiency and rates from 250 kW

to 2.5 MW [26]. An innovative hybrid system can increase the combined participation of different types of DG units such as wind turbines, fuel cells, and PV panels. Other add-on options including energy storage devices and diesel generators can also enhance the microgrid when in stand-alone mode (Figure 2.2).

Table 2.1 shows the characteristics of the common DG units in terms of rating, efficiency, grid connection technology, and fuel type [27]. According to the IEEE standard 1547-2003 [28], the DG units that form the microgrid are normally disconnected from the utility based on a network fault or a market decision. The microgrid is then forced in to autonomous operation mode and is vulnerable in terms of maintaining voltage and frequency, because of the contrasting characteristics of the connected DG units. Therefore, it is necessary to maintain the power supply within at least the threshold of required quality.

Table 2.1: The characteristics of most common DG units

Characteristic	Micro-turbines	Fuel cells	Wind Turbines	Photovoltaic panels	Fossil Fuels
Rating	20-500 kW	1 kW-5 MW	0.3 kW-5 MW	0.3 kW-2 MW	up to 100 MW
Efficiency	20-30(%)	40-60(%)	20-40(%)	5-15(%)	33(%)
Grid connection technology	power electronic converter	power electronic converter	induction generator and power electronic converter	power electronic converter	synchronous generator
Fuel type	natural gas, biogas, diesel, propane, hydrogen	natural gas, propane, hydrogen	wind	sunlight	oil, diesel, coal, natural gas

2.2 Inverter-Based DG Unit

Typical DG units provide electrical power through conversion processes that can be classified as: high frequency such as micro-turbine generator, variable frequency such as wind turbine, and direct energy such as photovoltaic and fuel cell. An interfacing power electronic converter is required to convert the produced energy from DC to a constant voltage and frequency AC power source. This converter is usually called a Voltage Source Inverter (VSI) system and is the most functional block in the inverter-based DG unit.

Figure 2.3 depicts the power circuit of the 3-phase VSI inverter-based DG unit and the associated control functions. The VSI system itself encompasses two main circuits with the

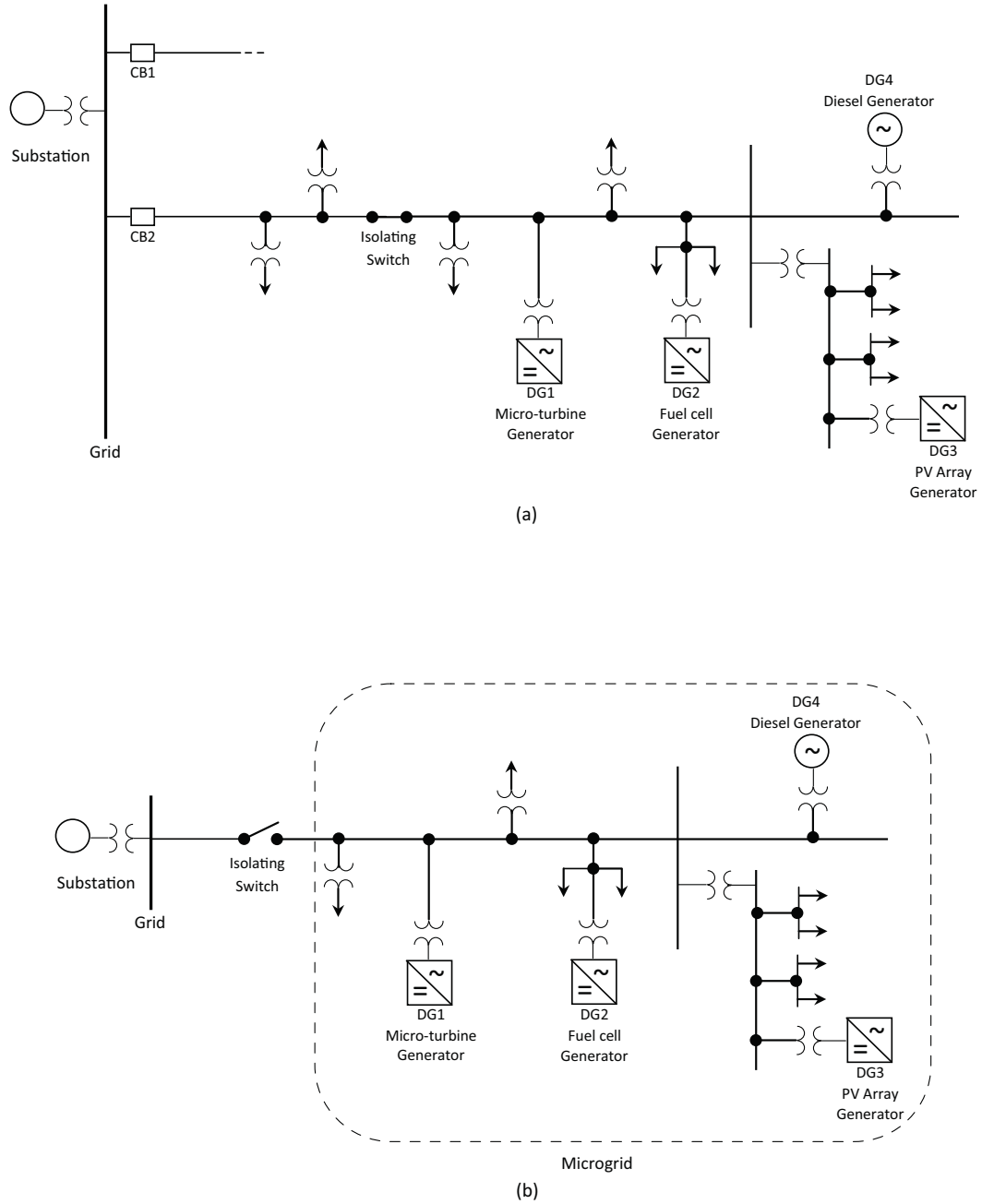

Figure 2.2: An example of the microgrid: (a) Grid-connected mode. (b) Microgrid mode

first being the power circuit that includes a three-leg VSI with an AC filter. The second is the control circuit that incorporates the VSI control loops that are designed to provide reliable operation. For example, in grid-connected mode, the voltage and frequency are established by the grid which dominates the overall system behaviour. In this case, the DG unit can be operated as a PQ generator, thus the control of the active and reactive power flows are largely required. Conversely, in the islanding mode, the system should provide regulated voltage and frequency or low power quality may occur. Therefore, voltage and frequency regulation must be considered as substantial control objectives, whereas power flow can be managed among the DG units provided they meet the total load demand. If not, the system has to undergo load shedding. Thus, sharing power in a microgrid can be regulated for optimising utilisation of the DG units, taking into account the inverter power rating. For these reasons, the power control loop in an inverter-based DG unit is essential for maintaining power supply quality. In addition to the power control loop and regardless of microgrid operation mode, the inner current control loop is also required to make the VSI system operate as a current-source amplifier. This ensures that accurate tracking exists and short transients occur for the inverter output current. The synchronisation technique is also crucial for adapting the inverter's behaviour to any microgrid operation mode. That is also required to implement a synchronous reference frame in the control scheme.

Moreover, the inverter current can be protected from low-order harmonic distortion by using a Pulse-Width-Modulation (PWM) technique. However, high frequency current distortion can be caused by the inverter switching frequency, which must be attenuated to meet the power quality standard for the connected DG unit. This is the main function of the inverter output filter.

Overall, the performance of the inverter-based DG unit largely depends on the effectiveness of the abovementioned control loops. This research will show the advantages of the proposed power controller for maintaining power supply quality in a microgrid scenario, and for both operation modes: grid-connected and islanding. The corresponding control loops for an inverter-based DG unit are presented in the following subsections.

2.2.1 Current Control

The current controller usually represents an important inner loop in the overall controller scheme of a three phase PWM-VSI system. Its main function is to provide accurate current tracking, acceptable dynamic response (short transient), and thus force the inverter to work as a current source amplifier. Clearly, the current control loop can improve the

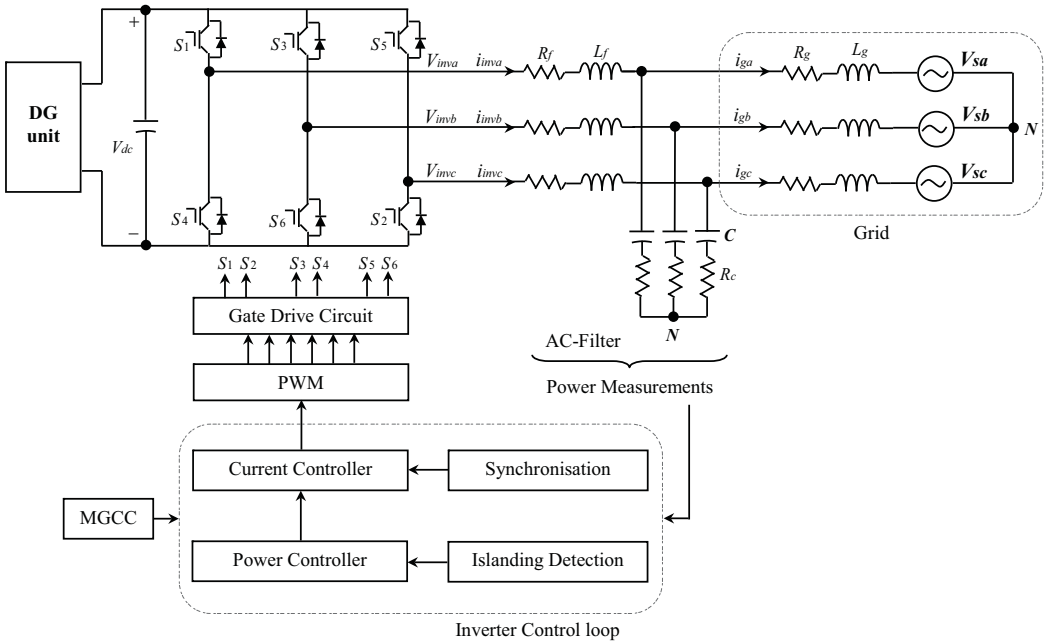

Figure 2.3: Power and control circuits of the VSI-based DG unit

inverter output current quality; however, there are many factors which can directly affect the performance of this controller, for example, grid parameters, transition between the operation modes, and load change. Thus, poor power quality and instability can still occur [6].

The current control strategy of the PWM-VSI system is one of the most important characteristics of modern electronic power converters. While an inverter-based DG unit is crucial for establishing microgrids, an appropriate current control strategy for the inverter is required to achieve high performance and met power quality requirements when DG units are flexibly connected to the grid. There are two main categories for current controllers: nonlinear controllers based on closed loop current type PWM, and linear controllers based on open loop voltage type PWM, and both are applied using the inner current feedback loop [29].

A hysteresis current controller (HCC) is a common type of nonlinear controller that is used for a 3-phase grid-connected VSI system. As shown in Figure 2.4a, this controller depends on a nonlinear feedback loop and the hysteresis comparators. The switching signals for the PWM are directly generated once the error exceeds the tolerance band h (see Figure 2.4b). Two types of HCC are proposed:

1. *Variable Switching Frequency Controller*: This type is also known as a free-running hysteresis controller and its main advantages are an outstanding dynamic response

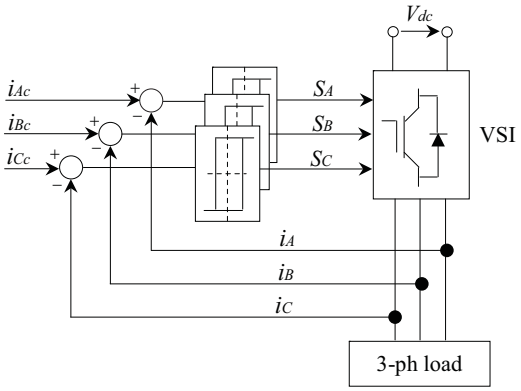

(a) Hysteresis controller

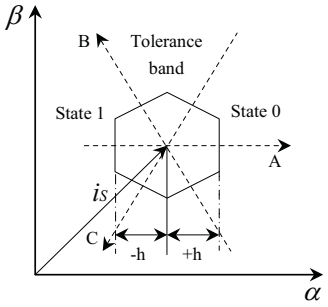

(b) Switching trajectory

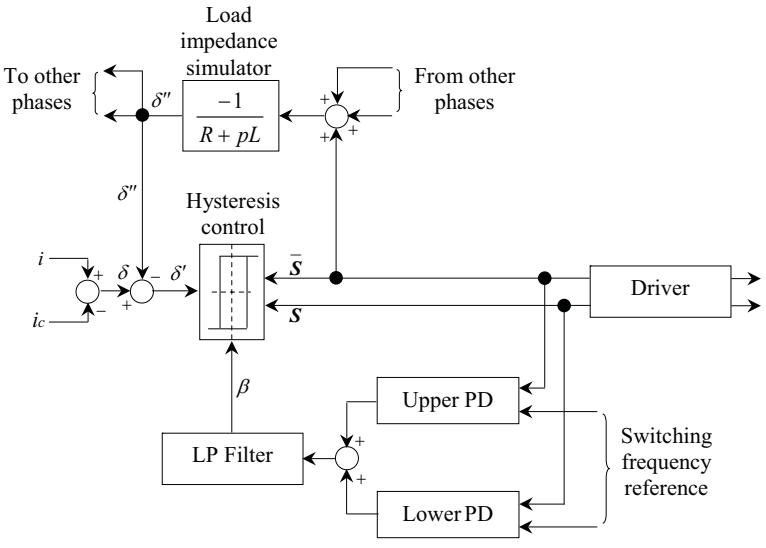

(c) Constant switching frequency controller

Figure 2.4: Common types of nonlinear current controllers

and an absence of tracking errors. It can be easily implemented and mainly depends on the load parameter changes. However, the current is independently controlled with a time delay, and the zero voltage vectors cannot be generated. Thus, a large current ripple with high total harmonic distortion (THD) may occur [30]. Moreover, the inherent randomness can be acquired due to the limit cycle of the operation, which causes relatively rough operation and makes protection for the inverter challenging. In addition, for a system that lacks neutral leaders, the hysteresis band is often decreased to half the value of the instantaneous error because of the interaction between the system and the three independent controllers. Therefore, the instantaneous current cannot remain exactly in a tolerance band. Furthermore, changing the comparator state in one phase influences the load voltage in the other two phases [31].

2. *Constant Switching Frequency Controller*: This type was developed to overcome the disadvantages of the variable switching frequency controller. The amplitude of the tolerance band is controlled either based on the ac-side voltage or by the Phase-Locked-Loop (PLL) technique [32]. Moreover, this controller can decouple the error signal through subtracting an interference signal that is driven from the inverter voltage. Thus, the problem of the interference and its impacts can be eliminated (see Figure 2.4c) [31]. In [33], the decoupling is also considered as important for improving performance without estimating the load impedance. Reliable operation can be obtained and overall the results were similar to those for the discontinuous switching model. In that case, the controller became more complex and thus undermined the main advantage of the hysteresis current controller, that is its simplicity.

Conversely, the linear current controller has been proposed as a solution to improving the inverter output current quality. This controller can independently compensate for the current error and the voltage modulation part. The linear current controller also allows the use of open loop modulators such as sinusoidal PWM, space-vector PWM, and optimal PWM. These can help improve the controller's behaviour because of positive attributes such as; constant switching frequency, optimum switching pattern, well-defined harmonic spectrum, and excellent DC-link voltage utilisation. In addition, the overall independent design of the control structure, and the open loop testing of the inverter, can be easily accomplished [34]. Four types of linear current controllers have been proposed:

1. *Stationary PI Controller*: This type is also known as a *Ramp Comparison Current*

Controller. As shown in Figure 2.5a, three PI regulators are used to compensate for the current error and to provide the voltage reference signals V_{Ac}, V_{Bc}, and V_{Cc} for a three-phase sinusoidal PWM. Along with this type of modulator, comparison with the triangular carrier signal is required to generate control signals S_A, S_B, and S_C for the inverter switches. To explain the function of the PI regulator, the integral part is to minimise the error at low frequency, while the proportional part and the zero placement are responsible for the amount of ripple. In this type, although the original triangular sub-oscillation PWM can directly drive this controller, the performance is imperfect, because the switching time is influenced by the output current ripple which is set through the feedback loop [35]. Moreover, the maximum slope of the reference voltage signal is designed to be no more than the slope of the triangle. Therefore, additional problems may emerge due to the multiple crossing of triangular limits. Overall, the main limitations are that good controller performance is only achieved when the harmonics of the current are in frequency less than the carrier, and the controller suffers from an inherent tracking error (amplitude and phase) [36].

2. *Synchronous Vector PI Controller*: In many industrial applications, a qualified current is required to guarantee robust system operation. For example, in vector-controlled ac motors, a small error in phase or amplitude causes inefficient performance and the space-vector control method is widely used to address such problem. Figure 2.5b depicts the schematic diagram of the synchronous vector controller which employs two PI compensators for two current vector components defined in a $d-q$ synchronous reference frame. The benefit of using this frame is that it transforms the three-phase (i_{ABC}) form of the inverter output current into two dc components (i_{dq}), thus simplifying the analysis and the calculations for the controller. The synchronous controller is also proposed for a stationary reference frame, particularly for the PWM that utilises this frame to synthesise the pulses for the controlled VSI system. Examples of using this type of controller can be found in [37, 38, 39].

3. *State Feedback Controller*: This controller is based on a state feedback control system instead of a PI regulator. The controller scheme can also be designed in stationary or synchronous rotating coordinates. Figure 2.5c shows the block diagram of a state feedback controller, which is designed based on multivariable state feedback theory and a stationary coordinate system. Reliable performance of this controller relies on the pole assignment technique which is used to drive the feedback gain matrix

$K = \begin{bmatrix} K_1 & K_2 \end{bmatrix}$. Thus, a sufficient damping can be only ensured when these gains are well-defined. In addition, by using the integral gain K_2, the static error can be minimised to zero, but an unacceptable transient period can still be obtained. Eventually, the disturbance inputs K_d and the feed-forward signals K_f should implement the feedback control law, so only a well-defined control algorithm can result dynamically correct compensation [40].

4. *Predictive Controller*: In this type, and at the beginning of each sampling time, the current error vector is predicted based on the actual error and the ac load parameters R, L, E. Then, during the next sampling period, the voltage reference vector can be generated for the PWM in order to minimise the forecasted error. The predictive controller can be classified into two types. The first is known as a *constant switching frequency predictive algorithm* which is shown in Figure 2.5d. This algorithm calculates the voltage reference vector V_{sc} once for each sampling period. Thus, the current vector is forced according to its command (i_{sc}), while the voltages of the inverter and load are assumed to be constant [41]. The main disadvantage of this algorithm is that it is impossible to achieve the inverter peak current. The second type is known as a *deadbeat current controller* which is an option solution when the voltage vector is required to null the error at the end of the sampling period [42]. This type is inherently sensitive to model and parameter mismatches.

In conclusion, the linear current controller based on PWM is explored as an adequate technique that provides excellent steady-state response, low current ripple, and high-quality sinusoidal waveforms. Moreover, the tendency is currently towards the methods that allow full digital implementation, even with some sacrifice accuracy. Therefore, the linear current controller represents a practical technique that can be digitally implemented with accurate results, in particular when the modern Artificial Intelligence (AI) applications are embedded in such a controller.

2.3 Microgrid Control

The robust and reliable operation of a microgrid relies substantially on the control scheme for the DG units. Therefore, an efficient power control loop for an inverter-based DG unit can play a key role in satisfying power quality requirements [43]. In other words, while the current control loop is used to improve the quality of the inverter output current, an outer power control loop, as shown in Figure 2.6, can also be integrated with the inner

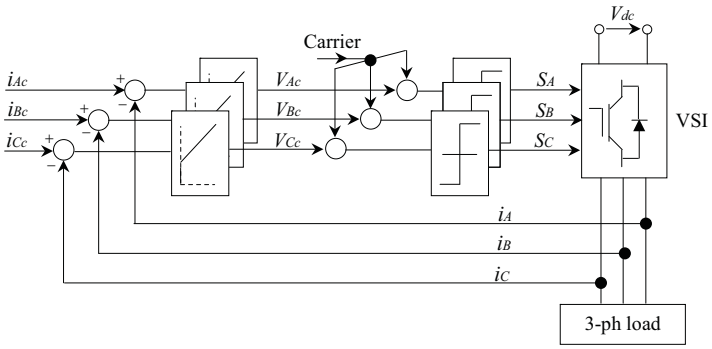

(a) Stationary PI controller

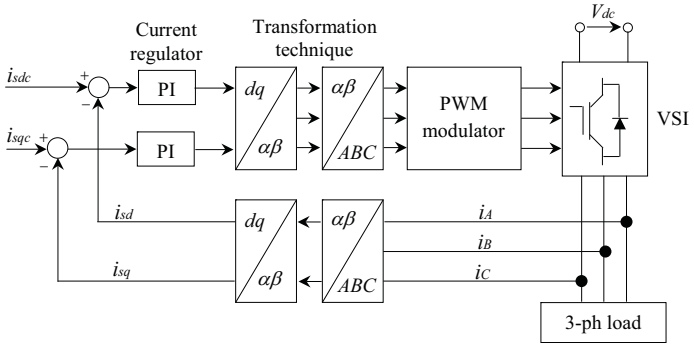

(b) Synchronous PI controller

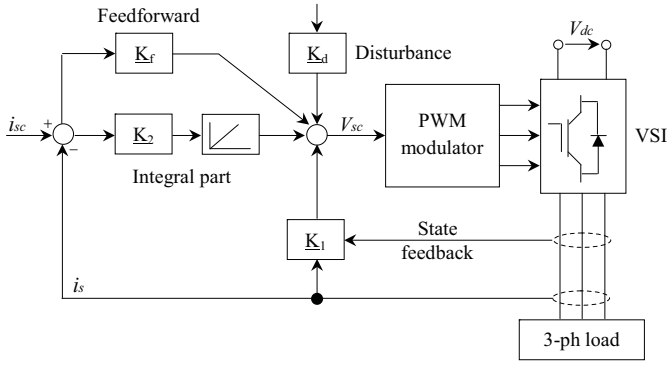

(c) State feedback controller

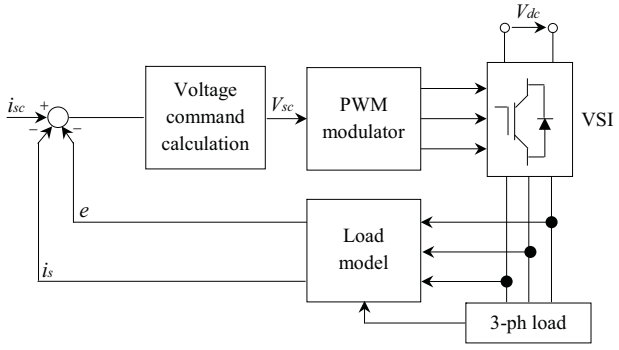

(d) Predictive controller

Figure 2.5: Common types of linear current controllers

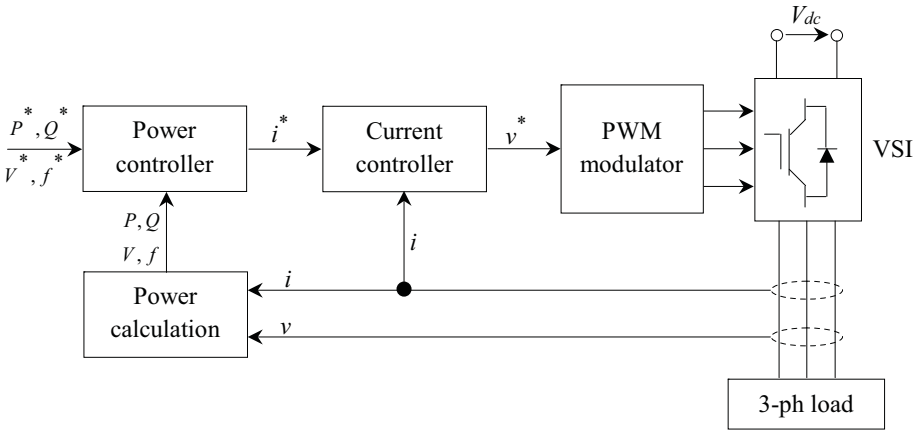

Figure 2.6: The schematic diagram of the power-controlled VSI system

current control loop to regulate the inverter output power. Moreover, it will ensure qualified reference current signals to the current controller. Accordingly, the inverter-based DG unit can be controlled in terms of the imposed power commands such as voltage, frequency, active power, and reactive power [37]. In this case, the DG unit can operate as a power-controlled current source. Consequently, and for both microgrid operation modes, the power controller can be selected based on crucial issues affecting power supply quality. For instance, the control of the power flow in grid-connected mode can be represented as the main control objective. That is because of the overall microgrid operation is completely dictated by the bulk power system, so there is no more pressing than power flow regulation for optimum DG unit utilisation. In contrast, significant operation problems are evident when the microgrid transits to the islanding operation mode. These problems are primarily related to the voltage drop and frequency deviation associated with the various characteristics of the connected DG units. The load sharing mechanism is an additional important issue that needs to be considered to obtain superior operation in both microgrid operation modes [44]. The following subsections present the main power control strategies that can be used for the inverter-based DG unit to satisfy the abovementioned issues, thus improving the quality of the power supply in microgrids.

2.3.1 Voltage and Frequency Control

As a function of load, managing both the microgrid voltage and frequency are essential control objectives, because DC/AC power converters and multi-types of the DG units have different operational properties. Thus, disturbances in the system voltage and frequency are may occur and affect the power supply for the end user [1]. In that case, it is necessary to explain such this problem based on the microgrid operation mode in two main points.

First, in the grid-connected mode, due to the stiff operation characteristics of the utility, the control of system voltage and frequency is mostly not needed. That is because the main grid can provide high voltage quality. However, this type of control can be an optional component only when the grid is weak which is commonly not the case. Second, in the islanding mode, the microgrid is completely responsible for maintaining voltage and frequency within acceptable limits. Thus, a proposed control approach should provide controlled voltage and frequency, and also pick up the load quickly with high power quality [45].

The microgrid voltage profile can also be influenced by various issues including harmonic distortion which can be defined as the deviation in the shape of voltage/current waveform from the standard sinusoid. This deviation is mainly caused by the high speed operation of the inverter switches and can lead to overheating of the load equipment which affects the power factor and the system resonance and disrupts functioning of electronic components. Therefore, the attenuation of the harmonic distortion in such systems is necessary and usually achieved either by using a coupling transformer or a specific type of filter [4]. The time of the transient period is another important challenge to be addressed in a microgrid. The switching between the two operation modes or load change usually causes sub-cycle voltage excursions. These may occur as very fast voltage changes, thus additional protection equipment is required to maintain the load. Therefore, fast dynamic response is another control objective that can help improve the profile of the inverter output power [46].

Severe and random voltage disturbances might be related to time-varying load in the non-dispatchable generations that supply fluctuated output power such as wind power generation and photovoltaic [47, 48]. After this, reactive power sources such as an inverter-based DG unit [49], active power filters (APFs) [50], and the synchronous compensators (DSTATCOMs) [51] are proposed for the voltage regulation at the point of common coupling (PCC) in a microgrid. These sources are used in a three-phase current controlled PWM-VSIs, and the axis-theory is applied as a control algorithm for balancing the three-phase system. Therefore, according to the typical operation of these applications, the reactive reference current is driven through the voltage controller to regulate the load voltage. An inner current controller is also used to regulate the output current. The performance of the voltage controller in providing relatively slow regulation against the disturbances, as well as the frequency restoration, was not considered in these applications. In other words, these applications used conventional PI regulators to control the voltage against

the nonlinear dynamic error, thus the voltage controller is not able to provide high control performance unless an intelligent technique is applied to find the best system parameters to deal with the disturbances. The fundamental frequency voltage must be controlled a stable close loop system to maintain appropriate voltage regulation.

Recently, the droop control method was proposed as a standard application to regulate the microgrid voltage and frequency [3, 52]. The overall scheme of this control is composed of three control loops: 1) the droop control loop that receives the measured and reference voltage and frequency signals and generates the reference active and reactive power vectors based on the droop characteristics; 2) the voltage control loop which relies on the output signals of the first loop and the computed values of voltage, active power, and reactive power, to produce the reference current vectors; and 3) the current control loop that is often responsible for providing the reference voltage signals for the PWM technique. In this controller scheme, conventional PI regulators are also used in the second and third control loops, and the control performance largely relies on the droop characteristics to regulate the microgrid voltage and frequency. Many researchers have evaluated this method for controlling the microgrid voltage and frequency. However, due to the droop characteristics, the frequency and voltage might drop at the values that make the DG unit operate in a new lower voltage and frequency, neither of which are close to their nominal values. Moreover, it is difficult to apply an intelligent technique for optimising the control parameters in real-time because the proposed controller is based on multi-loops which increase the number of parameters. Therefore, most researchers investigated optimisation approaches either to find the best placement of the DG units in order to improve the voltage profile [53] or to optimise the control parameters that offer stable operation for the best microgrid design [54].

2.3.2 Active and Reactive Power Control

Control over active and reactive power flows is essential for regulating the inverter output power. This method can help ensure reliable operation of the connected DG unit; help reduce the imported power from the grid; and support any contractual arrangement between the microgrid and the utility. Therefore, the active and reactive power control mode can also be explained based on the microgrid operation mode. For instance, in an autonomous microgrid mode, the control priority is maintaining the system voltage and frequency below the threshold of collapse. Therefore, the power flow control can be achieved, provided that regulation of the microgrid voltage and frequency is realised, and thus the system can

produce reliable power quality during this mode. Conversely, due to the high operation effects of the bulk power system in grid-connected mode, each DG unit operates as an active-reactive power source [5]. In this case, control over active and reactive power flows is very useful for maximising generation from the connected DG unit; thus, an economic operation strategy based on the market policies can be implemented for best power management between the microgrid and the utility. This can facilitate high market penetration for the micro-sources.

Recently, the power management between the microgrid and the utility has been targeted by many researchers to obtain best utilisation for the different types of DG units. For example, control of the combined active and reactive power is proposed to facilitate the connection between the single-phase hybrid microgrid and the electric power system [55]. In this work, the control structure is designed to compensate for the reactive power of the load, inject the active power to the load, and then pass the redundancy to the grid. However, this controller may not be feasible for the three phase system due to the complexity. The shunt active filter with energy storage is proposed to mitigate the voltage sag and improve the supplied power to the nonlinear load [56]. The control of this filter is coordinated with the synchronous generator, and the filter current was a unique feedback signal. Accordingly, the voltage sag is manipulated, while the active and reactive power reach a stable operation after a long transient period (9 s). In [57], the combination of the genetic algorithm and the power flow calculation is presented to allocate the location and sizing of the DG units relative to the electric power system. This method is useful for the DG units' installation to obtain best economic operating condition. However, the control of the active and reactive power flows was not considered against the disturbances in the real-time operation. In [58], the power flow control is proposed for a single-phase inverter-based DG unit in grid-connected operation mode. This controller regulates the active power and the reactive power by adjusting the power angle and the filter capacitor voltage, respectively. The objective behind this work was to achieve stable operation, low static error, and fast dynamic response. Similar observations can be found in [59, 60]. As a consequence, no method was proposed to regulate the active and reactive power automatically, thus reducing the imported power from the utility up to the limited ratio.

2.3.3 Power Sharing

While the microgrid is configured from multiple DG units connecting in parallel, sharing power among these units is an important scenario that can also improve the power supply

quality. In other words, load demand can be met distributing the load among the connected DG units, and thus obtaining reliable system operation [44]. Therefore, this scenario should be implemented while the power control strategy is proposed to improve the microgrid operation. In both microgrid operation modes, the proposed control methods are mostly used to regulate the inverter output power with the aim of achieving stable operation and fast dynamic response. This can provide constant power whether the load changes or is stable. Therefore, it is necessary to investigate a control strategy that can help inject sustained output power even when the load changes and thus increase the efficiency of the DG units, in particular those which supply constant power such as a photovoltaic panel.

Droop control of voltage and frequency is commonly proposed for sharing active and reactive power. In [3], three power management strategies based on the voltage-droop characteristics, voltage regulation, and reactive power compensation are proposed for a microgrid configured from multiple DG units. The frequency-droop characteristic is used to control the active power. The overall dynamic model is developed to investigate the system dynamic behaviour under the proposed power management strategies. In [61], the decoupling of active and reactive power flows in the grid-connected mode is presented to investigate power sharing between the microgrid and the utility. The events, arising from pre-planned switching and faults, that cause the islanding mode are presented with desired power sharing in [62]. The power derivative integral terms are introduced to address the slow load sharing with the conventional droop control and thus improve the transient performance [63]. The static droop control method is also used for power sharing in a microgrid in [52]. Accordingly, while the drawbacks of the droop method are explained in the penultimate sub-subsection, the above reviews focus on obtaining stable operation and fast dynamic response. Intelligent power sharing among the DG units is an important control objective in a microgrid, that can be targeted after considering power supply component quality. Therefore, power sharing is one of the objectives of this thesis.

In conclusion, the main purpose of microgrid control is to achieve robust and reliable operation of the connected DG units. Therefore, an efficient power control strategy can achieve the objective of improving the quality of the power supply in terms of; regulating the system voltage and frequency, controlling the active and reactive power flows independently, and sharing the load properly either between the microgrid and utility in grid-connected mode or among the DG units in the islanding mode. These can improve the overall operation of the microgrid, where the load can be quickly picked up, and also the microgrid can rapidly and seamlessly connect to, or disconnect from, the utility.

2.4 System Stability

System stability under the given operating conditions has become an important issue for microgrid operation. It is important, given the combination of different types of DG units and use of electronic power converters to interconnect these units, and can be efficiently analysed with the small-signal dynamic model. This model can be defined as an analytical approach that can verify the stability under the normal operating conditions. The overall dynamic model is combined from the linearised state-space equations that define each component of the system. After this, stability can be analysed through eigenvalue calculations. Subsequently, sensitivity analysis can be used to measure the dependency of the stability analysis on system variables. This is a complementary analytical method that depends on calculating the participation factor for each variable [64, 65].

Stability analysis of the microgrid operation has been investigated by many researchers. In [61], the transient stability was examined for the power system with a DG unit that interfaced via a power converter. This analysis was for a system with infinite bus, and the stand-alone operation of the power system network was not considered. For the stand-alone mode, [66] presented a control approach, for the parallel connected inverters, that could be modified for any ac system. The control objectives were to identify the reference signals of the generator angle and the flux, and to improve the dynamic performance of the system. In [67], small-signal stability was used to confirm that a proposed control method may escalate the oscillatory modes and yield poor damping, so the sensitivity analysis was employed to determine the proper feedback signals for the controller. The stability against change in load demand in a microgrid was examined in [68]. Due to the load change, moving the oscillatory modes towards new locations affected system stability. In [69], a dynamic model of voltage and current controllers based DG unit was developed to analyse system stability in the islanding mode. A small-signal dynamic model was also constructed for the microgrid that configured from multiple DG units in [70]. The droop control associated with the power average method is used for the purpose of the load sharing control in the islanding mode. The aim was to verify the accuracy of stability analysis against the simulation results of the nonlinear model.

To be brief, the small-signal dynamic model has been developed for numerous applications of the power system and microgrids. This method yielded accurate results that proved the validity of the designed systems. Therefore, the small-signal dynamic model is developed in this thesis to examine microgrid stability with the proposed power controller, and the sensitivity to the control parameters is also presented to assess the validity of the

proposed controller.

2.5 Conclusions

This chapter outlined the background theory and relevant literature including major reviews, that underpin and justify the need for this study on improving power supply quality in microgrids. The common types of the DG units are described with the aim of introducing their operation characteristics in terms of rating, sizing, efficiency, type of connection, and fuel type. Then, because the operation of these units depends on the control mode; the inverter-based DG unit is presented along with the most common types of the linear and nonlinear current controllers. The reviews show that the linear type is much better than nonlinear. For this reason, it becomes necessary to clarify the microgrid control that is largely responsible for qualifying the power supply. The control methods which are related to voltage and frequency restoration, active and reactive power regulation, and power sharing are introduced with the aim of exhibiting their aspects. Finally, small-signal dynamic model analysis of microgrid stability is targeted as a tool for measuring the system's reliability.

Chapter 3

MODERN HEURISTIC TECHNIQUE: PARTICLE SWARM OPTIMISATION ALGORITHM

The modern heuristic techniques mainly include the application of the Artificial Intelligence (AI) approaches such as Genetic Algorithm (GA), Particle Swarm Optimisation (PSO) algorithm, Ant Colony Optimisation (ACO), Stochastic Diffusion Search (SDS), Differential Evolution (DE), etc. [71]. The main aspect of these techniques is their flexibility for solving the optimisation problems that have different mathematical constraints. In a power system area, the competition between the electric utilities is gradually increased due to the deregulation of the electrical markets. For this reason, the generation expansion problem presents itself as an important issue that needs to be considered in order to achieve reasonable economic decisions. The applicable plan to address this problem is how to install new generation units that should meet the requirements of the power system such as load demand, power quality, reliability, operating conditions, and security [72]. In that case, while the generation expansion problem can be mathematically formulated such as high dimensional, mix-integer, nonlinear, and optimisation problem with an objective function, so the heuristic techniques have been developed to handle numerous qualitative problems which are common in the electric power field.

In general, many heuristic techniques have emerged to solve several optimisation problems in the power system area such as power system operation, voltage and reactive power control, capacitor placement, etc. These techniques are classified based on the type of search space and the objective function as follows. First, the *Linear Programming* (LP) is the simple optimisation technique that uses with the linear objective function and linear equality or inequality constraints [73]. This technique was applied for different power system problems such as economic dispatch [74, 75], planning and operation [76, 77, 78, 79], protection coordination [80, 81], maintenance scheduling [82], and state

estimation [83, 80, 84]. Similarly, an *integer linear programming* method is referred if and only if all or some variables are defined as integer values [73]. The application of this method was for power system security assessment [85], optimisation and design of the transmission system [86, 87, 88, 89], reliability analysis [90], planning of the distribution system [91], and load management [92]. Second, the *Nonlinear Programming* (NLP) is introduced for nonlinear objective function and constraints, but the researchers have noticed that it is a difficult field, and also valuable results are only achieved when all constraints are linear, so it is referred as *Linearly Constrained Optimisation* [93]. An extensive use of this technique was in the field of power system voltage security [94, 95], dynamic security [96, 97], reactive power control [98], planning and operation of the power system [99, 100, 101, 102, 103], optimal power flow [104, 105, 106, 107], capacitor placement [108], and unit commitment [109]. Third, *Stochastic Programming* is another technique that provides the probability functions of various variables in order to solve the problems that involve the uncertainty. It also has an alternative name which is called *Dynamic Programming* (DP) [110]. Although this method is widely used for optimisation problems, the numerical solution requires more computational process which increases the probability of suboptimal results because of the dimensionality problem. For instance, the application of using this method was for solving power optimisation problems such as unit commitment [111, 112], and power system planning and operation at the distribution system level [110, 113, 114, 115].

In the same way, Genetic Algorithm (GA) and Particle Swarm Optimisation (PSO) are computational-intelligence based techniques that proposed to solve the above problems. GA is a search method that emulates the evolutionary biology to find the approximate optimal solutions [116]. Although, a good solution can be located rapidly, it also has some negative aspects, namely: (1) the convergence moves toward the local solution rather than the global solution because only good genetic information can be passed, (2) it is difficult to run with sets of the dynamic data, and (3) in a particular optimisation problems and computation time, simple optimisation technique may gives better results than GA.

In contrast, the PSO is also an Evolutionary Computation (EC) technique that uses the dynamics of the swarm to find the solutions for the optimisation problems. The main aspect of this technique is that the size and nonlinearity of the problems do not largely affect the solution [117]. As reported in [118, 119], the best results are achieved by the PSO algorithm compared to other optimisation techniques. This is because it outperforms other methods, especially GA in some positive aspects, namely:

1. The PSO is easier to implement with less parameters for tuning.

2. The memory capability of the PSO is more effective than the GA because each particle is able to remember its own previous best position and its neighbours' best too.

3. The PSO is more efficient to maintain the diversity of the swarm. This is because the swarm uses the most successful information to move toward the best which is similar to the community social behaviour. While, the GA neglects the worse solution and passes only the good ones.

For these reasons, and based on the above review of the numerous heuristic techniques, PSO algorithm has been proposed in this work to solve an optimisation problem in order to improve the quality of the power supply in a microgrid operation scenario.

The remaining part of this chapter is divided into five main sections. Section 3.1 presents the basic concept of the Particle Swarm Optimisation technique. In Section 3.2, the implemented PSO algorithm is described in detail. Section 3.3 demonstrates the applied fitness function that is used to evaluate the search process of the PSO algorithm. In Section 3.4, the termination criterion is described to explain the strategy of stopping the search process of the algorithm. Finally, the conclusions are outlined in Section 3.5.

3.1 Particle Swarm Optimisation (PSO): Basic Concepts

The PSO algorithm was proposed by Kennedy and Eberhart in 1995. This algorithm simulates the social behaviour of the swarm such as schools of fish, flocks of birds, or swarm of bees where they find food together in a specific area. Therefore, this algorithm uses swam intelligence concept which can be defined as a collective behaviour of unsophisticated agents when they create coherent global functional patterns by interacting locally with their environment [120]. In nature, the journey of the swarm of bees is the best example to understand the conception of the PSO approach [121]. Imagine that this swarm searches to find higher concentration place of the flowers in the field. Initially, the swarm starts looking for the flowers in random locations and velocities with no prior knowledge about the field. At this stage, each bee can remember the locations of the most flowers, as well as knows the other locations of the abundance flowers which found by its neighbours. In that case, as shown in Figure 3.1a, depending on the location of the most flowers that is personally pointed, and the location that is discovered and reported by the rest of the swarm bees, the hesitant bee accelerates in both directions, and alters its trajectory to move towards best position based on the social influence that dominates its decision. After this, a bee or

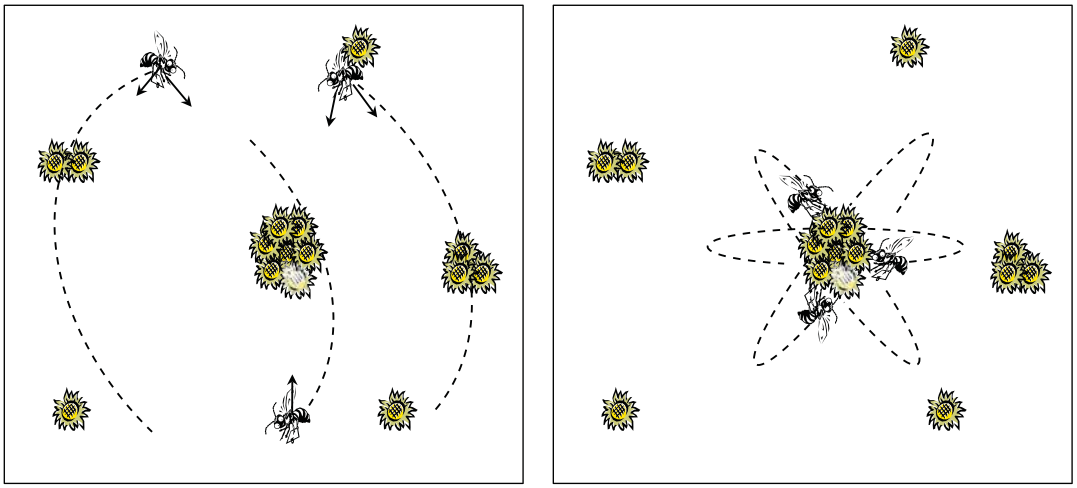

(a) Bees search for location of the most flowers (b) Bees attract to high flowers concentration area

Figure 3.1: Bees search process in a field

swarm may discover new place with higher density flowers compared to previous one, so they move to modify their locations towards this new place. In like manner, when a place with more flowers is discovered by one bee later, the whole bees of the swarm draw towards this location in addition to their own personal detection. Consequently, after exploring the field and flying over the best density places, the bees are being pulled back towards them. They keep checking the location that they fly over in order to find the absolute best density of the flowers against the last encountered location. Eventually, the bees drive themselves into one position with the highest concentration of the flowers, and then all bees of the swarm gather around this point. Moreover, they continually return back to same point when they are unable to find the highest flowers concentration as shown in Figure 3.1b.

In conclusion, it can be noticed that the bees' journey is accomplished based on three main concepts, namely: intelligence, social, and the computational characteristics, which are already used as a fundamental cornerstones of the PSO algorithm. For more explanations, these concepts are described in the next subsections as follows.

3.1.1 Social Concepts

The social concept usually refers to the interaction and the collective coexistence between the members of group of humans or other animals. In other words, this concept describes the living characteristics of such groups in the environment, irrespective of whether they are aware or not of their interaction, and regardless of the interaction is voluntary or involuntary. In the AI applications, the social term is widely used and its adjectives like

behaviour, orientation, interest, or need of each other play a vital role in establishing the idea of these applications. Therefore, while different social theories are considered in many AI approaches, the idea of the PSO algorithm is proposed based on two main theories as follows [120]. First, "*human intelligence results from social interaction*". That means activities like evaluation, comparison, and learning from experience help humans to be familiar with the environment and establish optimal patterns of behaviour and attitudes. Second, "*culture and cognition are inseparable consequences of human sociality*", which means the mutual social learning leads individuals to become more similar, thus the culture is acquired, and then more dealing between the individuals allows them towards more adaptive patterns of behaviour.

3.1.2 Swarm Intelligence

Swarm intelligence is the second concept that provides integrated operation of the PSO technique when it consolidates the social behaviour. This concept can be defined as a collective behaviour system that simulates the cooperative work of the swarm of ants, birds, or bees when they interact locally in nature. In other words, swarm intelligence is a kind of ability that almost uses to solve an optimisation problem in the artificial intelligence applications. Additionally, it is important to explain that swarm intelligence includes two fundamental concepts, namely: the concept of a swarm that suggests multiplicity, randomness, stochasticity, and messiness, and the concept of intelligence that suggests a method for solving a problem which is somehow successful. As a result, the members of the swarm "population" should be able to work based on five fundamental principles that clarify the concept of the swarm intelligence as follows [122, 123, 124].

1. *Proximity*: the population should be able to run in simple space and time computation.

2. *Quality*: the population should be able to respond to the quality factors in the environment.

3. *Diverse Response*: the population should not limit their activities over restricted spaces.

4. *Stability*: the population should not change their behaviour once the environment changes.

5. *Adaptability*: the population should be able to change their behaviour when it is necessary to obtain worthy results.

In a PSO, the term "population" refers to the particles which are subject to the best mode of behaviour. These particles can run in two modes: stochastic mode and deterministic mode. Accordingly, they frequently adjust their trajectories, after starting the search process, in order to find the best position. As shown in Figure 3.2, while each particle is able to move randomly, it is mostly attracted towards the current global best position X_{gbest}, as well as keeps its own best position X_{pbest} in memory. Also, when each particle discovers a new position which is better than any previously encountered positions, then it updates that as a new current best position [125]. Consequently, a number of current best positions results for all particles at any time of iterations, so the global best position can be pointed over all current best positions until the process achieves the objective or at a maximum number of iterations.

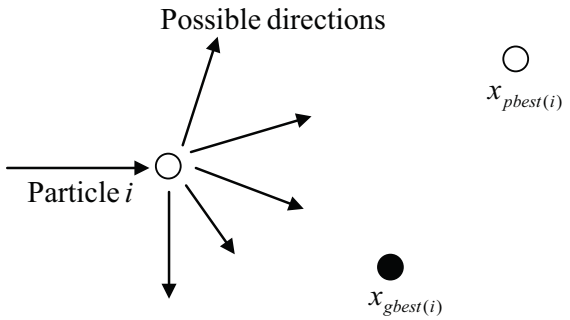

Figure 3.2: Schematic diagram of particle movement in a PSO technique

3.1.3 Computational Characteristic

A computational characteristic is another positive feature that can describe the computational process of the PSO algorithm. That is because the PSO algorithm mainly uses swarm intelligence which provides sufficient computational characteristics for most of AI approaches. In other words, swarm intelligence can be mathematically defined as an extension of evolutionary computation that employs softening parameterisation of logical operators such as AND, OR, and NOT. Recently, the AI approaches that proposed a concept based on swarm intelligence are widely used to solve the optimisation problems that occur in the most of engineering applications. However, due to the rapid increase of complexity, these approaches are useful when they are used in some applications, whereas may not give feasible results in others. Thereby, PSO has been proposed as an alternative

solution technique that employs a stochastic search process in order to find the optimum solution. This technique includes the scenarios of artificial life, social psychology, engineering, and computer science. PSO is also an extension of swarm intelligence concept and its states simultaneously change in many dimensions, so the main computational attributes of the PSO can be described as follows [120].

1. Updating all particles individually and in parallel.

2. Obtaining new particle's value depends on the previous value and its neighbours.

3. Using the same rules for all updates.

In conclusion, the above-mentioned overview of the PSO and other types of AI applications gives clear impression that PSO algorithm outperforms other applications. That is because this algorithm was proposed with the aim of overtaking the common downsides of the most techniques which are applied in different fields of science. Moreover, it mostly provided good performance and results in many applications of the power system areas. Therefore, PSO algorithm has been employed in this work in order to improve the quality of the power supply for microgrid operation scenario. The following sections describe the main structure of this algorithm in detail.

3.2 Developed Heuristic Technique: PSO Algorithm

In this section, the implemented PSO algorithm has been outlined based on the fundamental concepts described above. The essential steps of this algorithm are represented in a flowchart diagram shown in Figure 3.3. These steps describe that this algorithm is an iterative technique that searches the space to determine the optimal solution for an objective function (fitness function). The PSO algorithm evaluates itself based on the movement of each particle as well as the swarm collaboration. Each particle starts to move randomly based on its own best knowledge and the swarm's experience. It is also attracted towards the location of the current global best position X_{gbest} and its own best position X_{pbest} [125]. Therefore, the basic rules of this algorithm can be explained in three main stages:

1. Evaluating the fitness value of each particle.

2. Updating local and global best fitness and positions.

3. Updating the velocity and the position of each particle.

Mathematically, the search process can be expressed by simple equations, using the position vector $X_i = [x_{i1}, x_{i2}, ..., x_{in}]$ and the velocity vector $V_i = [v_{i1}, v_{i2}, ..., v_{in}]$ in the specific dimensional search space. In addition, the optimality of the solution in the PSO algorithm depends on each particle position and velocity update using the following equations [126]:

$$V_i^{k+1} = w.V_i^k + c_1.r_1[X_{pbest}^k - X_i^k] + c_2.r_2[X_{gbest}^k - X_i^k] \tag{3.1}$$

$$X_i^{k+1} = X_i^k + V_i^{k+1} \tag{3.2}$$

where i is the index of the particle; V_i^k, X_i^k are the velocity and position of particle i at iteration k, respectively; w is the inertia constant and it is often in the range [0 1]; c_1 and c_2 are the cognitive coefficients which are usually between [0 2]; r_1 and r_2 are random values which are generated for each velocity update; X_{gbest} and X_{pbest} are the global best position that is achieved so far based on the swarm's experience, and the local best position of each particle that is achieved so far, based on its own best position, respectively. Moreover, each term in Equation (3.1) can be defined according to its task as follows:

- The first term $w.V_i^k$ is called the *inertia component*; it is responsible for keeping the particles search in the same direction. The low value of the *inertia constant* w accelerates the swarm's convergence toward the optimum position, while the high value discovers the entire search space.

- The second term $c_1.r_1[X_{pbest}^k - X_i^k]$ is called the *cognitive component*; it represents the particle's memory. The particle tends to return to the field of search space in which it has high individual fitness and the *cognitive coefficient* c_1 affects the step size of the particle to move toward its local best position X_{pbest}.

- The third term $c_2.r_2[X_{gbest}^k - X_i^k]$ is called the *social component*; it is responsible to move the particle toward the best region found by the swarm so far. The *social coefficient* c_2 affects the step size of the particle to find the global best position X_{gbest}.

According to Equation (3.2), the position of each particle updates itself by using the new velocity and its previous position. In this case, a new search process starts over the updated search space in order to find the global optimum solution. This process repeats itself until it meets the termination criterion such as the maximum number of iterations or the required fitness value. Consequently, regenerating the swarm through a stochastic velocity term and the ability of understanding, the search process produces high performance operation

to find the global optimum solution. Therefore, the PSO algorithm has more advantages than other iterative searching methods such as the GA, which passes only good genetic information to the descendants.

On the contrary, a confined search space is the only significant limitation of the PSO algorithm. A fast solution can be achieved by selecting limited search space, but the optimality of the solution will be influenced if the global optimum value is located outside the boundaries. Extended boundaries however allow finding global optimum results, but need more time to determine the global optimal value in the search space. Therefore, more information about the limits of the parameters will help to determine the search boundaries.

In order to address this problem, a small-signal state-space model is developed in Chapter 7 for the purpose of investigating the dynamic stability for the microgrid. In this work, the linearised state-space model is defined to examine the system stability through the eigenvalue analysis. This model is also used with the aim of testing the sensitivity of the control parameters. Therefore, the PSO algorithm has been used to the find optimum power controller parameters, so appropriate ranges of the control parameters can be selected and prepared for the applied optimisation technique.

3.3 Fitness Function

The fitness function is a particular criterion that is used to evaluate an automatic iterative search such as PSO or GA. In this case, regarding the control objectives, the minimisation of error-integrating function is the most relevant function of the four error criteria techniques, namely: 1) *Integral Absolute Error* (IAE), *2) Integral Square Error* (ISE), *3) Integral Time Square Error* ($ITSE$), and *4) Integral Time Absolute Error* ($ITAE$); which offered the best results in the previous study [127]. The ISE and $ITSE$ are very aggressive criteria because squaring the error produces unrealistic evaluation for punishment. Also, the IAE is an inadequate technique compared with the $ITAE$ which represents more realistic error index because the error multiplies by time. For these reasons, the controller's objective function is formulated based on $ITAE$ in this work, which is calculated using *Simpson's 1/3 rule*.

Accordingly, many numerical approximations integrals can be used to find the integration for functions defined by set of values. Figure 3.4 shows the more sophisticated techniques that determine the definite integral from data values. These techniques can be described as follows.

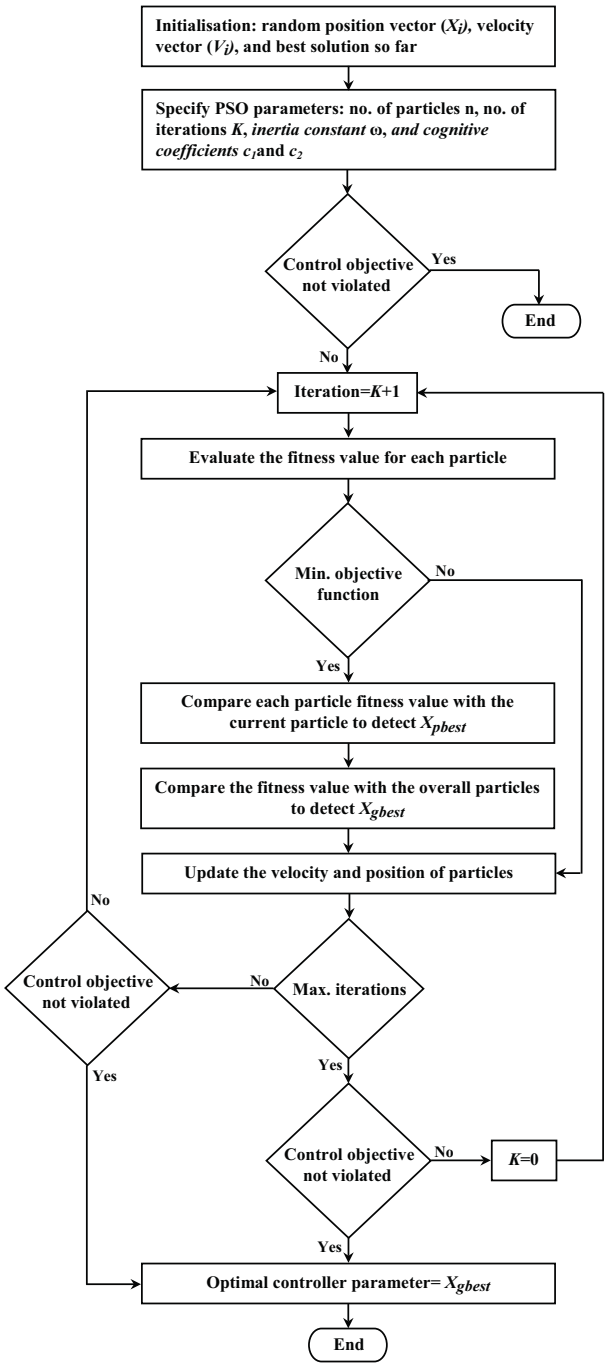

Figure 3.3: Flowchart diagram of the implemented PSO algorithm

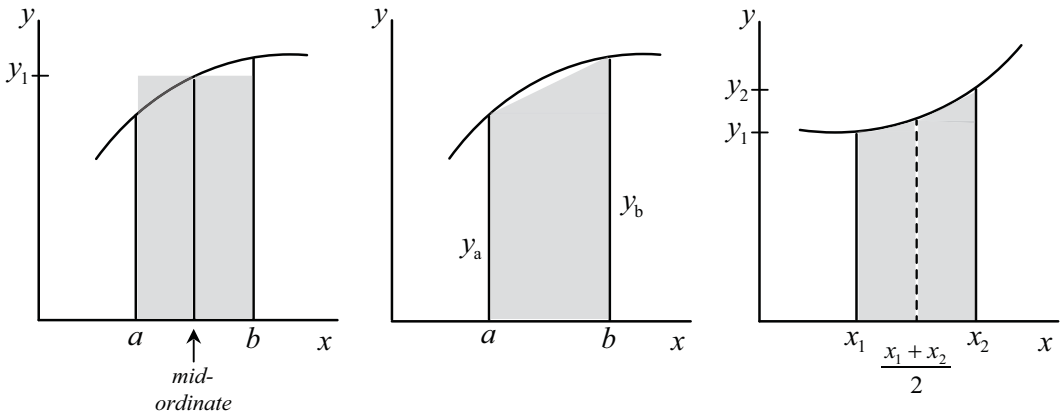

(a) Mid-ordinate rule (b) Trapezium rule (c) Simpson's rule

Figure 3.4: The most common numerical approximations integrals

1. *Mid-ordinate rule*: This method represents a function by a horizontal line ($y = A$, where A is a constant value) through the mid-ordinate line to delineate the upper extent of the area of a strip. As shown in Figure 3.4a, when there are two points, a straight line is draw through the value of the function at the mid-point between the two values, i.e. at $1/2(b-a)$. The estimated area is taken as being the value of the function y_1 at the mid-ordinate multiplied by $(b-a)$, which is given by:

$$\int_a^b f(x)dx \approx (b-a)y_1 \tag{3.3}$$

   Assuming that the area under the function between the ordinates is subdivided into n rectangular strips, the *mid-ordinate rule* can be separately applied to each strip and the estimated area expressed as:

$$\int_a^b f(x)dx \approx \frac{(b-a)}{n}(y_1 + y_2 + y_3 + ... + y_n) \tag{3.4}$$

2. *Trapezium rule*: This method assumes a function by a sloped line ($y = A+Bx$, where A and B are constants) joining the tops of two ordinates as shown in Figure 3.4b, the obtained area of the trapezium is half the sum of the parallel sides multiplied by its width, i.e. $1/2(y_a + y_b)(b-a)$. Thus, the estimated area can be expressed as:

$$\int_a^b f(x)dx \approx (b-a)\frac{1}{2}(y_a + y_b) \tag{3.5}$$

Similar to the first rule, the best value for the integration can be obtained when the area under the curve is subdivided into n equal width strips. In this case, the approximated area using *trapezium rule* can be expressed as:

$$\int_a^b f(x)dx \approx \frac{(b-a)}{n}[\frac{1}{2}(y_a + y_b) + y_1 + y_2 + ... + y_n] \tag{3.6}$$

3. *Simpson's rule*: This method uses the area under the function ($y = A + Bx + Cx_2$, where A, B, and C are constants) between x_1 and x_2 (see Figure 3.4c), which is given by:

$$\int_{x_1}^{x_2} (A + Bx + Cx^2)dx \approx \frac{1}{6}(x_2 - x_1)[y_1 + 4y_m + y_2] \tag{3.7}$$

where $y_1 = A + Bx_1 + Cx_1^2$, $y_2 = A + Bx_2 + Cx_2^2$, and $y_m = A + B(x_1 + x_2)/2 + C\{(x_1+x_2)/2\}^2$, which is located at the midpoint between x_1 and x_2, i.e. $(x_1+x_2)/2$. As shown in Figure 3.5, assuming that the area under the curve is divided into an even number of strips n, then the area of each double strips can be approximated using Equation (3.7), and the width of each double strips is $2(b-a)/n$. The reason for the double strip is to enable the central ordinate of each strip to give y_m value in Equation (3.7). This method called *Simpson's 1/3 rule*, and the integration between a and b can be expressed as:

$$\int_a^b f(x)dx \approx \frac{1}{3}\frac{b-a}{n}[y_a + 4y_1 + 2y_2 + 4y_3 + 2y_4 + 4y_5 + y_b] \tag{3.8}$$

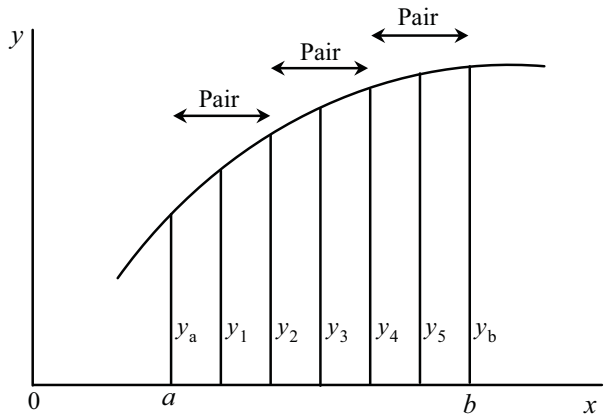

Figure 3.5: Area under the curve using Simpson's rule

In conclusion, the performance of these methods can be evaluated through the error value obtained by the numerical integration. This error can be defined as a difference between the true value of that integral and the calculated value. In other words, based on the results of an example of the integral, halving the width of strips and doubling the number of strips using the first two methods, respectively reduce the error to be proportional to the reciprocal of the square of the number of strips, whereas *Simpson's 1/3 rule* decreases the error to be proportional to the square of the fourth power of the number of strips. As a result, it can be noticed that *Simpson's 1/3 rule* is much better compared with the other rules, and an accurate results can be obtained within few strips.

3.4 Termination Criteria

In general, the termination criteria of a PSO algorithm can be either when the algorithm completes the maximum number of iterations or achieves an acceptable fitness value. In this work, the minimisation of the objective function is considered with the maximum number of iterations to find optimum power control parameters. The implemented PSO algorithm and its objective function are individually constructed for each DG unit that allows dealing with more than one DG unit under the supervision by the Microgrid Control Centre (MGCC) unit. In a more detailed, the performance of the applied PSO search process can be described as follows:

1. The $ITAE$ performance index is the objective function that is separately implemented on each control objective such as voltage, frequency, and active and reactive power. In this case, the results would be referred to the difference between the set-values which may either be defined locally or by the MGCC unit and the computed area of the controlled signals over the limited time which are calculated using *Simpson's 1/3 rule*. This function is incorporated using a MATLAB/M-file program, and the pseudo code of calculating this function is outlined in Algorithm 3.1. In this work, the results that show the performance of the $ITAE$ index with respect to the number of iterations are outlined in the next chapters, Subsections 4.4.1, 5.4.1, and 6.2.1.

2. The PSO is executed in three phases. First, as shown in Algorithm 3.2, PSO sequentially injects n particles when the control objective is being violated, thus the system reacts to each one as a control parameter value, and simultaneously the fitness value is calculated for each control objective as described in Algorithm 3.1. Second, after

Algorithm 3.1 *ITAE* using *Simpson's 1/3 rule*

Require: A difference between set-point and measured value of the control objective (*error*).

Ensure: A value of the objective function $f(x)$ for each particle over limited time.

1: $k = k + 1$, $k = 1 \rightarrow n$ particles
2: $t = t + 1$, (iteration counter)
3: IF control objective violated, THEN
4: Absolute the *error*
5: Compute $f(x)$ *Simpson's 1/3 rule.*
6: RETURN
7: ELSE
8: $f(x)$ =best so far;
9: ENDIF

the particles have been injected, the PSO algorithm runs to evaluate and compare the fitness value of each particle with the current values to select the local best position X_{pbest}. Then, the algorithm updates the particle's position according to Equations (3.1) and (3.2) in order to repeat the process until the global optimum parameter X_{gbest} is found, which represents the best selected value of the controller parameter. A MATLAB/M-file program is also used to implement this process and the pseudo code of these steps are outlined in Algorithm 3.3. In the next chapters, the movement behaviour of the particles are described for all cases that require new control parameters such as the transition from grid-connected to the islanded operation mode or at the load change condition. The figures shown in Subsections 4.4.1, 5.4.1, and 6.2.1 confirm that the particles finish their movements at the best positions, and the power control parameters stay at the optimum global values which satisfy the control objectives.

Algorithm 3.2 Injecting n particles of swarm

Require: Difference between set-point and measured value of the control objective (*error*), a swarm of n particles ($x_1 \rightarrow x_n$).

Ensure: A number of particles sequentially inject when control objective is violated $f(x) = x$, $x = x_1, x_2, ...x_n$.

1: $k = k + 1$, $k = 1 \rightarrow n$ particles
2: IF control objective violated, THEN
3: $f(x_k) = x_k$;
4: RETURN
5: ELSE
6: $f(x) = 0$;
7: ENDIF

Algorithm 3.3 Search process for finding optimum position X_{gbest}

Require: A difference between set-point and measured value of the control objective ($error$), a swarm of n particles ($x_1 \rightarrow x_n$),

Ensure: Find global best position $f(x) = X_{gbest}$ for minimum $ITAE$ value.

IF control objective violated, THEN
WHILE (criterion)
$t = t + 1$ (iteration counter)
FOR loop over all n particles
Evaluate objective function for each particle
Generate new velocity
Calculate new locations
Find the local best position
ENDFOR
Find the current global position
ENDWHILE
Find the final result X_{gbest}
$A = X_{gbest}$, save best global
$f(x) = X_{gbest}$
RETURN
ELSE
$f(x) = A$;
ENDIF

3.5 Conclusions

In this chapter, the PSO algorithm has been proposed for solving an optimisation problem that is related to improving the quality of the power supply in a microgrid scenario. The basic concept of this algorithm is described in this chapter along with the review of other techniques which are used in different optimisation problems. As a consequence, PSO algorithm has emerged as an efficient optimisation approach which can provide reliable solutions for wide range of optimisation problems. The implemented PSO algorithm is demonstrated in detail in this chapter, and the objective function and the termination criterion are also presented, with the aim of describing the complete operation scenario of this technique. In this project, the results that show the performance of the implemented PSO algorithm are included in the next three chapters based on the outlined optimisation problem. Therefore, according to the modelling results achieved in these chapters, the PSO algorithm has been proven as a logical process with high performance of operation. Moreover, the validity of the selected control parameters using this algorithm is proven through the stability analysis as shown in Chapter 7. Thus, the implementation advantages are as follows. First, few particles are required to tune the parameters that provide high speed optimisation process and robust convergence. Second, the so far best parameters can be used as initial values. Third, the algorithm can be individually constructed for each

control objective, so precise results can be expected. Consequently, it can be proven that the PSO algorithm exhibits high speed, high accuracy and high reliability.

Chapter 4

VOLTAGE AND FREQUENCY REGULATION BASED DG UNIT IN AN AUTONOMOUS MICROGRID OPERATION

In a microgrid, the voltage and frequency regulation in the islanding operation mode is considered to be an important issue due to the rapid growth in proliferation of the DG units. This problem occurs once the microgrid is subject to sadden changes such as the transition from the utility to the islanding operation mode or during load change condition. In this case, the quality of the power supply is directly affected by the collapsed voltage and frequency, so this problem needs to be addressed in order to obtain integrated microgrid operation. Moreover, the subject of this regulation is mostly investigated through the controlled VSI systems that is supposed to provide flexible control and operation of the connected DG unit. For this reason, it is important to propose the control strategy that would be responsible for ensuring acceptable limits of the microgrid voltage and frequency, thus improving the quality of the power supply whether the microgrid transfers from the grid to the islanding operation mode or during load change condition.

In this chapter, an optimal power control strategy is proposed for the VSI system based DG unit in an autonomous microgrid operation based on real-time self-tuning method. The aim of this controller is to improve the quality of power supplied by DG units connected in the microgrid. Voltage and frequency regulation, dynamic response, steady-state response, and harmonics distortion are the main performance parameters which are considered here, particularly when the microgrid is islanded or at the load change condition. The controller scheme is composed of an inner current control loop and an outer power control loop based on a synchronous reference frame and conventional PI regulators. The power controller is designed for voltage-frequency (Vf) power control mode. Particle Swarm Optimisation

is an intelligent searching algorithm that is applied for real-time self-tuning of the power control parameters. The proposed strategy is that when the microgrid is islanded or under load change condition, the DG unit adopts the Vf control mode in order to regulate the system voltage and frequency. The results show that the proposed controller offers an excellent response to satisfy the power quality requirements and proves the validity of the proposed strategy.

The remaining part of this chapter is divided into five main sections. Section 4.1 presents a mathematical foundation of a three-phase grid-connected VSI model. In Section 4.2, the VSI control strategy is demonstrated for microgrid in the islanding operation mode. Section 4.3 describes the proposed control strategy in detail. In Section 4.4, the simulation results are analysed to verify the aims of this work. Finally, the conclusions are outlined in Section 4.5.

4.1 Modelling of Three-Phase Grid-Connected VSI System

A typical model of the three-phase grid-connected VSI with an LC filter is depicted in Figure 4.1, where R_s and L_s represent the equivalent lumped resistance and inductance of the filter, the coupling transformer if applicable, and the grid as detected by the inverter. C is the filter capacitance and V_s is the grid voltage.

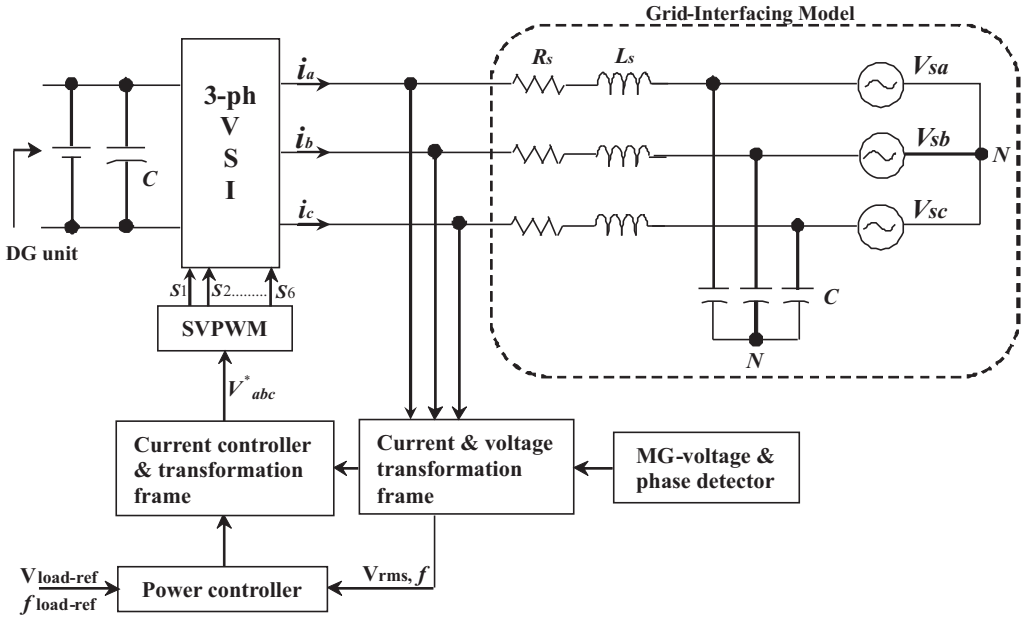

Figure 4.1: 3-phase grid-connected VSI model

In the *abc* reference frame, the state space equations of the system equivalent circuit

are given by [128]:

$$\frac{d}{dt}\begin{bmatrix} i_a \\ i_b \\ i_c \end{bmatrix} = \frac{R_s}{L_s}\begin{bmatrix} i_a \\ i_b \\ i_c \end{bmatrix} + \frac{1}{L_s}\left(\begin{bmatrix} V_{sa} \\ V_{sb} \\ V_{sc} \end{bmatrix} - \begin{bmatrix} V_a \\ V_b \\ V_c \end{bmatrix}\right) \tag{4.1}$$

Using Park's transformation, Equation (4.1) can be expressed in the dq reference frame as:

$$\frac{d}{dt}\begin{bmatrix} i_d \\ i_q \end{bmatrix} = \begin{bmatrix} -\frac{R_s}{L_s} & \omega \\ -\omega & -\frac{R_s}{L_s} \end{bmatrix}\begin{bmatrix} i_d \\ i_q \end{bmatrix} + \frac{1}{L_s}\left(\begin{bmatrix} V_{sd} \\ V_{sq} \end{bmatrix} - \begin{bmatrix} V_d \\ V_q \end{bmatrix}\right) \tag{4.2}$$

where ω is the coordinate angular frequency, and the Park's transformation can be defined as:

$$i_{dq0} = T i_{abc} \tag{4.3}$$

where

$$i_{dq0} = \begin{bmatrix} i_d \\ i_q \\ i_0 \end{bmatrix},\ i_{abc} = \begin{bmatrix} i_a \\ i_b \\ i_c \end{bmatrix} \tag{4.4}$$

$$T = \frac{2}{3}\begin{bmatrix} cos\theta & cos(\theta - \frac{2\pi}{3}) & cos(\theta + \frac{2\pi}{3}) \\ -sin\theta & -sin(\theta - \frac{2\pi}{3}) & -sin(\theta + \frac{2\pi}{3}) \\ \frac{1}{2} & \frac{1}{2} & \frac{1}{2} \end{bmatrix} \tag{4.5}$$

$\theta = \omega_s t + \theta_o$ is the synchronous rotating angle, θ_o represents the initial value. To be continued with this modelling, the state apace equations of the proposed power control mode and the current controller can be found in Subsections 4.3.1 and 4.3.2, respectively.

4.2 VSI Control Strategy in Islanding Mode

In contrast to large generators, DG units can be classified into three energy source types, namely: variable speed (variable frequency) source such as wind energy, high speed (high frequency) source such as micro-turbine generators, and direct energy conversion source such as photovoltaic and fuel cells. For this reason, it is necessary to use a VSI to interface the DG unit to the grid and provide flexible operation [6]. As shown in Figure 4.1, the power circuit of the VSI based DG unit is associated with the control structure, so the

controlled operation of the DG unit relies on the inverter control mode. For instance, in the grid-connected mode, the DG unit operates as a PQ generator and the inverter should follow the active-reactive power (PQ) control mode, while voltage and frequency regulation are not required because the grid voltage is fixed. However, in the islanded mode, the DG units are expected to meet the load demand with respect to the quality of power supply. In this case, the voltage and frequency are not fixed, and the inverter should follow the Vf control mode taking into account the inverter power rating for power sharing issues [129]. Therefore, an appropriate power control mode can result in the high performance operation of the DG unit. The following subsection presents the most relevant power control strategy for the islanding operation mode.

4.2.1 Vf Control Strategy

For a reliable operation of the microgrid, it is necessary to ensure the seamless transition between the microgrid modes, and also keep a stable operation during the islanding mode in terms of regulating the microgrid voltage and frequency with respect to the load demand. In this case, the DG units must follow the load demand and maintain the voltage and frequency within threshold limits, so the Vf control mode has to be adopted by one or more DG units in order to satisfy the above requirements [130]. The block diagram of this application is shown in Figure 4.2. Since the reference voltage and frequency values can be defined locally or by the Microgrid Control Centre (MGCC), the frequency can be measured by the Phase-Locked-Loop (PLL) application, and the V_{rms} is given by [46]:

$$V_{rms} = \sqrt{V_d^2 + V_q^2} \tag{4.6}$$

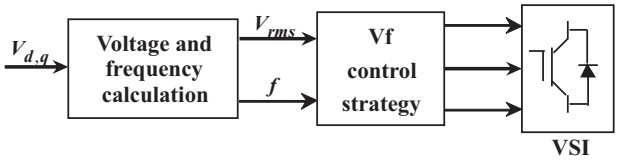

Figure 4.2: VSI based Vf power controller

4.3 The Proposed Control Strategy

This section presents the proposed power controller for a three-phase grid-connected VSI system. As shown in Figure 4.3, the controller scheme consists of three main blocks, namely: power controller, linear current controller, and PSO algorithm for real-time self-

tuning of the power control parameters. The following subsections describe the functionality of each block in more detail.

4.3.1 Power Control Strategy

The purpose of using this strategy is to improve the quality of power supply in terms of the control objective mode. As shown in Figure 4.3, the left side depicts the block diagram of the proposed power controller based on two PI regulators. This controller represents the outer control loop which is employed to generate the reference current vectors i_d^* and i_q^*. Consequently a relatively slow change of the reference current trajectory would ensure high quality of the inverter output power, indicating that the control objective has been achieved. In this work, the Vf control strategy based on the PSO algorithm is proposed for the VSI based DG unit; the system voltage and frequency are the main control objectives which must be achieved during the islanding operation mode. This strategy is designed to respond to sudden changes such as starting the islanding operation mode, or at load change condition. In this case, the controller regulates the voltage and frequency based on their reference values (V_{ref} and f_{ref}), and the PSO is an intelligent process which provides optimum control parameters in order to release qualified reference current vectors. Accordingly, in a *dq* reference frame and based on two PI regulators, the reference current vectors can be expressed as:

$$i_d^* = (V_{ref} - V)(K_{pv} + K_{iv}/s) \tag{4.7}$$

$$i_q^* = (f_{ref} - f)(K_{pf} + K_{if}/s) \tag{4.8}$$

4.3.2 Current Control Strategy

The objective of this controller is to ensure accurate tracking and short transients of the inverter output current. As shown in Figure 4.3, the right side depicts the block diagram of the current control loop the design of which is based on a synchronous reference frame. The linear current controller based on SVPWM and open loop voltage type is utilised with the inner current feedback loop. This controller is usually used in a way that the voltage is applied to the inductive $R - L$ impedance, so that an impulse current in the inductor has a minimum error. The PLL block is required to detect the voltage phase angle in order to implement Park's transformation in the control scheme. Two PI regulators are used to

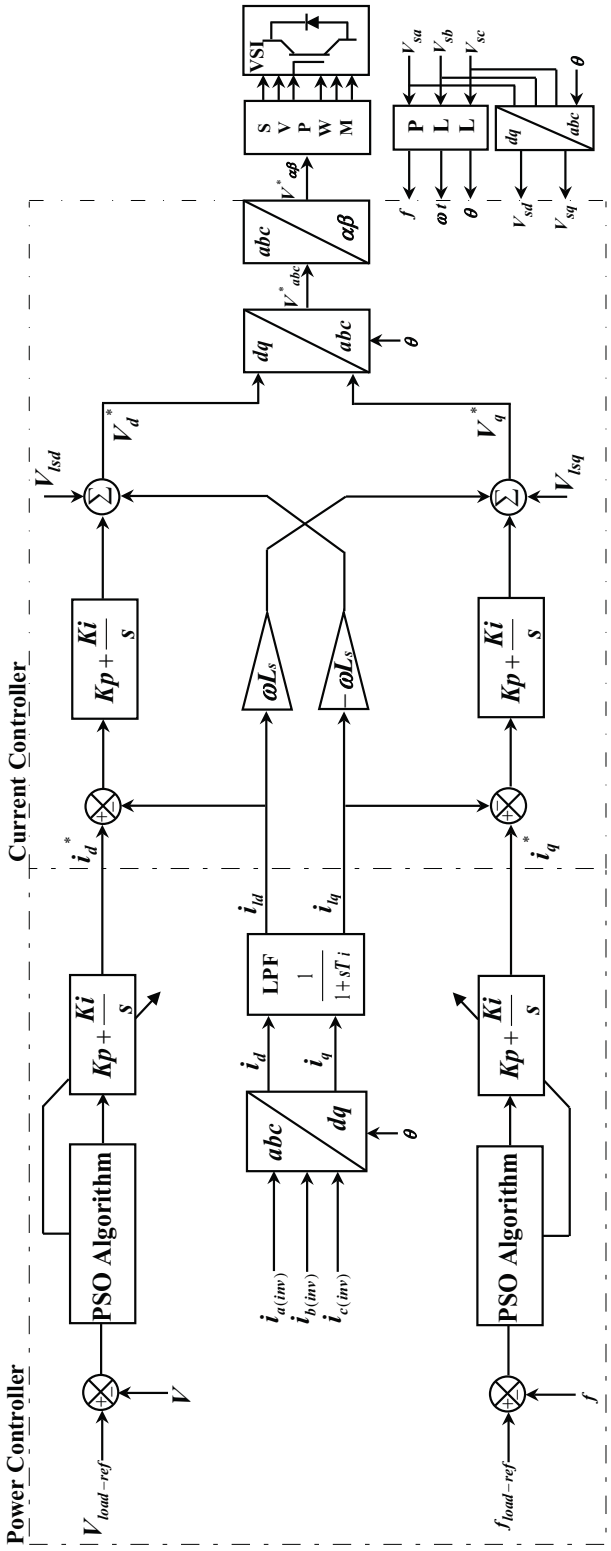

Figure 4.3: The proposed power controller scheme

eliminate current error, and both the inverter current loop and the grid voltage feed-forward loop are employed to improve the steady state and dynamic performance. Consequently, the output signals of the controller represent the reference voltage signals in the dq frame. It is followed by the inverse Park's transformation and Clarke's transformation (see Appendix A), so that the controller generates the reference voltage signals in $\alpha\beta$ stationary frame, synthesising six pulses for the SVPWM in order to fire the Insulated-gate Bipolar Transistor (IGBT) inverter. Moreover, use of the SVPWM technique ensures that the controller provides the desired output voltage vectors with less harmonic distortion. Appendix B presents more information about the SVPWM technique.

In the synchronous dq frame, based on Equation (4.2), the reference voltage signals can be expressed as:

$$\begin{bmatrix} V_d^* \\ V_q^* \end{bmatrix} = \begin{bmatrix} -K_p & -\omega L_s \\ \omega L_s & -K_p \end{bmatrix} \begin{bmatrix} i_d \\ i_q \end{bmatrix} + \begin{bmatrix} K_p & 0 \\ 0 & K_p \end{bmatrix} \begin{bmatrix} i_d^* \\ i_q^* \end{bmatrix} + \begin{bmatrix} K_i & 0 \\ 0 & K_i \end{bmatrix} \begin{bmatrix} X_d \\ X_q \end{bmatrix} + \begin{bmatrix} V_{sd} \\ V_{sq} \end{bmatrix} \tag{4.9}$$

where the superscript "$*$" denotes the reference values, $\frac{dX_d}{dt} = i_d^* - i_d$, and $\frac{dX_q}{dt} = i_q^* - i_q$.

Using Clarke's transformation, Equation (4.9) can be transformed into $\alpha\beta$ stationary frame, as shown in the following equation:

$$\begin{bmatrix} V_\alpha \\ V_\beta \\ V_0 \end{bmatrix} = \frac{2}{3} \begin{bmatrix} V_a \\ V_b \\ V_c \end{bmatrix} \begin{bmatrix} 1 & \frac{-1}{2} & \frac{-1}{2} \\ 0 & \frac{\sqrt{3}}{2} & \frac{-\sqrt{3}}{2} \\ \frac{1}{2} & \frac{1}{2} & \frac{1}{2} \end{bmatrix} \tag{4.10}$$

Furthermore, the inductor current is obtained using a Low Pass Filter (LPF) [46]. In this work, the LPF is presented as a first-order transfer function which is given by:

$$f \frac{1}{1 + sT_i} = f_l \tag{4.11}$$

where f is the filter input value, f_l is the filtered value, and T_i is the time constant.

4.4 Simulation Results

The model of a three-phase grid-connected VSI system and the proposed controller are simulated using MATLAB/Simulink environment, and are depicted in Figure 4.1. The PSO algorithm is implemented through a MATLAB/M-file program, and the model parameters

are defined as follows: $L_s = 5$ mH, R_s=1.4 Ω, f=50 Hz, filter capacitance C=50 μF, and the input capacitor of the dc side is set to 5000 μF. One DG unit with rating 50 kW is used. Typically, the current control parameters are set to K_p=12.656 and K_i=0.00215. For the SVPWM-based current controller, switching and sampling frequency are fixed at 10 kHz and 500 kHz, respectively. All results are in a per-unit (p.u.) system, and the following objectives are investigated:

4.4.1 PSO Algorithm Results

As described in Chapter 3, the PSO algorithm is proposed in order to find optimum Vf power control parameters based on the minimum value of the error-integrating function. In this chapter, PSO algorithm and its objective function are individually constructed for each control objective for one DG unit, which allows dealing with more than one DG unit under the supervision by the MGCC. The voltage and frequency are two control objectives which are considered in this work. The set-point values for voltage (V_{ref}) and frequency (f_{ref}), which can be noticed in Equations (4.7) and (4.8), respectively are assumed to be set by the MGCC, so the function of the applied optimisation technique is to find the optimal power control parameters based on minimum error between the set-points and their measured values. In this work, Table 4.1 shows the parameters of the applied PSO algorithm which sets to optimise 50 particles for each cycle of 50 iterations. More explanation about the selections of these parameters can be found in Chapter 3, Sections 3.2, 3.3 and 3.4. The search spaces of the parameters of the voltage control loop K_{pv} and K_{iv} are limited to [0 -20] and [0 $5e^{-3}$], respectively. Similarly, the search boundaries of the parameters of the frequency control loop K_{pf} and K_{if} are set to [0 30] and [0 $5e^{-3}$], respectively. The simulation results shown in Figures 4.4 and 4.5 depict the differences between the set-value and the computed area of the controlled signals over the limited time; which are calculated using Simpson's 1/3 rule. It can be seen that the error decreases rapidly with the number of iterations, and the solution is steady towards the end.

Table 4.1: The Applied PSO Parameters

PSO Parameters Description	K_{pf}	K_{if}	K_{pv}	K_{iv}
Acceptable violation (p.u.)	±0.01	±0.01	±0.1	±0.1
Initial velocity (V)	0	0	0	0
Initial fitness value (best so far)	800	800	800	800
Inertia constant (w)	0.05	0.5	0.05	0.5
Cognitive coefficients (c_1&c_2)	0.09	0.1	0.09	0.1

To explain the movement behaviour of the swarm, Figures 4.6 to 4.9 and 4.10 to 4.13 depict the simulation results of the search process of the candidate particles for both cases: starting in islanding mode and load change condition, respectively. These particles select their trajectories based on their best fitness values. The results show that the particles finish their movements at the best positions, and the power control parameters stay at the optimum global values which are indicated in Table 4.2.

Table 4.2: Power Controller Parameters

Control Parameters	Islanding Operation Mode	Load Change Condition
K_{pf}	3.010859051739	2.561841587350
K_{if}	3.779371678977e-04	3.778269709488e-04
K_{pv}	-0.993692883859	-1.012858708331
K_{iv}	0.003377691047	0.0031963506784

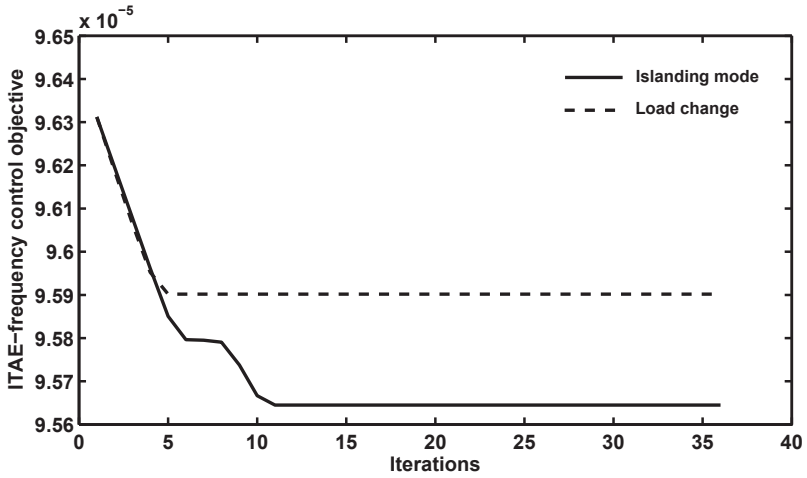

Figure 4.4: Fitness values of the frequency control objective

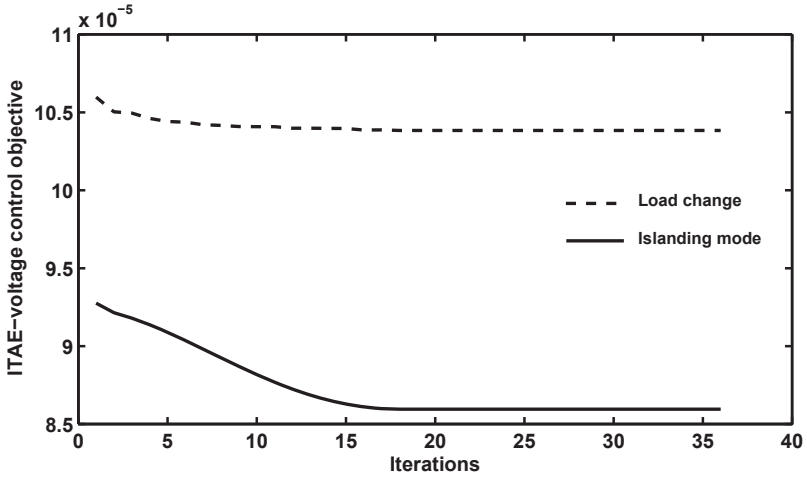

Figure 4.5: Fitness values of the voltage control objective

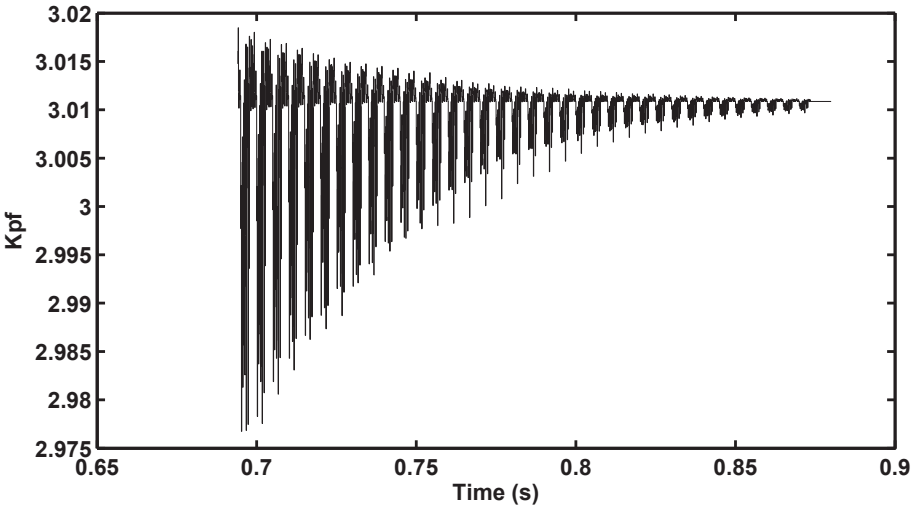

Figure 4.6: Search process of K_{pf} when the microgrid is islanded

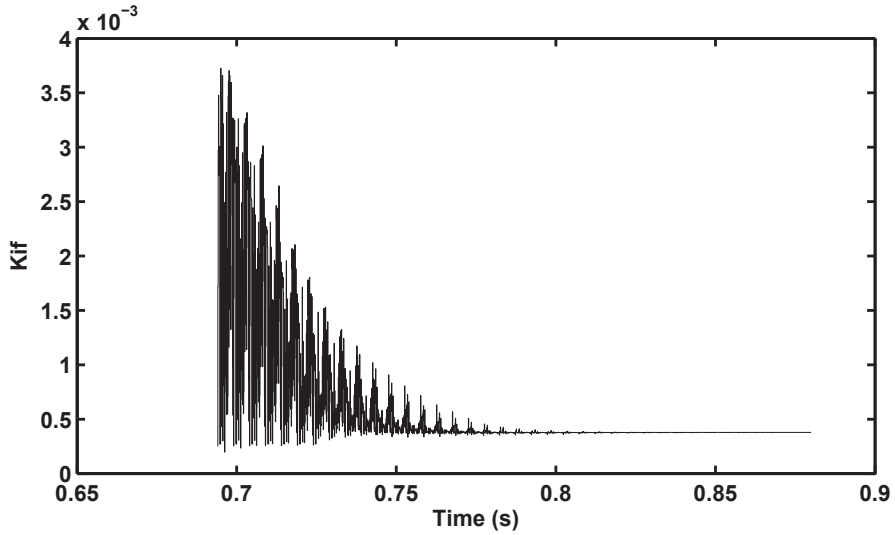

Figure 4.7: Search process of K_{if} when the microgrid is islanded

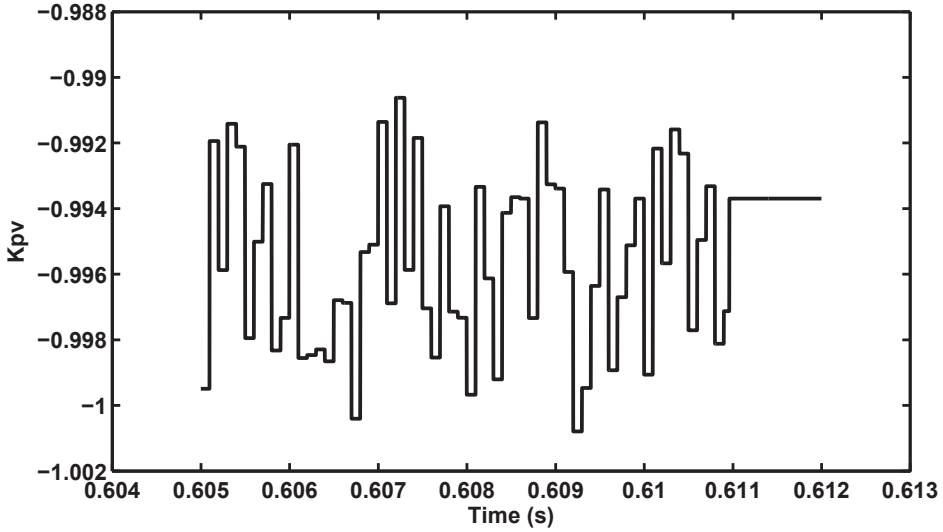

Figure 4.8: Search process of K_{pv} when the microgrid is islanded

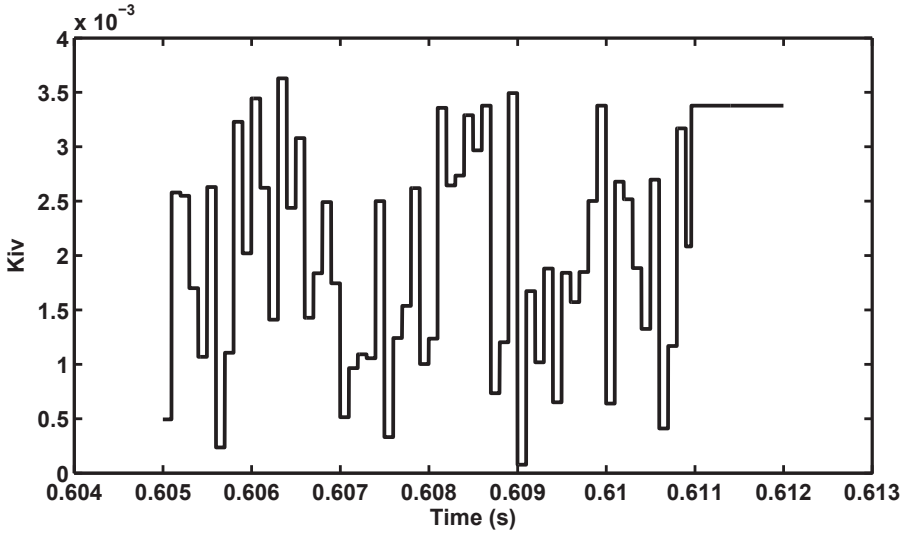

Figure 4.9: Search process of K_{iv} when the microgrid is islanded

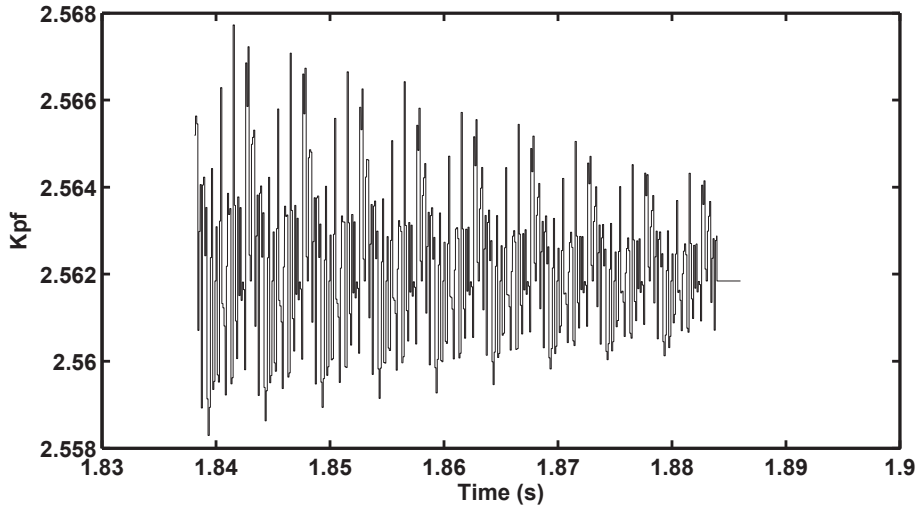

Figure 4.10: Search process of K_{pf} at the load change condition

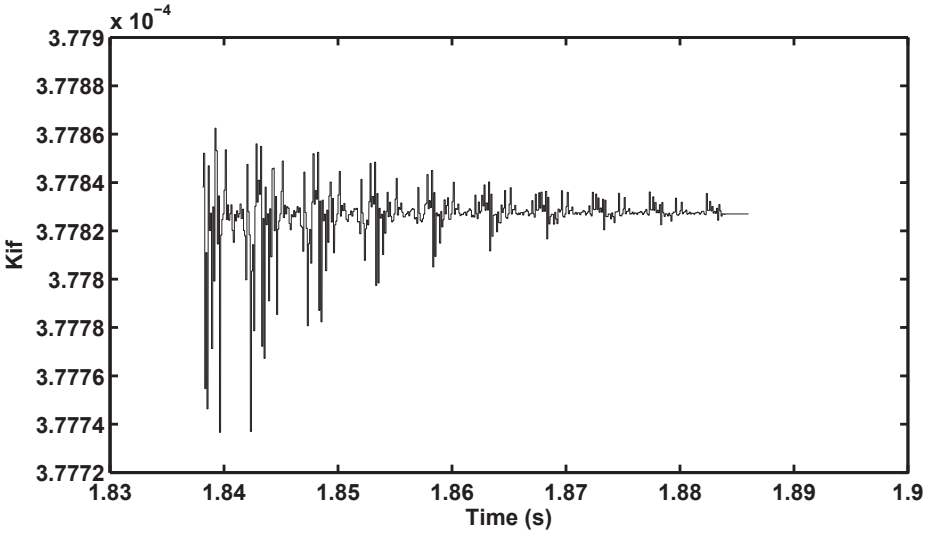

Figure 4.11: Search process of K_{if} at the load change condition

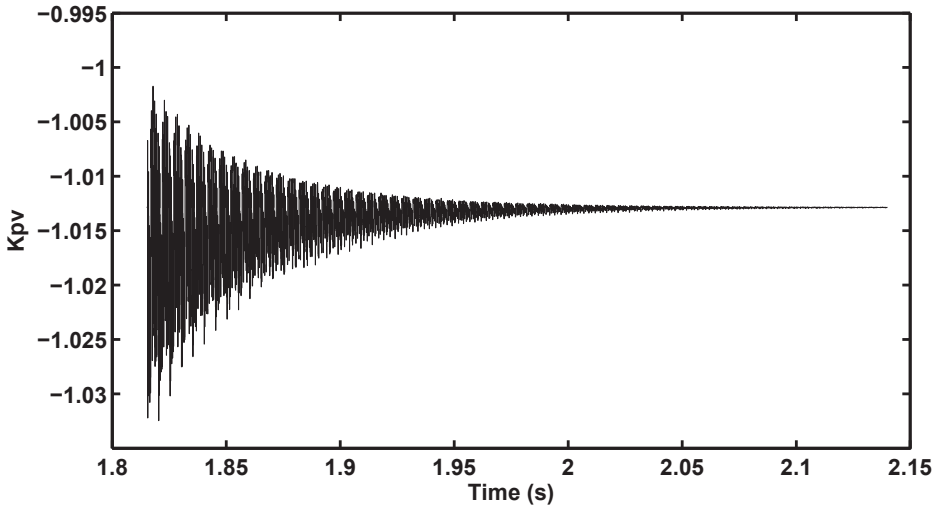

Figure 4.12: Search process of K_{pv} at the load change condition

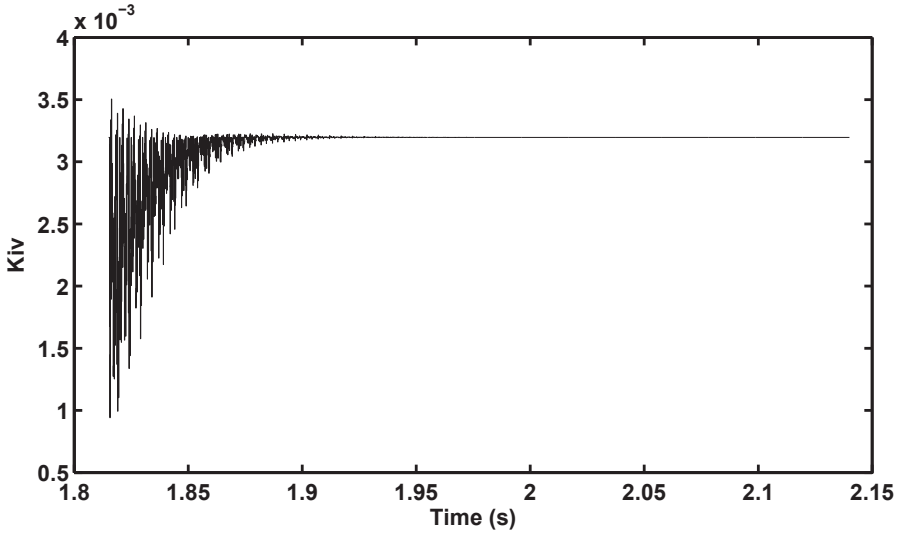

Figure 4.13: Search process of K_{iv} at the load change condition

4.4.2 Voltage and Frequency Regulation

To evaluate the proposed controller scheme, the simulation starts in the grid-connected mode, so the microgrid voltage and frequency are mainly established by the grid which is responsible to maintain their profiles.

At 0.6 s, the microgrid switches to the islanding operation mode. As shown in Figure 4.14, the load power is considered to be active power for simplicity and set to 4.65 (p.u.). The DG unit adopts the Vf power control mode based on PSO algorithm in order to mitigate the voltage drop and avoid a severe deviation of the frequency caused by a sudden move to the islanding mode or load change. In this mode, and as presented in Equations (4.7) and (4.8), the V_{ref} and f_{ref} of the proposed controller are set to 1 (p.u.). As a result, since the PSO algorithm and its results are discussed in Subsection 4.4.1, Figures 4.15 and 4.16 depict the results of the controlled voltage and frequency. These figures are resulted from the reaction between the proposed power controller and the applied PSO technique. For example, at 0.6 s, the system is islanded and Figure 4.16 shown that the frequency is going to fall around 0.7 s. At this time, the PSO algorithm started searching on new power control parameters (see Figures 4.6 and 4.7), because the frequency is decreased and reached the threshold limit ($\pm$0.01 p.u.). This process occurs even through the transient period. Thus, the frequency restored to be within the acceptable limits, and Figure 4.16 is a consequence of an automatic response of the proposed power controller. Consequently, the proposed controller reacts to starting the islanding mode and provides voltage and frequency equal to 0.96 p.u. and 0.9914 p.u., respectively.

At 1.8 s, the active load power is decreased to 4.55 p.u., so the PSO algorithm searches again to find the optimal parameters of the Vf power controller based on minimum error of the fitness function. As shown in Figures 4.15 and 4.16, the proposed controller still offers an excellent behaviour and maintains the system voltage and frequency equal to 1.067 p.u. and 1.0018 p.u., respectively.

Consequently, according to the acceptable limits which are outlined in Table 4.1, it can be noticed that the proposed strategy restores the microgrid voltage and frequency close to their reference values within $\pm$0.1 and $\pm$0.01 (0.5 Hz), respectively.

4.4.3 Dynamic and Steady State Response

In order to verify the dynamic response of the proposed controller, the inverter output current is stepped two times. First, when the microgrid is islanded at 0.6 s, then once the load is changed at 1.8 s. Figures 4.17 and 4.18 show the simulation results of the inverter

output line current. For both cases, it can be seen that the transient time is short and the current reaches steady state within two cycles.

For the steady-state response, Figures 4.19 and 4.20 depict the microgrid phase voltage and the inverter output line current of the islanding operation mode and load change condition, respectively. In this work, since the inverter output filter is utilised to bypass switching harmonics, and a LPF with low enough cut-off frequency to ensure sufficient attenuation for the harmonic content of the *dq* current vectors is used, the results show that the waveforms are high-quality sinusoids with a unity power factor. Also, Figures 4.21 and 4.22 show the spectrum of the line current when the microgrid is islanded and during the load change, respectively. The THD values are 1.79% and 0.44% which are well below the 5% THD allowed in IEEE Std 1547-2003 [28].

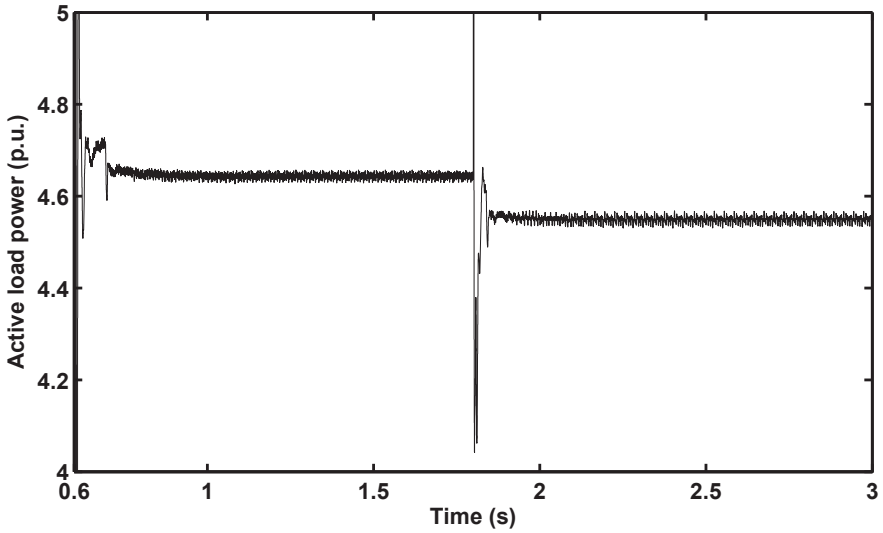

Figure 4.14: The active load power

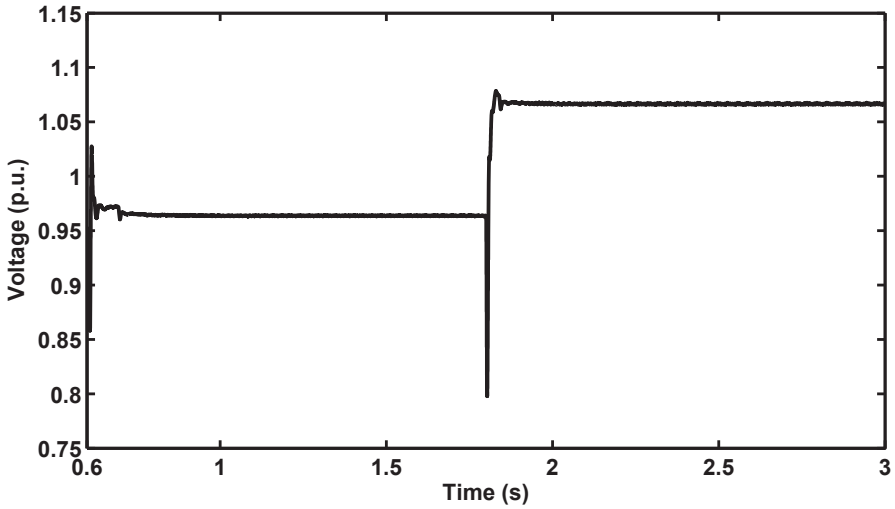

Figure 4.15: The microgrid voltage regulated by Vf controller

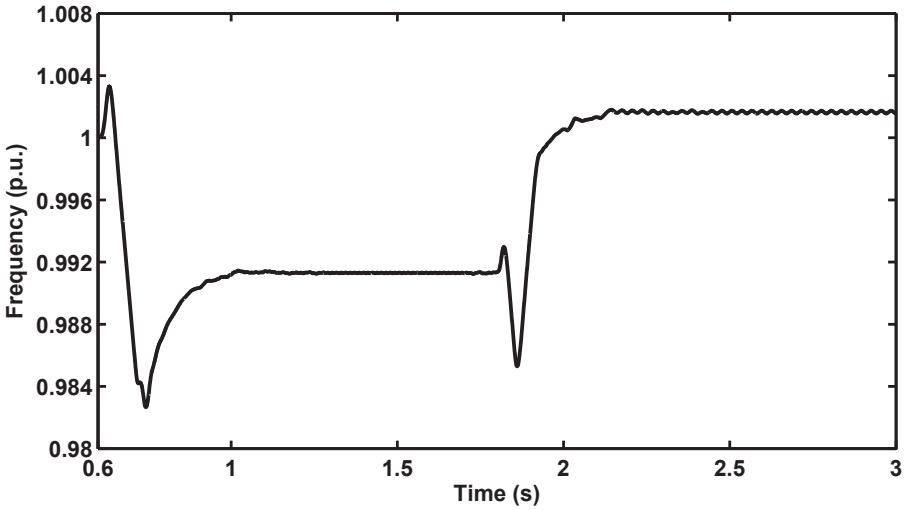

Figure 4.16: The microgrid frequency regulated by Vf controller

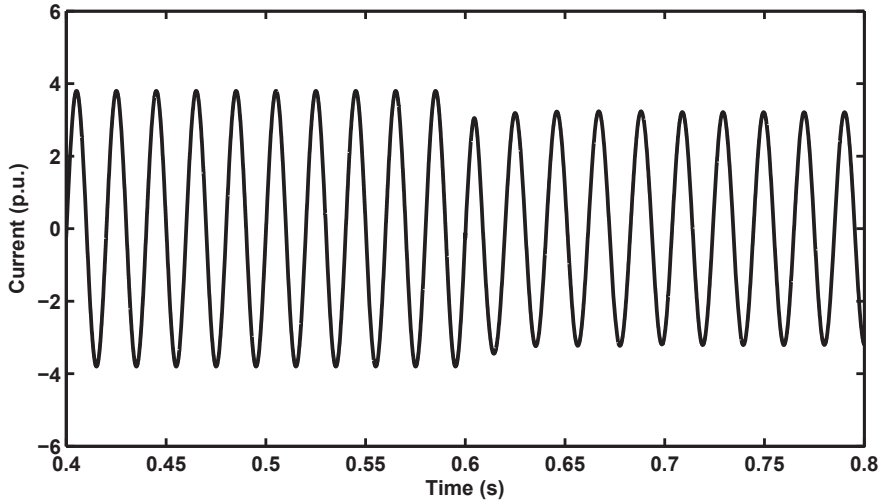

Figure 4.17: The dynamic response when the microgrid is islanded at 0.6 s.

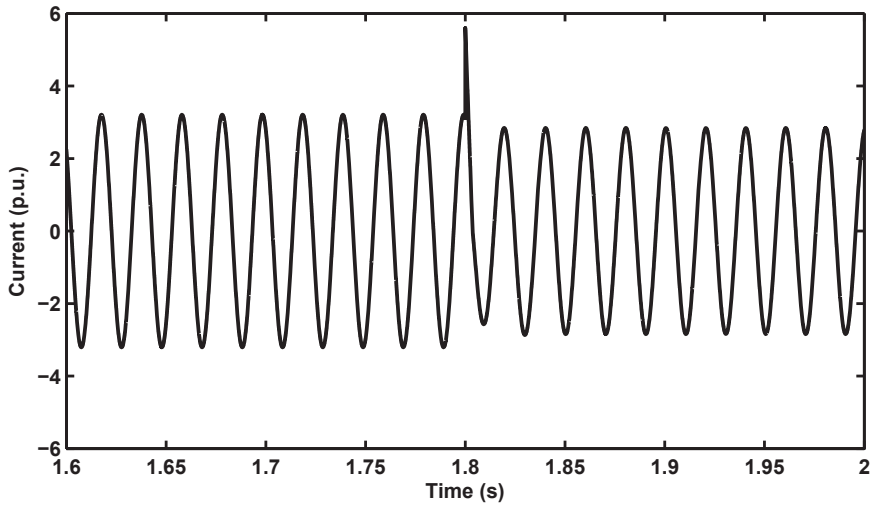

Figure 4.18: The dynamic response when the load is changed at 1.8 s.

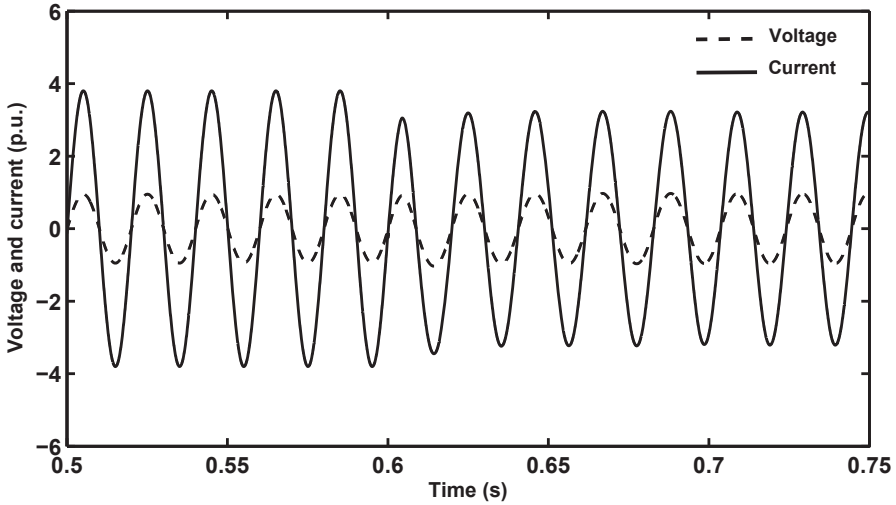

Figure 4.19: Transient and steady-state responses in islanding mode

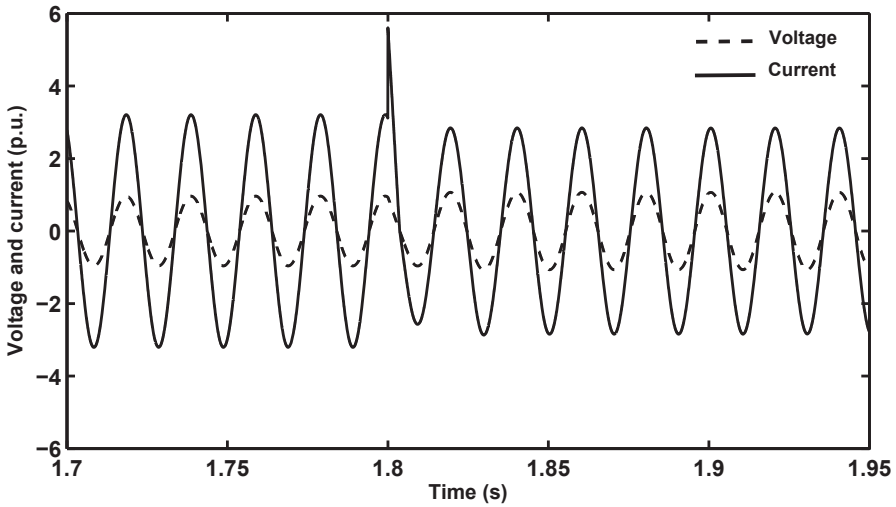

Figure 4.20: Transient and steady-state responses during load change

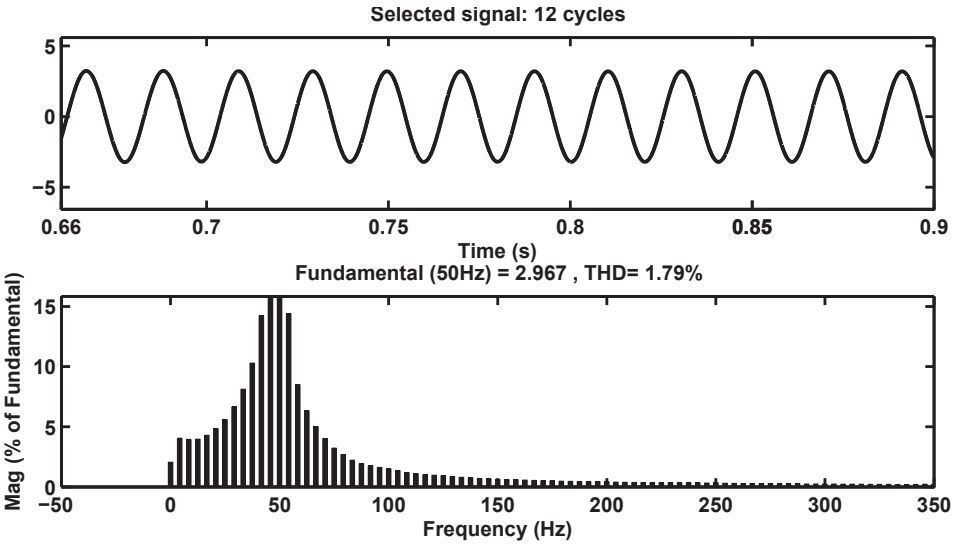

Figure 4.21: Spectrum of the VSI line current of the islanding operation mode

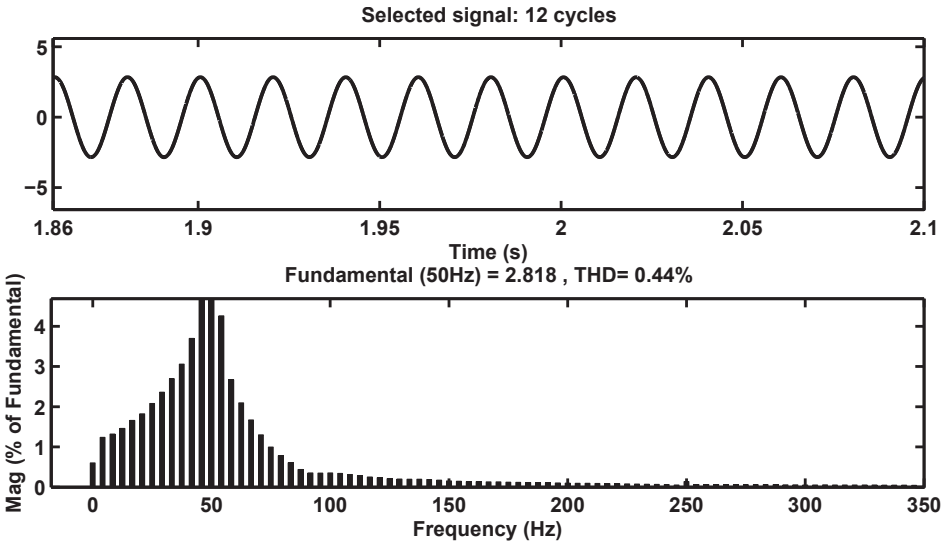

Figure 4.22: Spectrum of the VSI line current during the load change

4.5 Conclusions

In this chapter, an optimal power control strategy has been proposed for an inverter based DG unit in order to improve the quality of the power supply in an autonomous microgrid operation. The proposed controller scheme consists of an inner current control loop and an outer Vf power control loop. The PSO algorithm has been incorporated into the Vf control mode to implement real-time self-tuning method in order to regulate the microgrid voltage and frequency, especially when the microgrid transits to the islanding operation mode or during load change. In addition, the controller is designed to investigate the dynamic response, steady-state response, and driving the harmonic currents through the inverter. The simulation results show that the proposed controller offers an excellent response of regulating the microgrid voltage and frequency, and achieves short transient time with satisfactory harmonics distortion level. Consequently, this controller can be used by more than DG unit in a microgrid scenario, considering the power sharing issue.

Chapter 5

POWER FLOW CONTROL IN GRID-CONNECTED MICROGRID OPERATION UNDER VARIABLE LOAD CONDITIONS

In the grid-connected mode, the system is obviously in steady state voltage and frequency due to the bulk power system. Therefore, with respect to the generation, load and market policies, the main function of this mode is to satisfy the load demand with the aim of reducing the imported power from the grid (Peak Shaving). In this case, the microgrid behaves either as a constant load power that draws power from the grid when the load demand is more than the rated power of the microgrid or as a source of the power supply that injects the excess power to the grid when the required load is less than the rated power of the microgrid. For this reason, the output active and reactive power of the connected DG units should be regulated via a controller regarding to their reference values. This controller should also be able to provide stable operation, fast dynamic response, and low static error. Therefore, it is necessary to propose an appropriate power control mode for the connected DG unit that helps to provide the pre-defined active and reactive power.

In this chapter, an optimal power flow controller is proposed for a utility connected microgrid based on a real-time self-tuning method. The purpose of this work is to control the flow of the active and reactive power between the main grid and the microgrid composed of DG units. Sharing power at the desired ratio by the DG units is the main performance parameter which is considered during the load change. This chapter also shows the response of the controller in situations where the load is either higher or greatly lower than the rated power of the DG unit. In this work, the controller scheme is composed of an inner current control loop and an outer power control loop based on a synchronous reference frame and the conventional PI regulators. The power controller is designed for active-reactive power

(PQ) control strategy. Particle Swarm Optimisation is an intelligent searching algorithm that is applied for real-time self-tuning of the power control parameters. In this work, the proposed strategy is that the required load power is shared equally between the microgrid and the utility based on the PSO algorithm during the load change. The utility supplies the difference power when the load is more than the power generated by the microgrid, while it injects the extra power to the grid when the load is less than the power generated by the microgrid. The results show that the proposed controller offers an excellent response and proves the validity of the proposed strategy.

The remaining part of this chapter is divided into five main sections. Section 5.1 presents a mathematical foundation of a three-phase grid-connected VSI model. In Section 5.2, the VSI control strategy is demonstrated for the grid-connected operation mode. Section 5.3 describes the proposed control strategy in detail. In Section 5.4, the simulation results are analysed to verify the aims of this work. Finally, the conclusions are outlined in Section 5.5.

5.1 Modelling of Three-Phase Grid-Connected VSI System

A typical model of the three-phase grid-connected VSI with an LC filter is depicted in Figure 5.1, where R_s and L_s represent the equivalent lumped resistance and inductance of the filter, the coupling transformer if applicable, and the grid as detected by the inverter. C is the filter capacitance and V_s is the grid voltage.

In the *abc* reference frame, the state space equations of the system equivalent circuit are given by [128]:

$$\frac{d}{dt}\begin{bmatrix} i_a \\ i_b \\ i_c \end{bmatrix} = \frac{R_s}{L_s}\begin{bmatrix} i_a \\ i_b \\ i_c \end{bmatrix} + \frac{1}{L_s}\left(\begin{bmatrix} V_{sa} \\ V_{sb} \\ V_{sc} \end{bmatrix} - \begin{bmatrix} V_a \\ V_b \\ V_c \end{bmatrix}\right) \tag{5.1}$$

Using Park's transformation, Equation (5.1) can be expressed in the dq reference frame as:

$$\frac{d}{dt}\begin{bmatrix} i_d \\ i_q \end{bmatrix} = \begin{bmatrix} -\frac{R_s}{L_s} & \omega \\ -\omega & -\frac{R_s}{L_s} \end{bmatrix}\begin{bmatrix} i_d \\ i_q \end{bmatrix} + \frac{1}{L_s}\left(\begin{bmatrix} V_{sd} \\ V_{sq} \end{bmatrix} - \begin{bmatrix} V_d \\ V_q \end{bmatrix}\right) \tag{5.2}$$

where ω is the coordinate angular frequency, and the Park's transformation can be defined as:

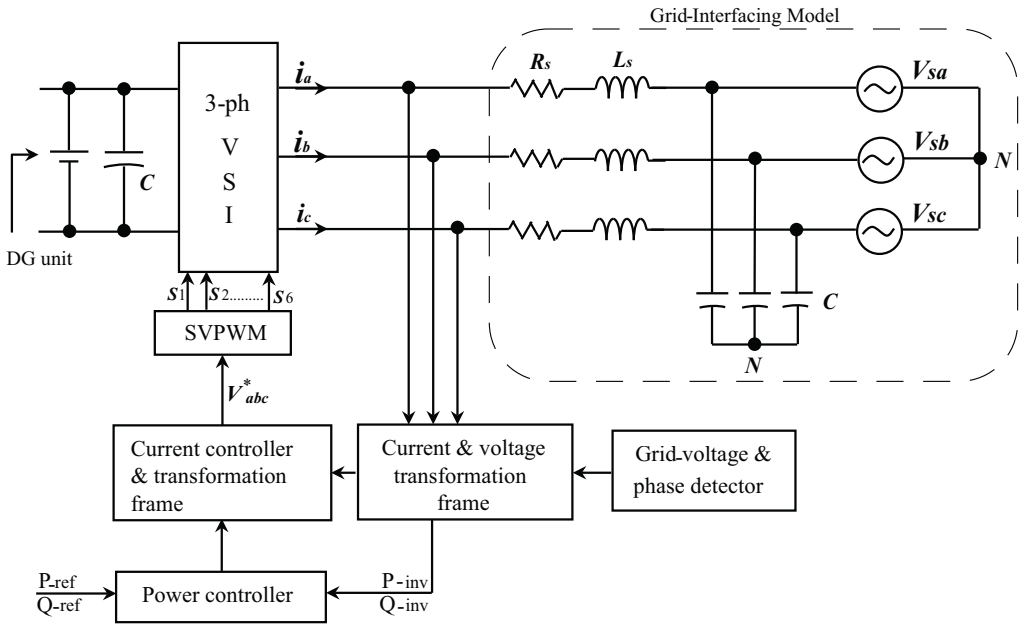

Figure 5.1: 3-phase grid-connected VSI model

$$i_{dq0} = T i_{abc} \tag{5.3}$$

where

$$i_{dq0} = \begin{bmatrix} i_d \\ i_q \\ i_0 \end{bmatrix}, \; i_{abc} = \begin{bmatrix} i_a \\ i_b \\ i_c \end{bmatrix} \tag{5.4}$$

$$T = \frac{2}{3} \begin{bmatrix} cos\theta & cos(\theta - \frac{2\pi}{3}) & cos(\theta + \frac{2\pi}{3}) \\ -sin\theta & -sin(\theta - \frac{2\pi}{3}) & -sin(\theta + \frac{2\pi}{3}) \\ \frac{1}{2} & \frac{1}{2} & \frac{1}{2} \end{bmatrix} \tag{5.5}$$

$\theta = \omega_s t + \theta_o$ is the synchronous rotating angle, θ_o represents the initial value. While the same current control strategy presented in Subsection 4.3.2 is used in this work, the state apace equations of the proposed power control mode and the current controller can be seen in Equations (5.8), (5.9), and (4.9), respectively.

5.2 VSI Control Strategy in Grid-Connected Mode

In grid-connected mode, the microgrid should be flexibly capable to export and import the power with the utility. Thus, an adequate control strategy would help to control the

flow of the generated power from or to the microgrid. As shown in Figure 5.1, the power circuit of the VSI based DG unit is associated with the control structure, so the inverter control strategy is responsible for providing controlled operation of the connected DG unit. For instance, while the microgrid operates either as a controllable load or source of the power supply, in both cases: the connected DG unit operates as a PQ generator and the inverter should follow the PQ control mode for the purpose of regulating the dispatched active and reactive power between the microgrid and the utility. The main goal of this mode is to reduce the abundant load from the utility. Therefore, it is necessary to propose an appropriate power control mode to ensure high performance operation of the connected DG unit. The following subsection presents the most relevant power control strategy which is proposed for the grid-connected operation mode.

5.2.1 PQ Control Mode

As long as the voltage and frequency are in a stable condition, the PQ control mode is an application that can be used either to import less power from the utility (Peak Shaving) in grid-connected mode, or to generate stable active and reactive power in standalone mode. The PQ mode is usually applied for DG units which supply constant power, so a photovoltaic cell is an example of using this application [131]. In this case the amplitude and phase angle of the inverter current are controlled in order to inject the pre-set active and reactive power values, which can be defined locally or by the Microgrid Control Centre (MGCC). Figure 5.2 shows the block diagram of the PQ control strategy. The measured values of the active and reactive power can be expressed [65]:

$$P_{inv} = \frac{3}{2}(V_{(d)inv}.i_{(d)inv} + V_{(q)inv}.i_{(q)inv}) \tag{5.6}$$

$$Q_{inv} = \frac{3}{2}(V_{(q)inv}.i_{(d)inv} - V_{(d)inv}.i_{(q)inv}) \tag{5.7}$$

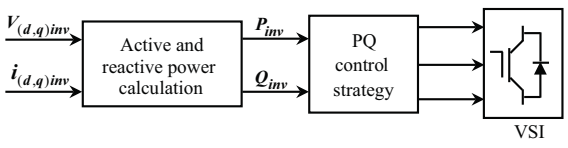

Figure 5.2: VSI based PQ controller

5.3 The Proposed Control Strategy

This section presents the proposed power controller for a three-phase grid-connected VSI system. As shown in Figure 5.3, the controller scheme consists of three main blocks, namely power controller, linear current controller, and PSO algorithm for real-time self-tuning of the power control parameters. While the current controller shown in the right side of Figure 5.3 is described in 4.3.2, and the applied optimisation technique is explained in Chapter 3, the following subsection explains the functionality of the proposed power control mode in detail.

5.3.1 Power Control Strategy

The purpose of using this strategy is to control the power flow between the microgrid and the utility in terms of supplying controlled active and reactive power to the load. As shown in Figure 5.3, the left side depicts the block diagram of the proposed power controller based on two PI regulators. This controller represents the outer control loop which is employed to generate the reference current vectors i_d^* and i_q^*. Consequently, a relatively slow change of the reference current trajectory would ensure high quality of the inverter output power, indicating that the control objective has been achieved. In this work, the PQ control strategy based on the PSO algorithm is proposed for the VSI based DG unit; the active and reactive power being the main control objectives which must be achieved once the DG unit connects to the grid, or at the load change condition. In this mode, while the decoupling between the active and reactive power has been achieved by Equations (5.6) and (5.7), the controller regulates the inverter output active and reactive power based on their reference values (P_{ref}) and (Q_{ref}), and the PSO algorithm is an intelligent process that provides optimum control parameters in order to release qualified reference current vectors. Accordingly, in a dq reference frame and based on PI regulators, the reference current vectors can be expressed as:

$$i_d^* = (P_{ref} - P_{inv})(K_{pp} + K_{ip}/s) \tag{5.8}$$

$$i_q^* = (Q_{ref} - Q_{inv})(K_{pq} + K_{iq}/s) \tag{5.9}$$

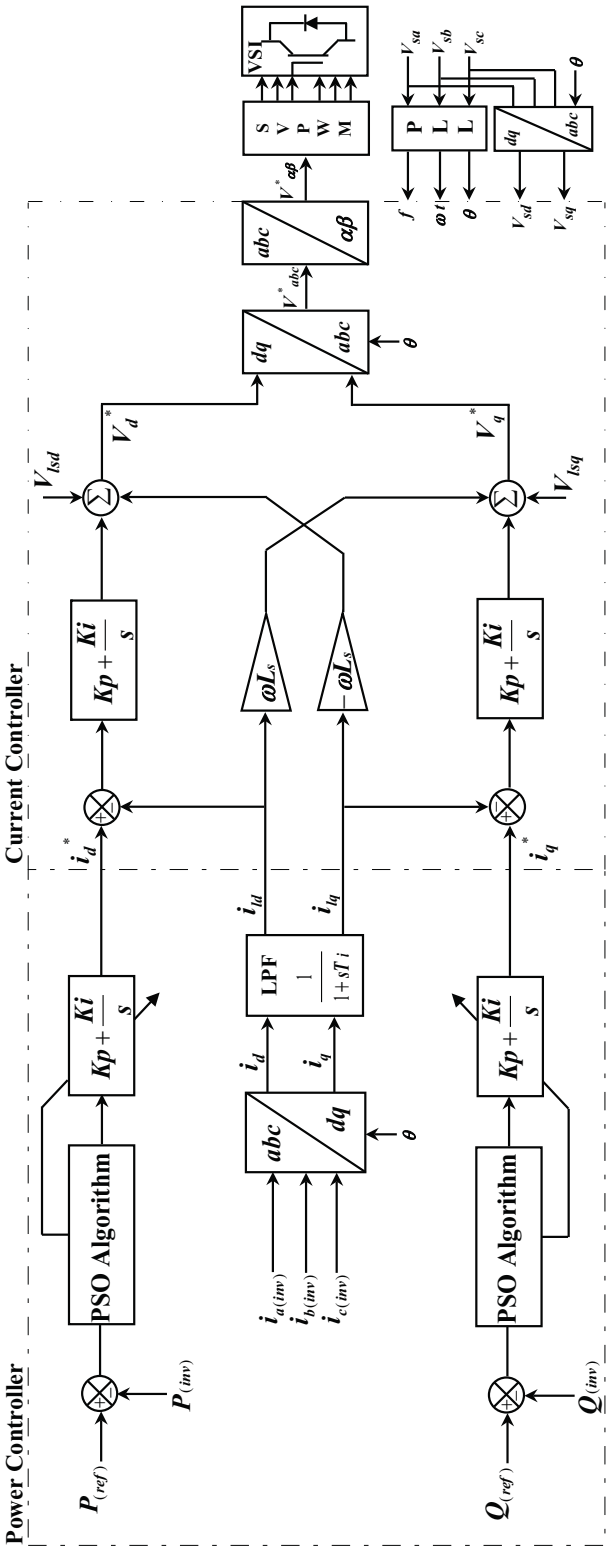

Figure 5.3: The proposed power controller scheme

5.4 Simulation Results

The model of a three-phase grid-connected VSI system and the proposed controller are simulated using MATLAB/Simulink environment, and are depicted in Figure 5.1. The PSO algorithm is implemented through a MATLAB/M-file program, and the model parameters are defined as follows: $L_s = 4$ mH, R_s=1.55 Ω, f=50 Hz, filter capacitance C=50 µF, and the input capacitor of the dc side is 5000 µF. The output power of the DG unit is 50 kW. The current control parameters are typically set to K_p=12.656 and K_i=0.00215. For the SVPWM-based current controller, switching and sampling frequency are fixed at 10 kHz and 500 kHz, respectively. All results are in a p.u. system.

In this model, the proposed controller of the DG unit is designed based on PQ control mode, and the PSO algorithm is incorporated to find the global optimum parameters of this controller. In order to illustrate the power flow control of the DG unit and to verify the performance of the proposed controller, the following subsections describe the simulation results of the applied optimisation technique and the control of the power flow for three cases.

5.4.1 PSO Algorithm Results

As described in Chapter 3, the PSO algorithm is proposed in order to find optimum power control parameters based on the minimum value of the error-integrating function. In this work, this algorithm is separately implemented on each control objective. The active and reactive power are two control objectives which are considered in this chapter. The set-point values for active power (P_{ref}) and reactive power (Q_{ref}), which can be noticed in Equations (5.8) and (5.9), respectively are assumed to be set by the MGCC, so the function of the applied optimisation technique is to find the optimal power control parameters based on minimum error between the set-points and their measured values. In this work, Table 5.1 shows the parameters of the applied PSO algorithm which sets to optimise 50 particles for each cycle of 50 iterations. More explanation about the selections of these parameters can be found in Chapter 3, Sections 3.2, 3.3 and 3.4. The search spaces of the parameters of the active power control loop K_{pp} and K_{ip} are limited to [0 -30] and [0 $5e^{-3}$], respectively. Similarly, the search boundaries of the parameters of the reactive power control loop K_{pq} and K_{iq} are set to [0 30] and [0 $5e^{-3}$], respectively. The simulation results shown in Figures 5.4 and 5.5 depict the differences between the set-value and the computed area of the controlled signals over the limited time; which are calculated using Simpson's 1/3 rule. It can be seen that the error decreases rapidly with the number of iterations, and the

Table 5.1: The Applied PSO Parameters

PSO Parameters Description	K_{pp}	K_{ip}	K_{pq}	K_{iq}
Acceptable violation (p.u.)	±0.1	±0.1	±0.1	±0.1
Initial velocity (V)	0	0	0	0
Initial fitness value (best so far)	800	800	800	800
Inertia constant (w)	0.05	0.5	0.05	0.5
Cognitive coefficients (c_1&c_2)	0.09	0.1	0.09	0.1

solution is steady towards the end.

To explain the movement behaviour of the swarm, Figures 5.6 to 5.9 and 5.10 to 5.13 depict the simulation results of the search process of the candidate particles for both cases: starting in grid-connected mode and load change condition, respectively. These particles select their trajectories based on their best fitness values. The results show that the particles finish their movements at the best positions, and the power control parameters stay at the optimum global values which are indicated in Table 5.2.

Table 5.2: Power Controller Parameters

Control Parameters	Grid-connected Mode	Load Change Condition
K_{pp}	-8.22704243936770	-5.097866092873157
K_{ip}	0.002041621568561	0.002003759695014
K_{pq}	6.219856307217065	5.929097564864147
K_{iq}	0.003440760963308	8.027506198352e-04

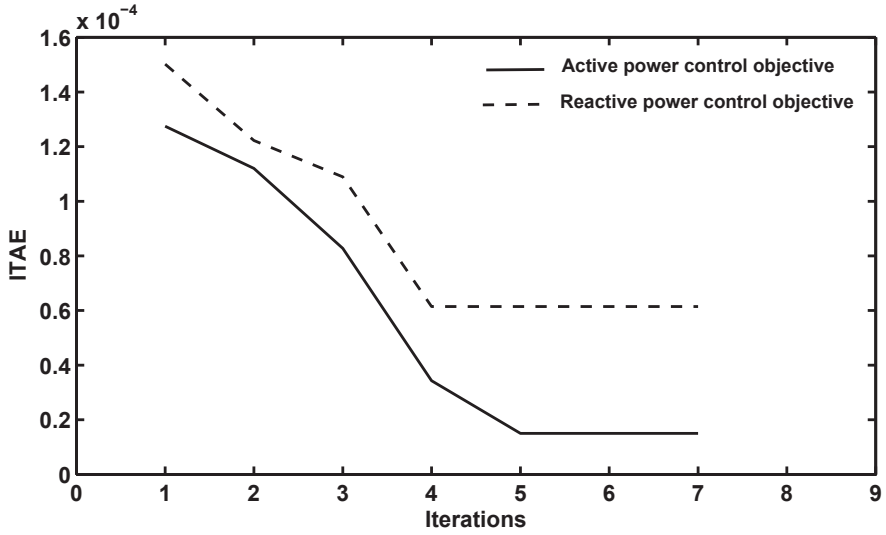

Figure 5.4: Fitness values when the DG unit is connected to the grid

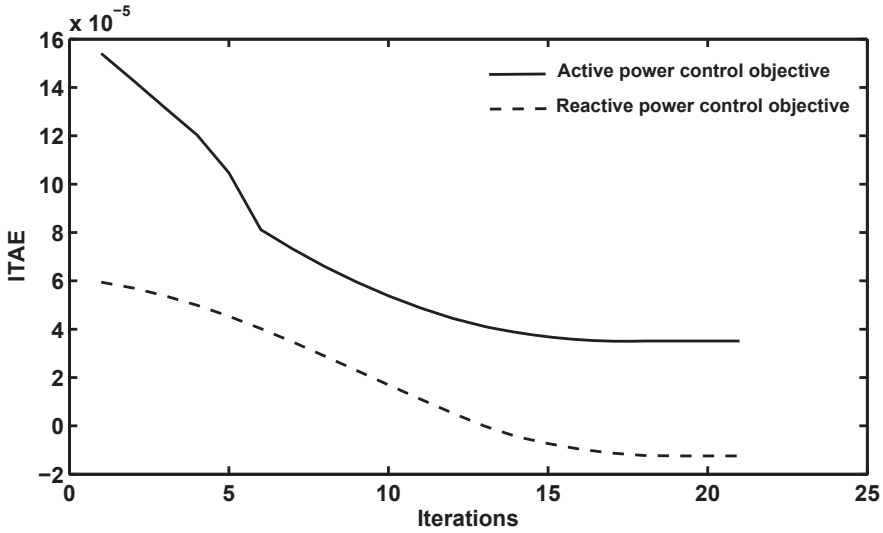

Figure 5.5: Fitness values at the load change condition

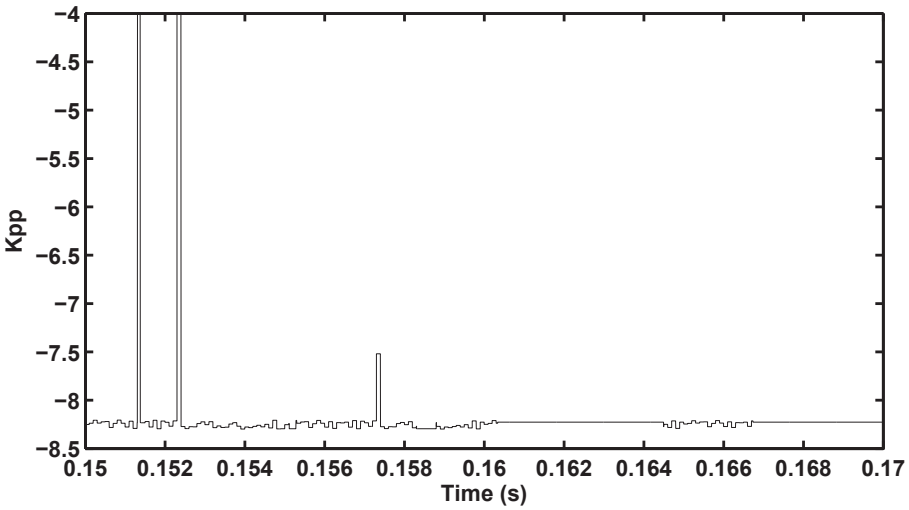

Figure 5.6: Search process of K_{pp} when the DG unit is connected to grid

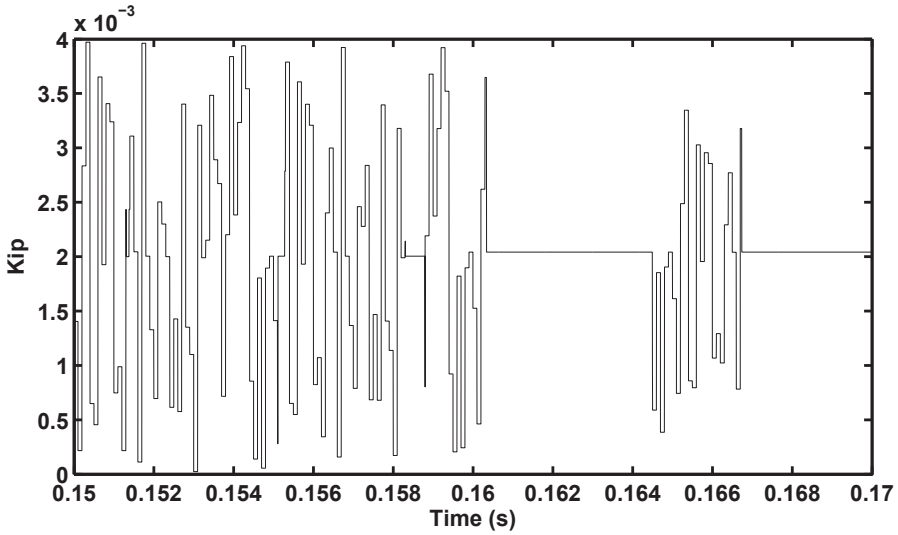

Figure 5.7: Search process of K_{ip} when the DG unit is connected to grid

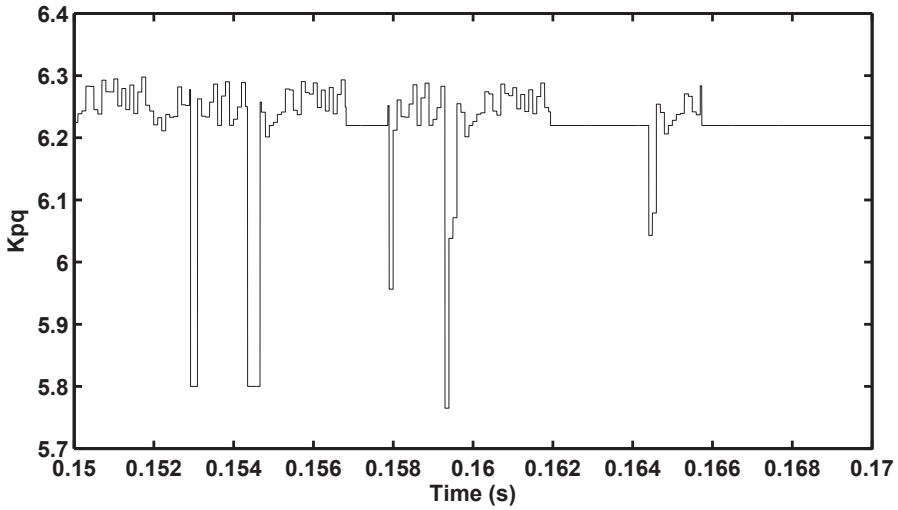

Figure 5.8: Search process of K_{pq} when the DG unit is connected to grid

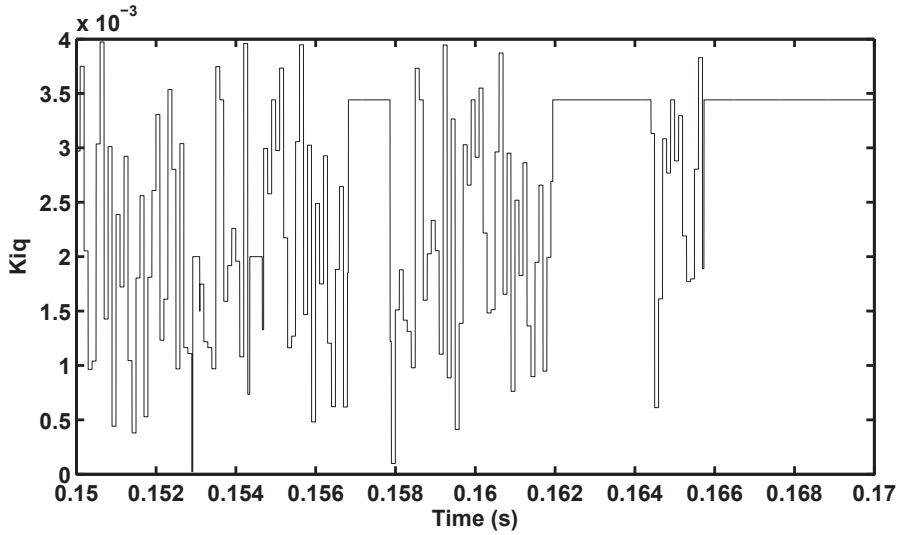

Figure 5.9: Search process of K_{iq} when the DG unit is connected to grid

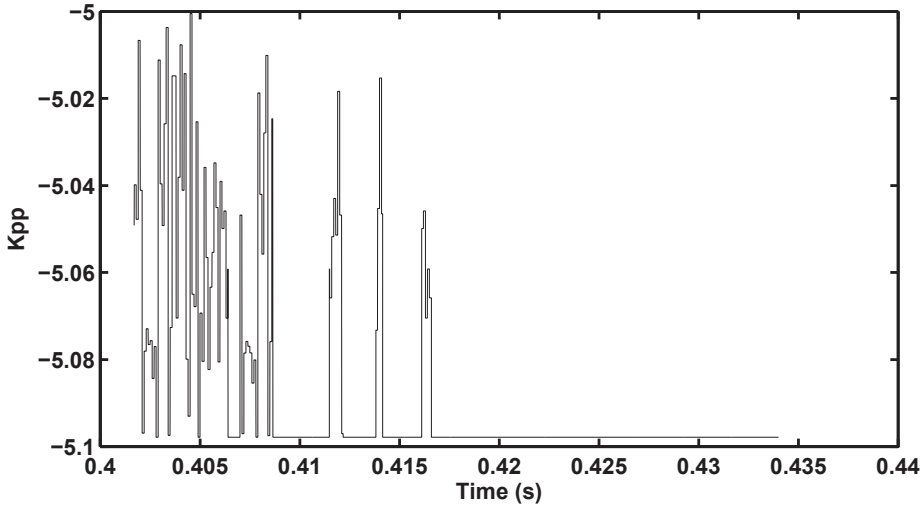

Figure 5.10: Search process of K_{pp} at the load change condition

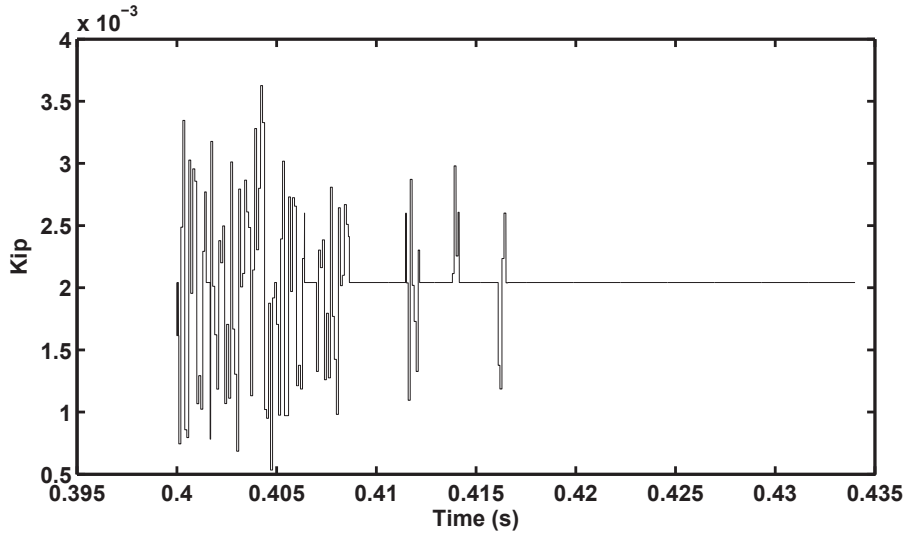

Figure 5.11: Search process of K_{ip} at the load change condition

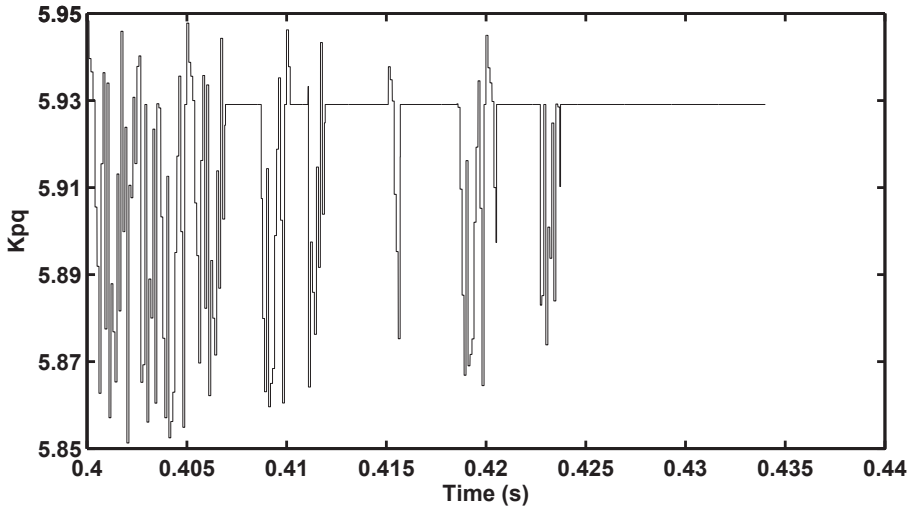

Figure 5.12: Search process of K_{pq} at the load change condition

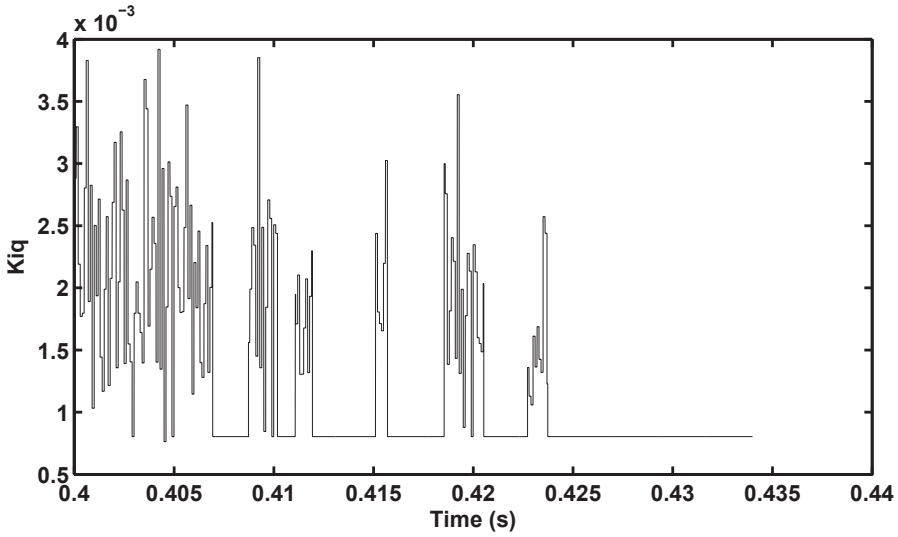

Figure 5.13: Search process of K_{iq} at the load change condition

5.4.2 Case 1: Power Flow of the DG unit with Utility

At 0.15 s, the DG unit connects to the grid and the model starts to operate in grid-connected mode. It is expected that the load would be shared based on the designed control mode of the DG unit. In such a system, it is desired that 50 per cent of the load is supplied by the DG units, while the rest of the load is supplied by the grid. At this stage (see Figure 5.14) the load is set to 2 p.u. active power and 0.56 p.u. capacitive reactive power; thus the set-points of the active and reactive power over the PQ control mode based-DG unit are set to 1 p.u. and -0.28 p.u. respectively. The PSO search process of this stage is depicted in Figures 5.6 to 5.9. The resulting controlled active and reactive power flows in the microgrid system are shown in Figures 5.15 and 5.16. It can be clearly seen that the power flow is controlled perfectly, and the load is halved between the grid and the DG unit.

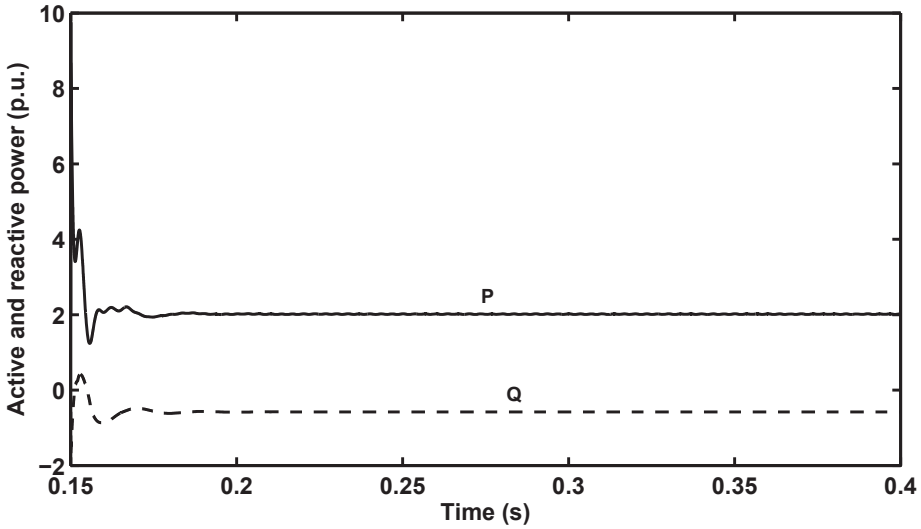

Figure 5.14: The load power once DG unit is connected to the grid

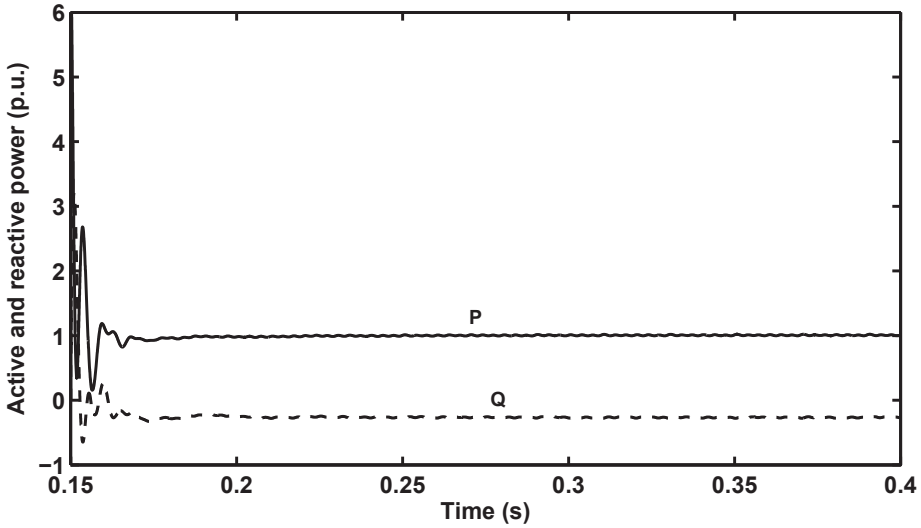

Figure 5.15: The output power of the DG unit

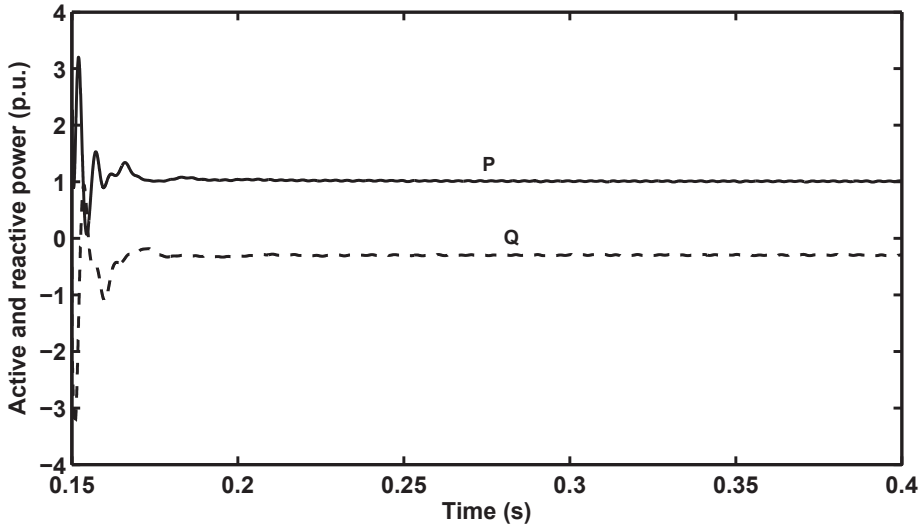

Figure 5.16: The supplied power by the grid

5.4.3 Case 2: Load Change during Grid-Connected Mode

As shown in Figure 5.17, the load is increased to 2.4 p.u. active power and 0.48 p.u. inductive reactive power at 0.4 s. In this case, the set-points of the active and reactive power over the PQ control mode based DG unit are changed to 1.2 p.u. and 0.24 p.u. respectively. Thus, while Figures 5.10 to 5.13 depict the search process of the PSO algorithm to find the optimal parameters of the power controller, Figures 5.18 and 5.19 show the supplied power by the DG unit and the grid, respectively. The load power is still shared equally between the DG unit and grid, so it is clear that an excellent power flow control has been achieved during the load change condition.

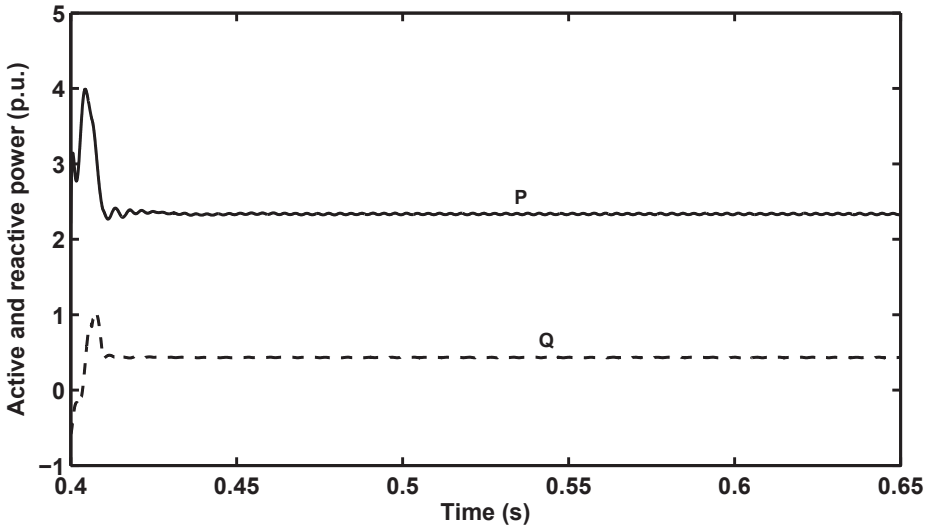

Figure 5.17: The load power at the load change condition

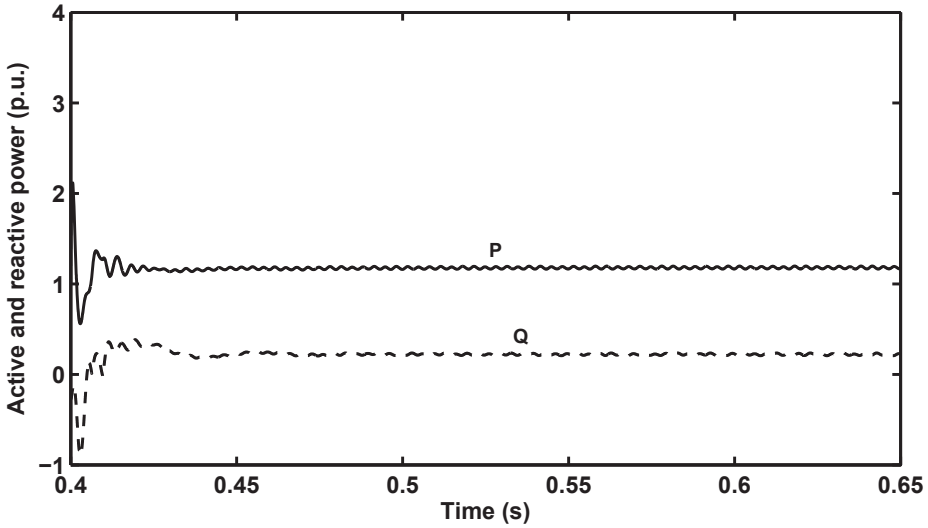

Figure 5.18: The output power of the DG unit

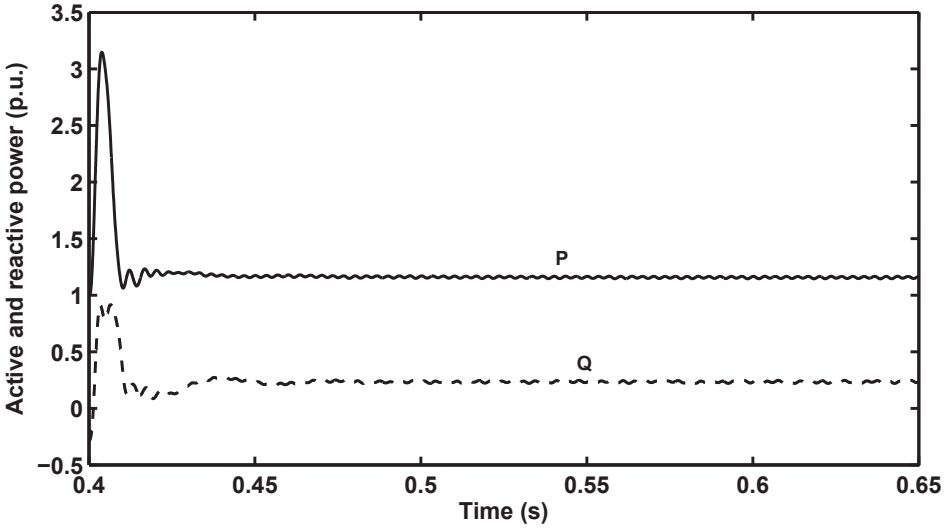

Figure 5.19: The supplied power by the grid

5.4.4 Case 3: Power Exchange between the Microgrid and Utility

In this case the PSO algorithm is disabled, and the control parameters are the same as in the previous case. The aim of this stage is to show the response of the power controller when the power requirement of the load is more or less than the power generation of the microgrid. Also, when the load is not required to be shared equally, or for any practical reason that needs to stop the optimisation technique, the interruption can be done through the MGCC unit either by setting the reference active and reactive power values equal to their measured values or by forwarding the measured values. Thus, the control strategy can be used with or without the optimisation technique.

As shown in Figures 5.20 and 5.21, the load is increased to 2.63 p.u. active power and 0.53 inductive reactive power at 0.65 s. In this case, the balance power is supplied by the grid, while the DG unit still injects a sustained output power. Now, the load is decreased to 0.9 p.u. active power and 0.17 p.u. inductive reactive power at 0.9 s. In this instance, the load is supplied by the DG unit and its excess power is automatically fed to the grid. This demonstrates that the proposed controller offers stable and satisfactory power flow between the microgrid and the utility.

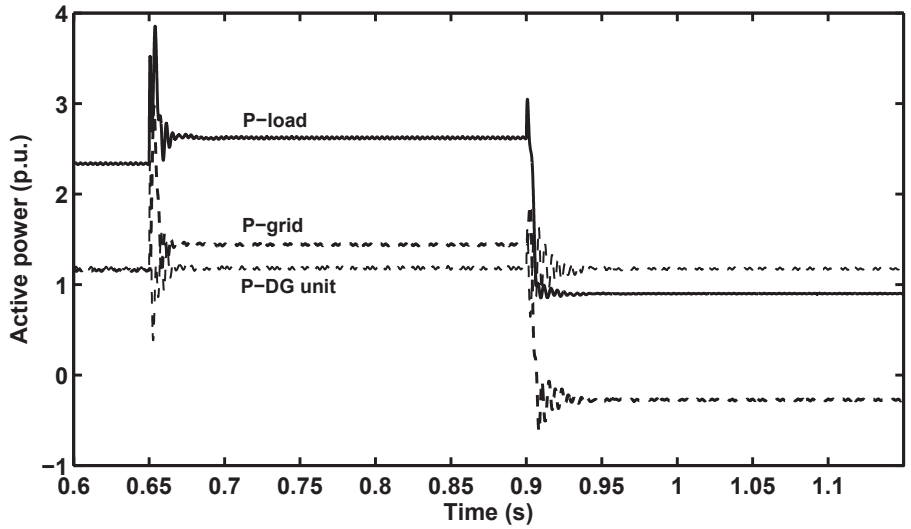

Figure 5.20: Active power flow in the microgrid system

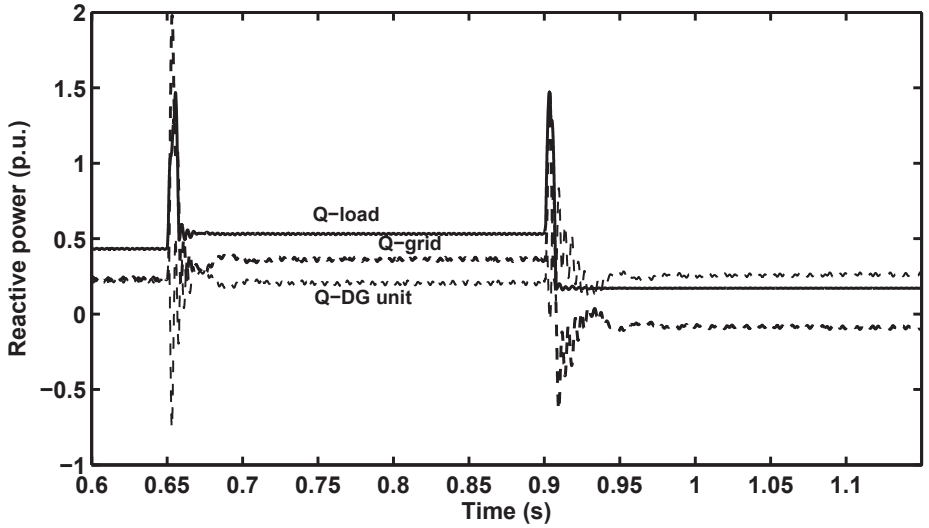

Figure 5.21: Reactive power flow in the microgrid system

5.5 Conclusions

In this chapter, an optimal power flow controller has been proposed for grid-connected microgrid operation mode. That is the controller has been proposed to regulate the injected active and reactive power by which DG unit is connected to the grid. The controller scheme consists of an inner current control loop and an outer PQ power control loop. The PSO algorithm has been incorporated into the PQ control mode to implement a real-time self-tuning method, in order to share the load equally during the load change condition. In addition, the controller is designed to investigate the power flow as to whether the load is higher or significantly lower than the power generation of the DG unit. The simulation results show that the proposed controller based PSO offers an excellent response, halving the load power between the microgrid and the utility during the load change. The simulation results also demonstrate the achievement of a satisfactory power flow when the load power is larger or significantly lower than the rated power of the DG unit.

Chapter 6

POWER QUALITY ENHANCEMENT IN AN AUTONOMOUS MICROGRID OPERATION

In a microgrid, the improvement of the quality of power supply and the proper load sharing between the DG units are the most important issues that need to be investigated in the islanding operation mode. In this mode, whether the isolating from the grid occurs due to the network fault or market decision or during load change condition, the voltage and frequency are being more susceptible for collapse. Also, because each DG unit behaves like a voltage-controlled current source, that is a main reason to inject or absorb large amounts of the active and reactive power among the DG units, thereby inadequate power can be shared between them. In other words, these are the common attributes of the power quality problems which have a huge economic impact for the end user, thus the microgrid must maintain an acceptable quality of the power supply. Therefore, designing an appropriate output control mode for each DG unit can help to address these problems, thus improve the quality of the power supply by the microgrid.

In this chapter, an optimal power control strategy is presented for an autonomous microgrid operation based on a real-time self-tuning method. The purpose of this work is to improve the quality of power supply of the microgrid where some DG units are connected to the grid. Voltage and frequency regulation, and power sharing are the main performance parameters which are considered in this work, particularly during the transition from grid-connected to islanding operation mode and also during load change. In this work, two typical DG units are connected in parallel to configure the microgrid. The controller scheme is composed of an inner current control loop and an outer power control loop based on a synchronous reference frame and the conventional PI regulators. The power controller employs two typical strategies: active-reactive power (PQ) control strategy and voltage-frequency (Vf) control strategy. Particle Swarm Optimisation (PSO) is an intelligent

searching algorithm that is applied for real-time self-tuning of the power control parameters. The proposed strategy in this work is that both DG units adopt the Vf control mode once the microgrid is islanded in order to regulate the microgrid voltage and frequency, whereas during the load change, only the second DG unit invokes the PQ control mode to ensure maximum power exportation. The results show that the proposed controller offers an excellent response to satisfy the power quality requirements and proves the validity of the proposed strategy.

The remaining part of this chapter is divided into three main sections. Section 6.1 presents the description of the system structure. In Section 6.2, the simulation results are analysed to verify the aims of this work. Finally, the conclusions are outlined in Section 6.3.

6.1 System Structure

As described in the last two chapters, two typical models of the three-phase grid-connected VSI system are presented in Sections 4.1 and 5.1. These models are used in two power control modes: voltage-frequency control mode for the islanding operation mode and active-reactive power control mode for the grid-connected operation mode. The system voltage and frequency regulation and the control of the active and reactive power flow were the main aims of using these power control types for the purpose of improving the quality of the power supply.

In this chapter, the microgrid model shown in Figure 6.1 is configured from two typical DG units. The same power controller schemes, Vf and PQ, are used in this model. These controllers are described in detail in Subsections 4.3.1 and 5.3.1. The PSO algorithm is also incorporated in each power control mode which already integrated with a linear current controller (see Subsection 4.3.2) to provide reference voltages signals to the SVPWM-VSI system. The following section presents the simulation results of the microgrid model that is run in a stand-alone mode. The control of the microgrid voltage and frequency, power sharing among the DG units, and achieving stable operation are the main control objectives whether the system begins in islanding mode or during load change.

6.2 Simulation Results

As depicted in Figure 6.1, the models of the three-phase grid-connected VSI systems and the proposed controllers are simulated for the microgrid using MATLAB/Simulink envi-

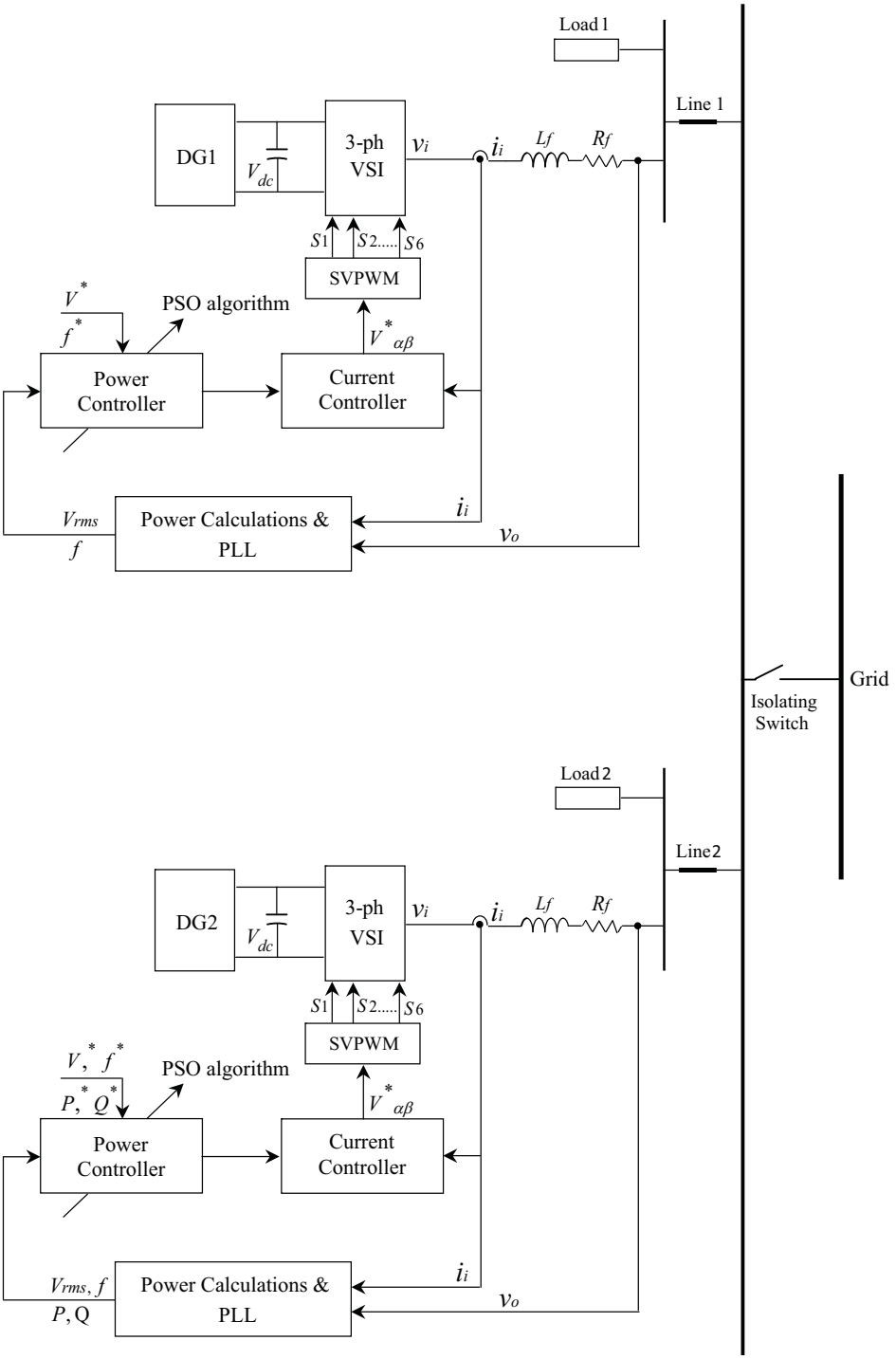

Figure 6.1: The block diagram of the microgrid model

ronment. Also, the PSO algorithm is implemented through a MATLAB/M-file program for each DG unit. The model parameters are defined as follows: L_s = 5 mH, R_s=1.5 Ω, f=50 Hz, and the filter capacitance C=50 µF. Two typical DG units are used, and the output power of each DG unit is 50 kW. The input capacitor of the dc side is set to 5000 µF. Typically, the current control parameters are set to K_p=12.656 and K_i=0.00215. For the SVPWM-based current controller, switching and sampling frequency are fixed at 10 kHz and 500 kHz, respectively. Figures 6.17 to 6.24 show the results of the simulated model. All results are in a p.u. system, and the following objectives are investigated:

6.2.1 PSO Algorithm Results

As described in Chapter 3, the PSO algorithm is proposed in order to find optimum power control parameters based on the minimum value of the error-integrating function. In this work, the PSO algorithm is individually constructed for each DG unit that allows dealing with more than DG units under the supervision by the MGCC. The voltage, frequency, active, and reactive power are four control objectives which are considered in this work. The set-point values of these control objective (V_{ref}, f_{ref}, P_{ref}, and Q_{ref}) which can be noticed in Equations (4.7), (4.8), (5.8) and (5.9), respectively are assumed to be set by the MGCC. Thus, based on minimum error between the set-points and their measured values, the PSO technique runs to find the optimal power control parameters. In this work, Table 6.1 shows the parameters of the applied PSO algorithm which sets to optimise 50 particles for each cycle of 50 iterations. More explanation about the selections of these parameters can be found in Chapter 3, Sections 3.2, 3.3 and 3.4. The search spaces of the parameters of the voltage-frequency control loop K_{pv}, K_{iv}, K_{pf}, and K_{if} are set to [0 -30], [0 $5e^{-3}$], [0 30], and [0 $5e^{-3}$], respectively. Similarly, the search boundaries of the parameters of the active-reactive power control loop K_{pp}, K_{ip}, K_{pq}, and K_{iq} are limited to [0 -30], [0 $5e^{-3}$], [0 30], and [0 $5e^{-3}$], respectively. The simulation results shown in Figures 6.2, 6.3, and 6.4 depict the differences between the set-value and the computed area of the controlled signals over the limited time; which are calculated using Simpson's 1/3 rule. It can be seen that the error decreases rapidly with the number of iterations, and the solution is steady towards the end.

To explain the movement behaviour of the swarm, Figures 6.5 to 6.8 and 6.9 to 6.16 depict the simulation results of the search process of the candidate particles for both cases: starting in islanding mode and load change condition, respectively. These particles select their trajectories based on their best fitness values. The results show that the particles

finish their movements at the best positions, and the power control parameters stay at the optimum global values which are indicated in Table 6.2.

Table 6.1: The Applied PSO Parameters

PSO Parameters Description	K_{pf}	K_{if}	K_{pv}	K_{iv}	K_{pp}	K_{ip}	K_{pq}	K_{iq}
Acceptable violation (p.u.)	$\pm$0.01		$\pm$0.05		$\pm$0.1		$\pm$0.1	
Initial velocity (V)	0		0		0		0	
Inertial fitness value	800		800		800		800	
Inertia constant (w)	0.05	0.5	0.05	0.5	0.05	0.5	0.05	0.5
Cognitive coefficients(c_1&c_2)	0.09	0.1	0.09	0.1	0.09	0.1	0.09	0.1

Table 6.2: Power Control Parameters

Control Parameters	Starting Islanding Mode	Load Change Condition
K_{pf}	4.107100235325	3.355005953343
K_{if}	0.002108453626	0.002109635421
K_{pv}	-1.50149664105	-1.80398178128
K_{iv}	0.003848222141	0.002576811582
K_{pp}	-	-1.95714161463
K_{ip}	-	0.001070485685
K_{pq}	-	3.807097417772
K_{iq}	-	0.003704792613

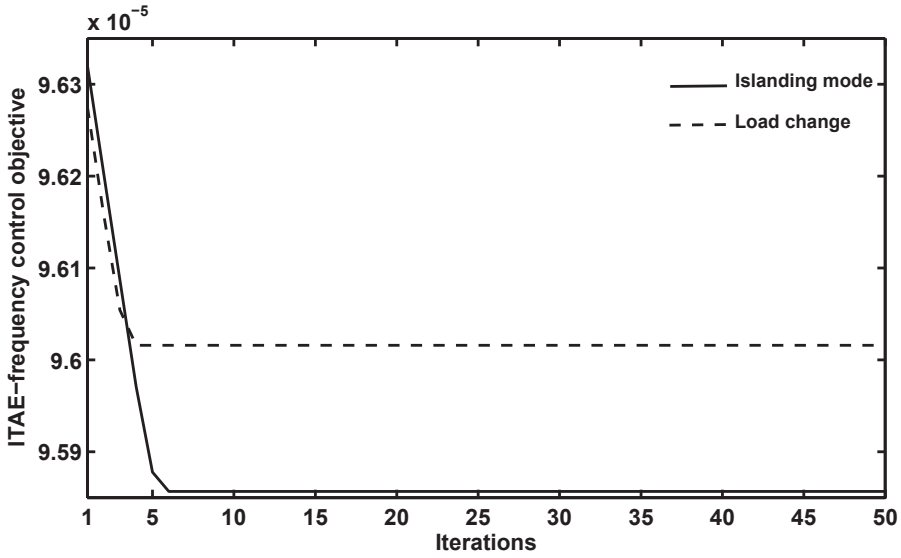

Figure 6.2: Fitness values of the frequency control objective

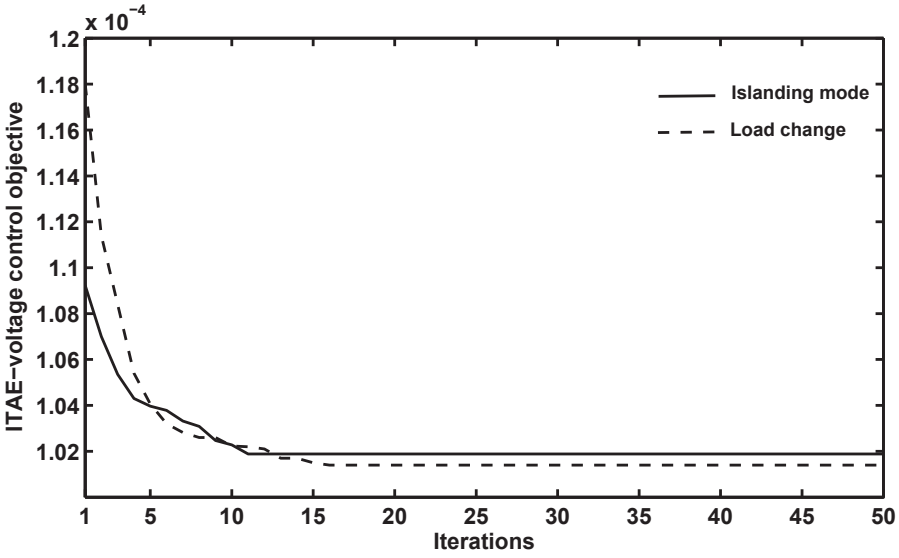

Figure 6.3: Fitness values of the voltage control objective

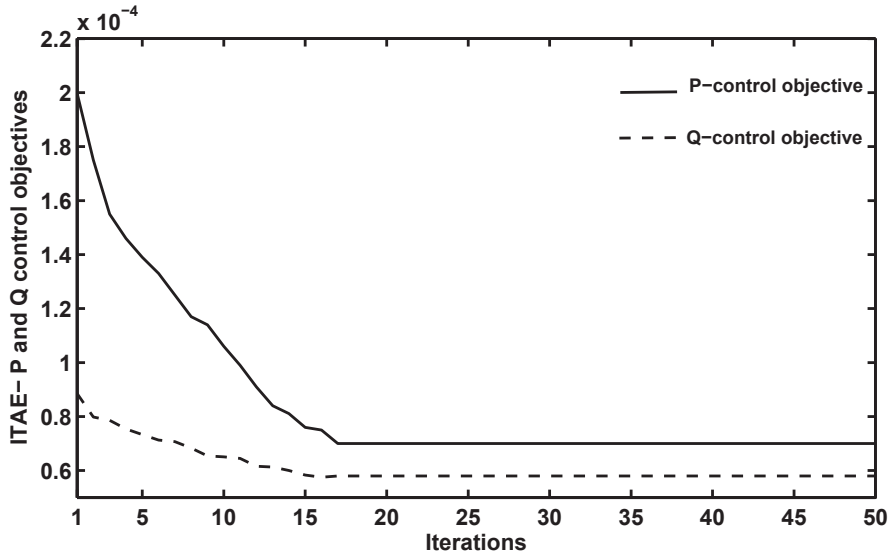

Figure 6.4: Fitness values of the active and reactive power control objectives

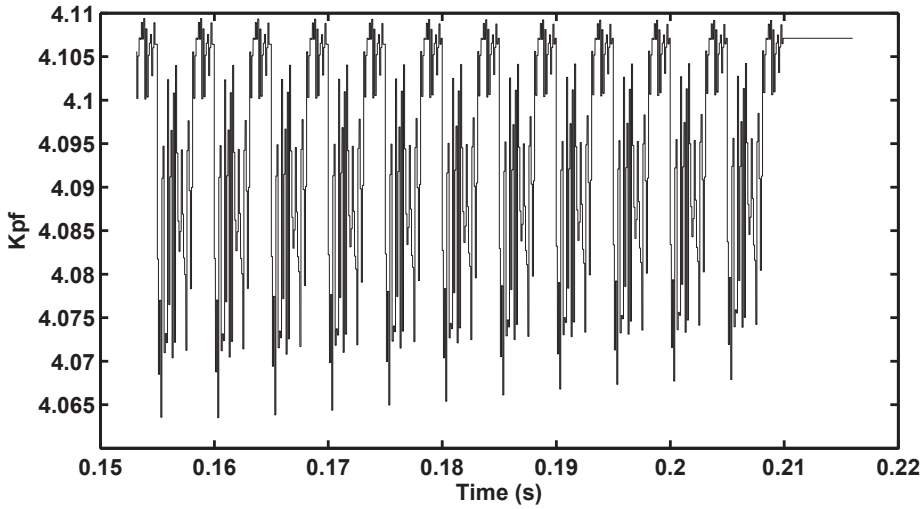

Figure 6.5: Search process of K_{pf} when the system is islanded

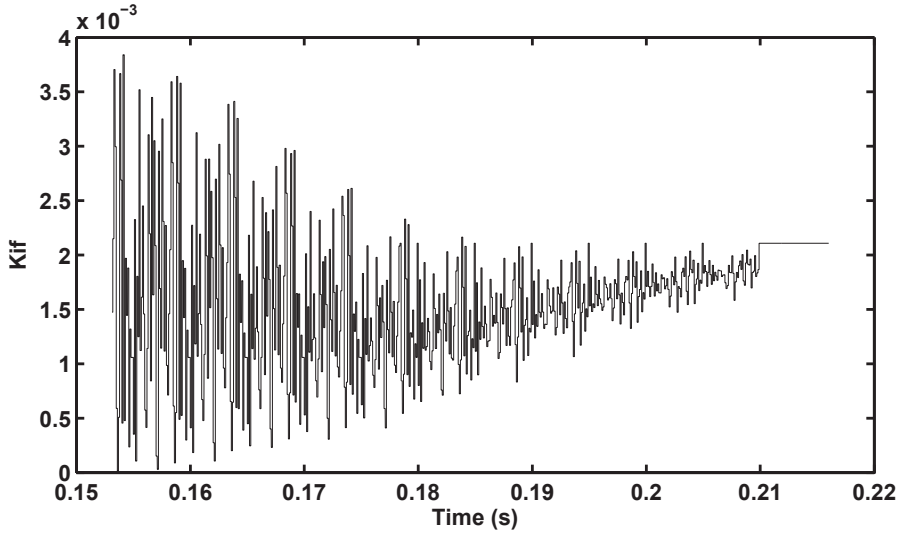

Figure 6.6: Search process of K_{if} when the system is islanded

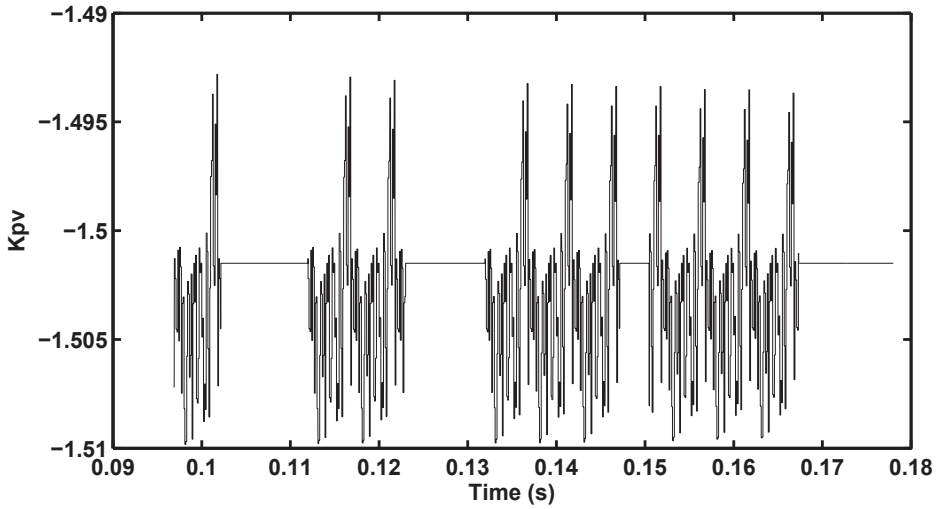

Figure 6.7: Search process of K_{pv} when the system is islanded

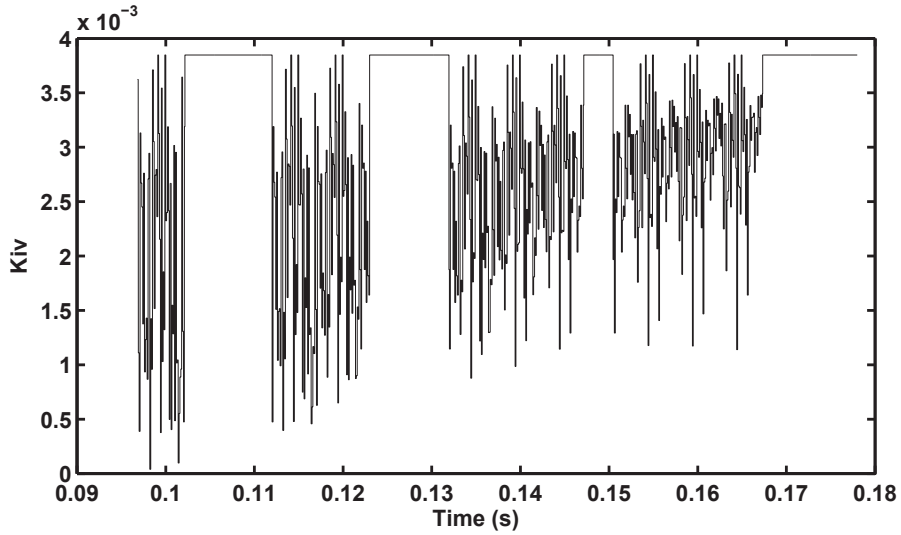

Figure 6.8: Search process of K_{iv} when the system is islanded

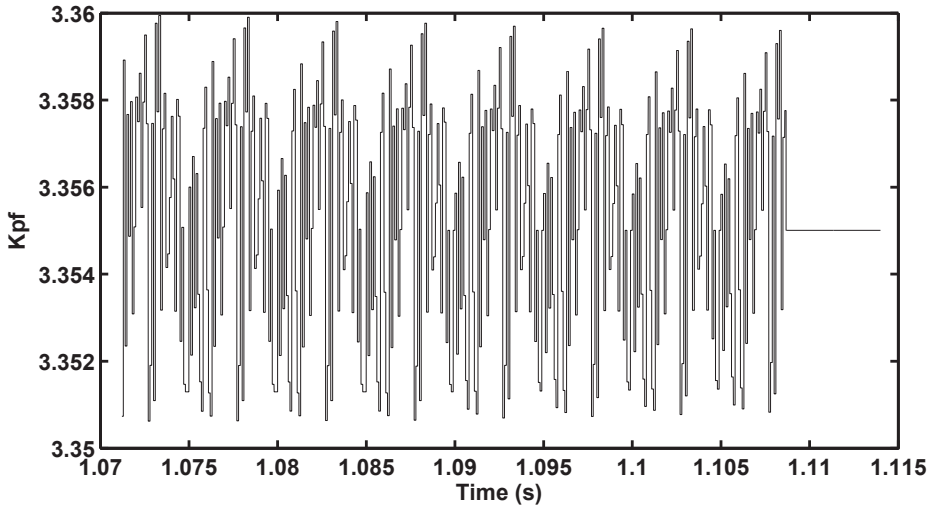

Figure 6.9: Search process of K_{pf} at the load change condition

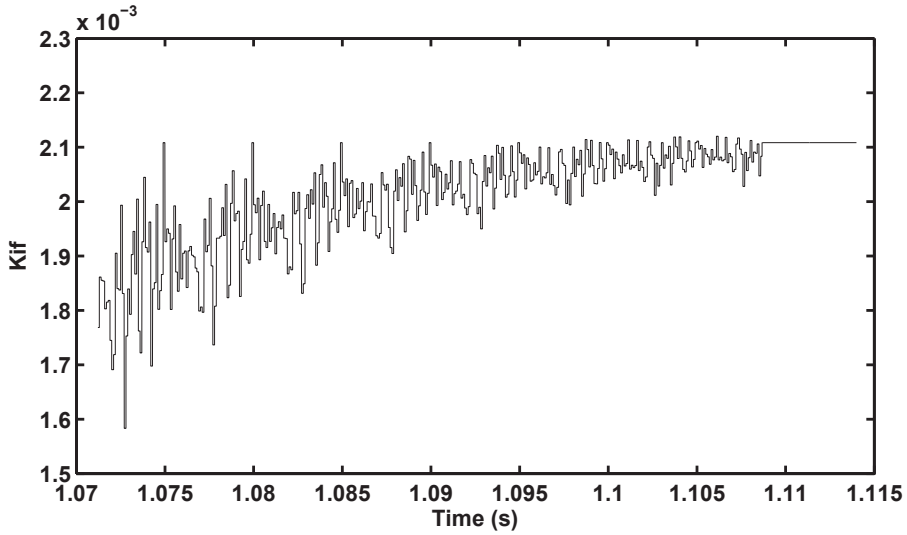

Figure 6.10: Search process of K_{if} at the load change condition

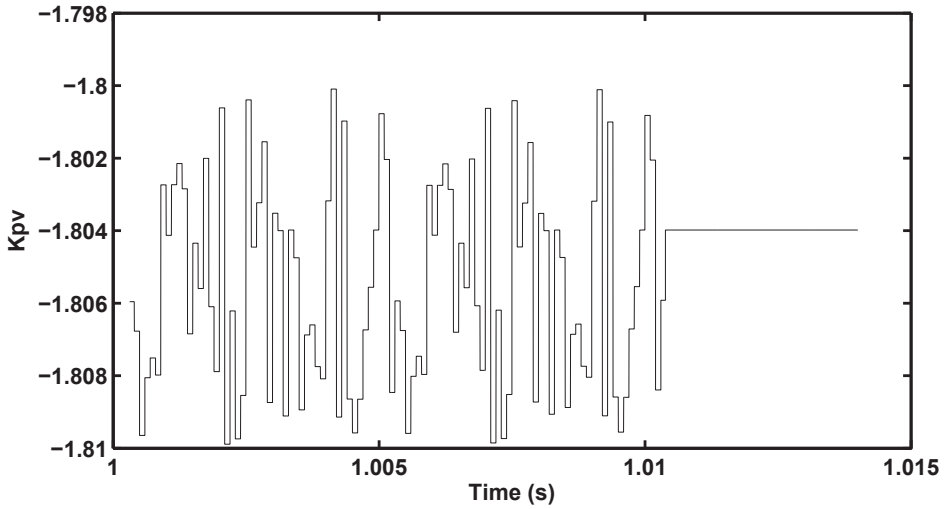

Figure 6.11: Search process of K_{pv} at the load change condition

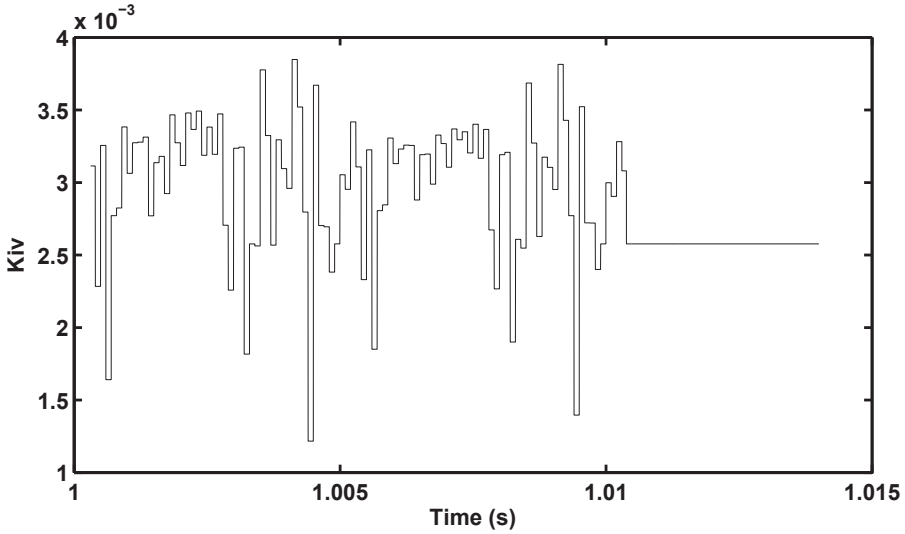

Figure 6.12: Search process of K_{iv} at the load change condition

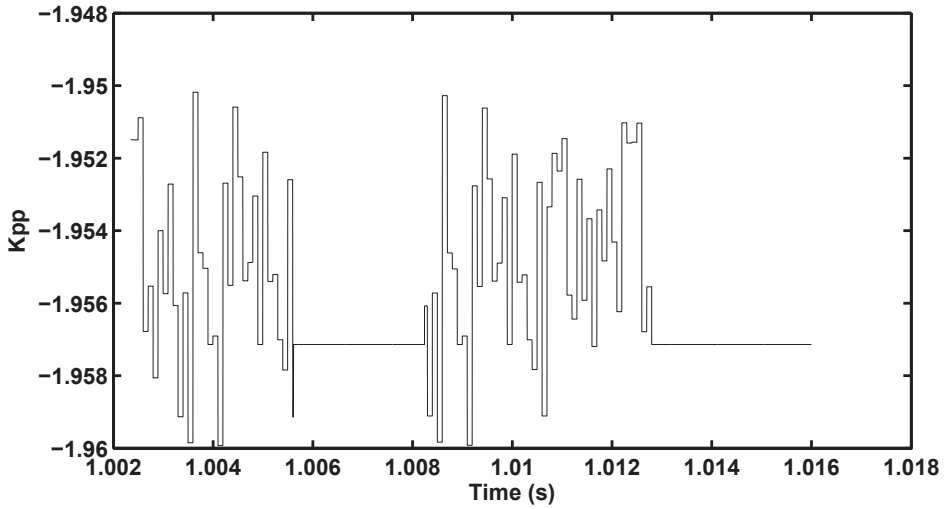

Figure 6.13: Search process of K_{pp} at the load change condition

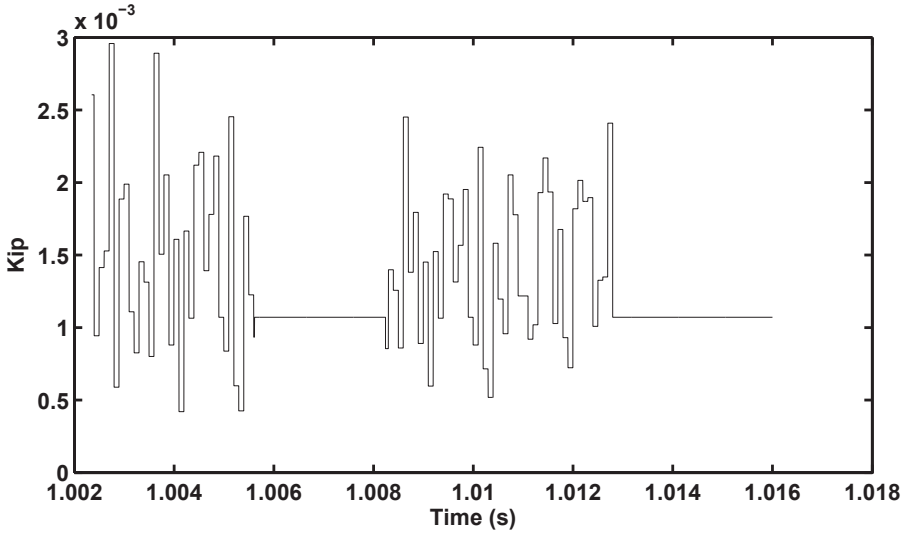

Figure 6.14: Search process of K_{ip} at the load change condition

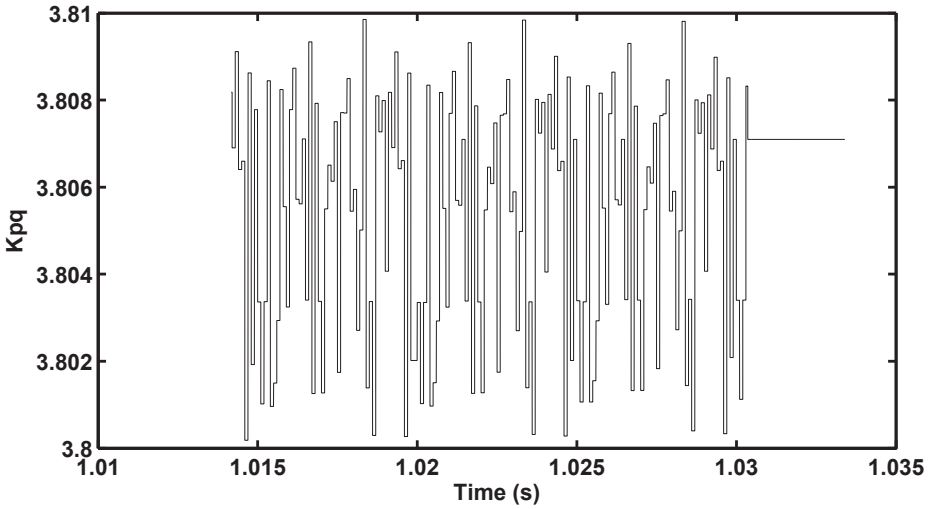

Figure 6.15: Search process of K_{pq} at the load change condition

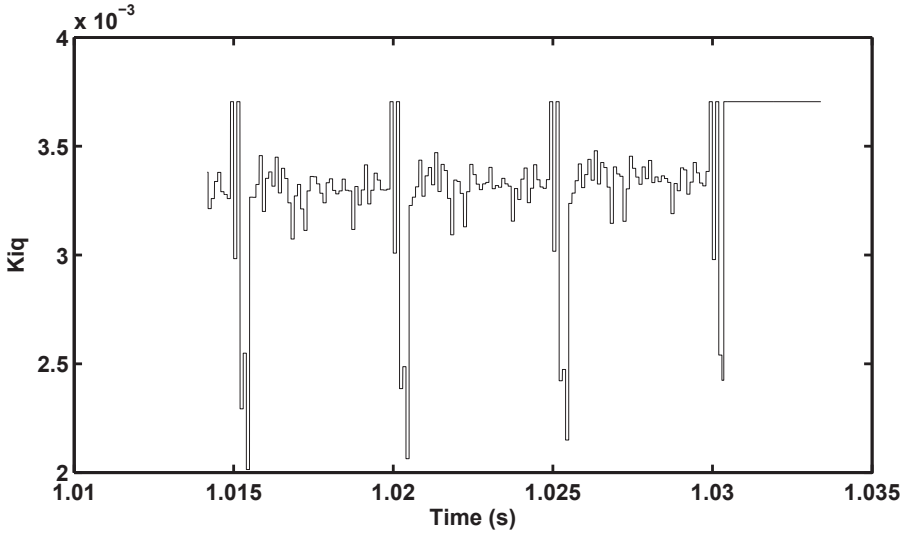

Figure 6.16: Search process of K_{iq} at the load change condition

6.2.2 Voltage and Frequency Regulation

To evaluate the proposed controller scheme, the simulation starts in grid-connected mode, so the microgrid voltage and frequency are mainly established by the grid which is responsible for maintaining their profiles.

At 0.09 s, the microgrid switches to the islanding operation mode. As shown in Figures 6.17 and 6.18, the active and reactive load power are set to 2 p.u. and 0.62 p.u., respectively. At this stage, both DG units adopt the Vf power control mode based PSO algorithm in order to mitigate the voltage drop and avoid a severe deviation of the frequency caused by a sudden move to the islanding mode or load change. In this mode, and as denoted in Equations (4.7) and (4.8), the V_{ref} and f_{ref} of both DG units are set to 1 (p.u.). The implemented PSO algorithm results are reported in Subsection 6.2.1, Figures 6.19 and 6.20 depict the results of the controlled voltage and frequency. It can be noticed that the proposed controller reacts to starting the islanding mode and provides, after a short transient, voltage and frequency equal to 0.9544 p.u. and 0.998 p.u., respectively.

At 1 s, the active and reactive load power are decreased to 1.9 p.u. and 0.37 p.u., respectively. In this case, and as shown in Figures 6.19 and 6.20, the Vf control mode which is adopted by the first DG unit offers an excellent behaviour and maintains the microgrid voltage equal to 1.047 p.u. and the frequency around 1.0044 (p.u.). Consequently, according to the acceptable limits which are outlined in Table 6.1, it can be noticed that the proposed strategy restores the microgrid voltage and frequency close to their reference values within ±0.05 and ±0.01 (0.5 Hz), respectively.

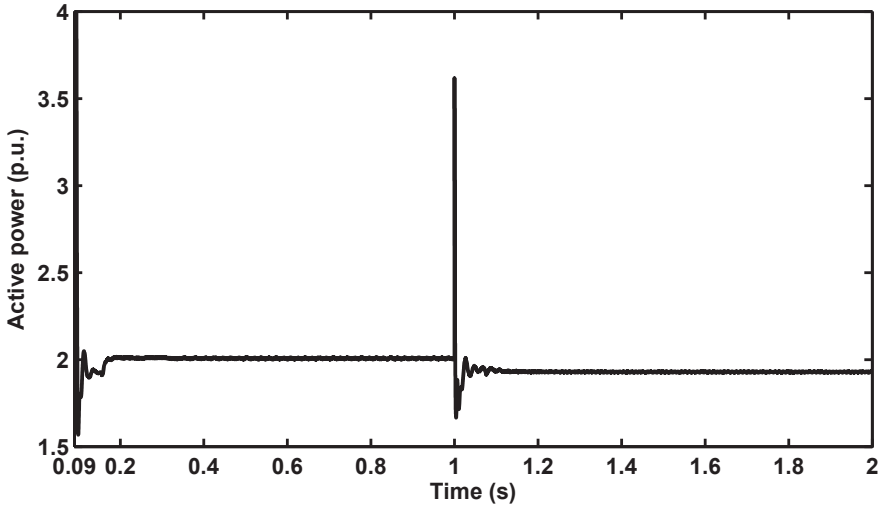

Figure 6.17: Active load power in islanding mode

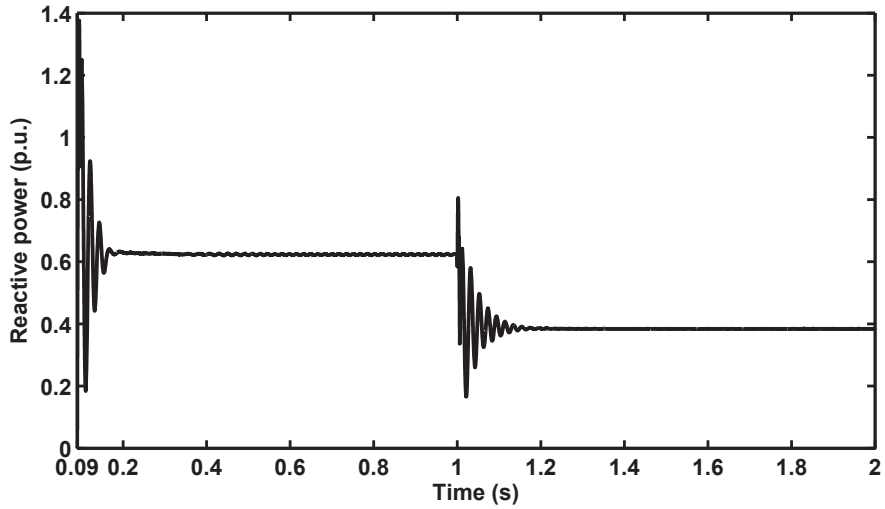

Figure 6.18: Reactive load power in islanding mode

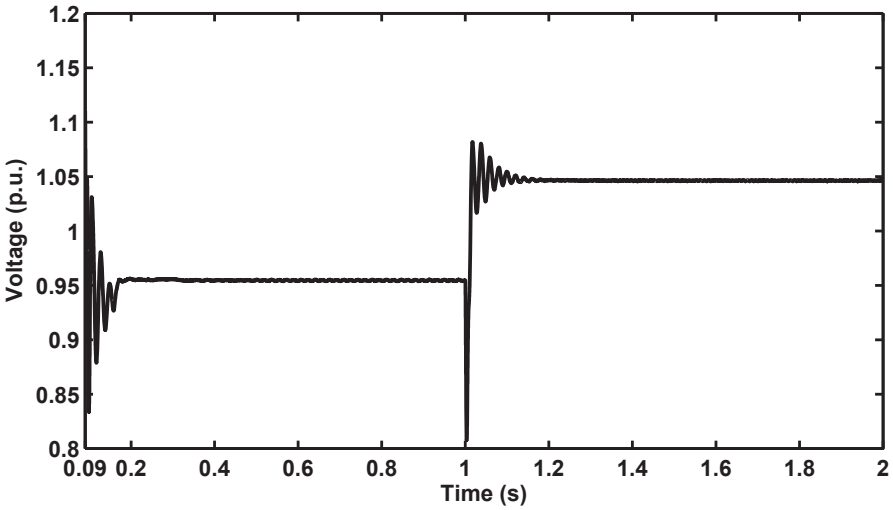

Figure 6.19: The microgrid voltage regulated by Vf control mode

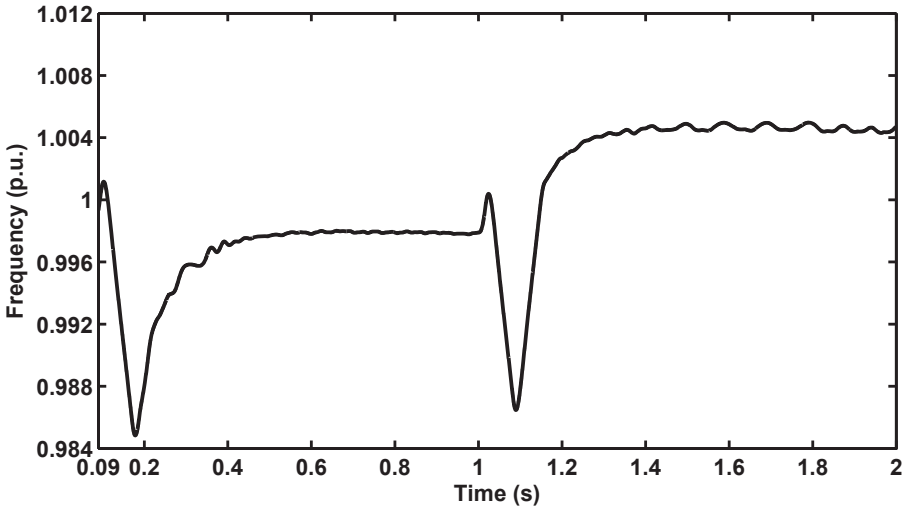

Figure 6.20: The microgrid frequency regulated by Vf control mode

6.2.3 Power Sharing

To ensure a proper utilisation of the DG units, the principle of sharing power is an adequate method to achieve appropriate distribution of the consumed power that is generated by multiple DG units. In this case, sharing power among multiple DG units mainly depends on their output control mode and the microgrid operation mode with respect to the load demand.

In this work, once the microgrid is islanded at 0.09 s, the proposed controllers of both DG units are switched to Vf power control mode in order to establish voltage and frequency close to their reference values. In this case, the PSO algorithm runs to find the global best parameters of this controller, and the power is expected to be shared equally among the DG units. In this simulation, for 2 p.u. active load power and 0.62 p.u. reactive load power, both DG units share the load power equally as expected. Figures 6.21 to 6.24 show that the output power of each DG units is equal to 1 p.u. active power and 0.31 p.u. reactive power.

However, at the load change, the second DG unit is set to produce a sustained output power by using PQ control mode, while the first DG unit keeps operating in Vf control mode being responsible for voltage and frequency regulation and also to generate the redundancy of the load demand. In this model, the P_{ref} and Q_{ref} of the second DG unit which are denoted in Equations (5.8) and (5.9) are arbitrarily set to 1 p.u. and 0.31 p.u., respectively. To verify this scenario, the load is changed at 1 s, and the active and reactive load power are reduced to 1.9 p.u. and 0.37 p.u., respectively. Thus, as shown in Figures

6.23 and 6.24, it can be seen that the second DG unit keeps its output stable, which proves the validity of the PQ control mode. In contrast, as shown in Figures 6.21 and 6.22, the output active and reactive power of the first DG unit are decreased to 0.9 p.u. and 0.06 p.u., respectively. In case of non-identical DG units, when the islanding mode occurs, and according to Equations (5.6) and (5.7), the measured values of the active and reactive power for each DG unit can be set as their reference values during the load change. This is because it is expected that the microgrid meets the total load demand based on its maximum generated power; otherwise, the microgrid must undergo the load shedding strategy.

Consequently, the results perfectly prove the proposed strategy of using one DG unit for voltage and frequency regulation and the second for maximum power exportation. This scenario is useful when the microgrid includes hybrid and more than two DG units. Hence, the PQ control strategy can be used for the DG units which produce constant or adjustable output power such as photovoltaic panels.

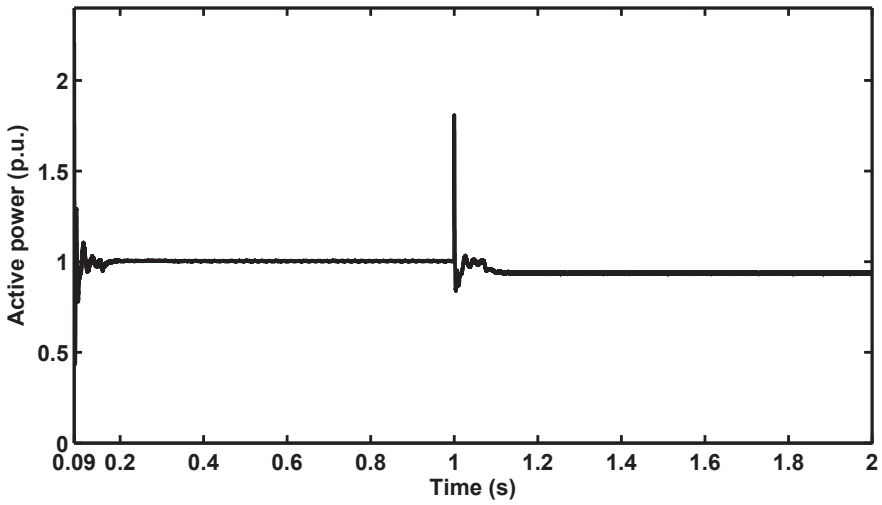

Figure 6.21: Active power generated by first DG unit

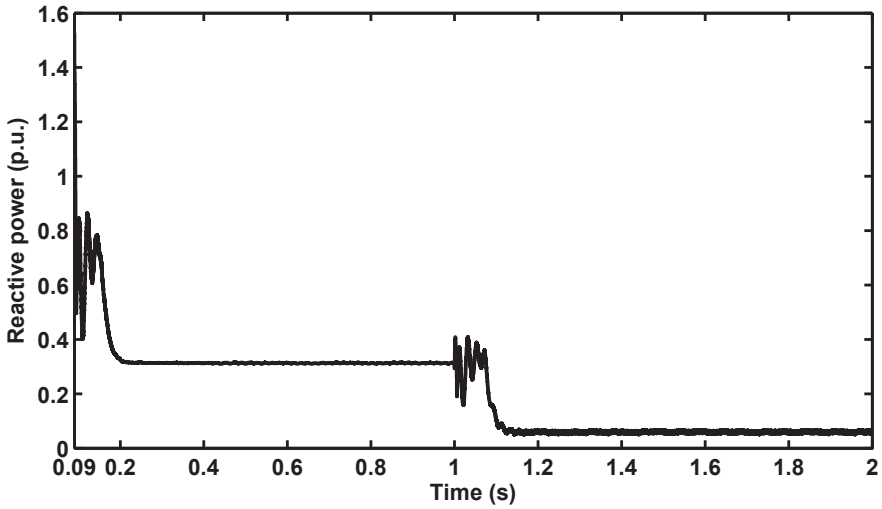

Figure 6.22: Reactive power generated by first DG unit

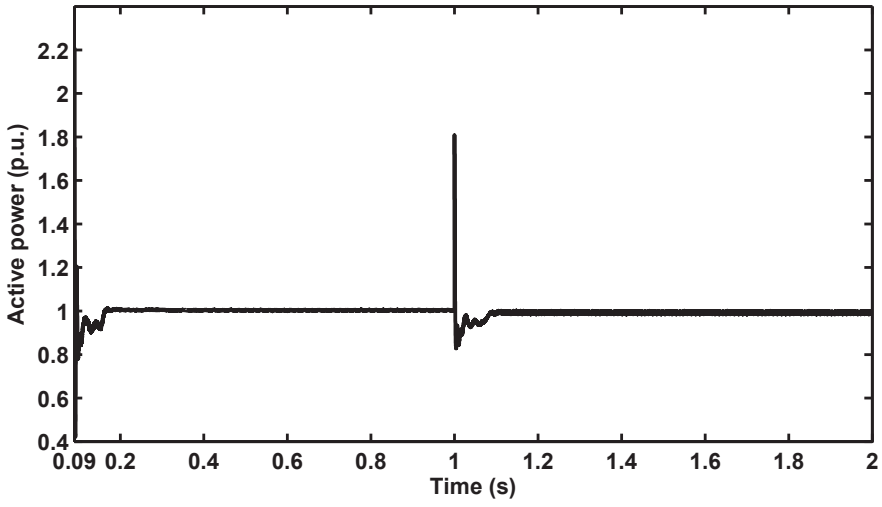

Figure 6.23: Active power generated by second DG unit

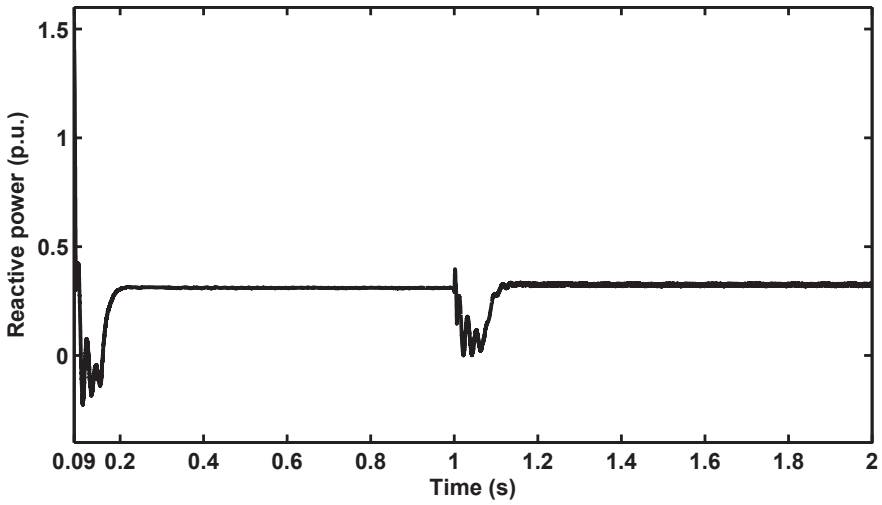

Figure 6.24: Reactive power generated by second DG unit

6.3 Conclusions

In this chapter, an optimal power control strategy has been proposed for an autonomous microgrid operation. The controller scheme consists of an inner current control loop and an outer power control loop. In this work, two different power control strategies were utilised for two typical DG units; the Vf control strategy was adopted when the microgrid starts the islanding operation mode to maintain the microgrid voltage and frequency within acceptable limits, while the PQ control strategy was considered only by the second DG unit during the load change to produce the maximum power. The PSO algorithm is incorporated into both power control strategies in order to implement real-time self-tuning regardless of whether the microgrid starts the operation in islanding mode or during load change condition. The simulation results show that the proposed strategy offers an excellent response of regulating the microgrid voltage and frequency, and achieves adequate power sharing with different control modes.

Chapter 7

STABILITY ANALYSIS OF MULTIPLE DG UNITS IN AN AUTONOMOUS MICROGRID OPERATION

The small-signal stability is one of the most important issues of the system's reliable operation. It can be defined as the ability of the power system to return to normal operating condition following a small physical disturbance. The stability analysis substantially depends on the linearised state-space equations that define the characteristics of the power system model. Thus, stability can be easily studied by determining the solution of the system characteristic equation [132]. In an autonomous microgrid operation, the DG units are responsible for maintaining the system voltage and frequency while sharing active and reactive power among them. In this case, the system being more susceptible for unstable operation, thereby the stability is largely required to be investigated in order to know whether the system is within an acceptable stability limit or not.

In this chapter, the stability analysis is presented for an autonomous microgrid operation. The small-signal model is developed in order to examine the dynamic stability for the given operating point and under the proposed power controller. This model is constructed in form that enables testing the stability for multiple DG units in such a system. Therefore, the stability analysis of the microgrid operation that is proposed in Chapters 4 and 6 has been targeted in this work. System oscillatory modes and the sensitivity to the control parameters are the main performance indices which are considered, particularly when the microgrid is islanded or under load change condition. The complete small-signal model is linearised and used to define the system state matrix which is employed for eigenvalue analysis. The results prove that the stability analysis is fairly accurate and the controllers offer reliable system operation.

The remaining part of this chapter is divided into seven main sections. Section 7.1 describes the small-signal dynamic model for an autonomous microgrid. In Section 7.2, the state-space model is developed for the proposed controlled VSI system. Section 7.3 presents the state-space models of the network and load. In Section 7.4, the microgrid sub-models are combined to form the overall system model. Section 7.5 demonstrates the eigenvalue and sensitivity analysis which are used in this analysis. In Section 7.6, the results are presented to confirm the aim of this work. Finally, the conclusions are outlined in Section 7.7.

7.1 Small-Signal Model of Autonomous Microgrid

In this work, the small-signal dynamic model of the microgrid is divided into three individual sub-models, namely: inverter, network, and load. The model of each inverter includes the dynamics of the power controller, current controller, an output LC filter and the coupling inductance (if applicable). These dynamics are described based on their own reference $d-q$ frame, while for the purpose of the whole microgrid analysis, all the sub-models must be represented in a common reference $D-Q$ frame, so the inverter output signals can be converted into a common reference $D-Q$ frame using the following transformation technique [7]:

$$[X_{DQ}] = [T][X_{dq}] \tag{7.1}$$

$$[T] = \begin{bmatrix} cos(\theta) & -sin(\theta) \\ sin(\theta) & cos(\theta) \end{bmatrix} \tag{7.2}$$

where $\theta = \omega_s t + \theta_o$ is the synchronous rotating angle, θ_o represents the initial value. Accordingly, the following sections describe the modelling approach for the sub-models that form the overall small-signal model of the microgrid.

7.2 State-Space Model of a 3-phase VSI System

The schematic diagram of the controlled VSI system is shown in Figure 7.1. This system can be divided into two main circuits. First, the power circuit that includes the inverter and the output LC filter. Second, the control circuit which involves the power controller, current controller, and the power calculation loop that sets the local feedback signals.

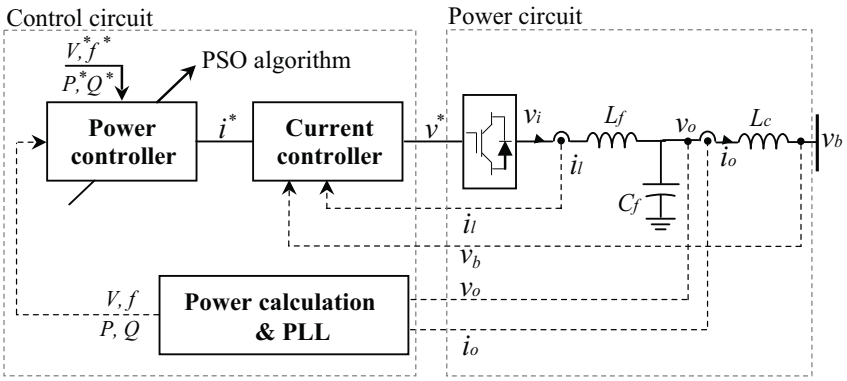

Figure 7.1: The controlled VSI system

While the frequency can be measured using a Phase-Locked-Loop (PLL), the local values of the voltage, active and reactive power can be calculated as follows:

$$V = \sqrt{V_d^2 + V_q^2} \tag{7.3}$$

$$P = \frac{3}{2}(V_d.i_d + V_q.i_q) \tag{7.4}$$

$$Q = \frac{3}{2}(V_q.i_d - V_d.i_q) \tag{7.5}$$

Assuming that the DG unit is a constant DC source, the dynamics of the DC bus can be ignored. Also, because the inverter is a switch-mode device with a sufficiently high switching frequency, the switching action does not impact the states when a good attenuation of the switching frequency ripple is achieved through the output LC filter [133]. In this work, the state-space models of the remaining parts are developed as follows:

7.2.1 Vf Control Mode

Figure 7.2 shows the block diagram of the proposed Vf control mode. System voltage and frequency are regulated with standard PI controllers based on real-time self-tuning method using the PSO algorithm. This strategy is proposed to respond to sudden changes such as starting the islanding operation mode or load change. In this case, the controller regulates the microgrid voltage and frequency based on their reference values V^* and f^*, which may either be defined locally or by the Microgrid Control Centre (MGCC). The main function of this controller is to generate the reference current vectors i_d^* and i_q^*, so a relatively slow change of the reference current trajectory would ensure high quality of the inverter output

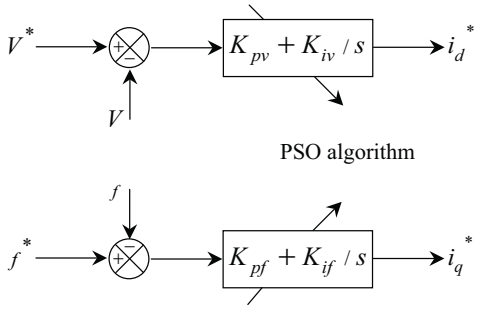

Figure 7.2: The block diagram of the proposed Vf control mode

power, which indicates that the control objective has been achieved. The corresponding state-space equations can be expressed as:

$$\frac{d\gamma_d}{dt} = V^* - V, \qquad \frac{d\gamma_q}{dt} = f^* - f \tag{7.6}$$

where γ_d and γ_q are the state variables of the PI regulators of the voltage and frequency control loops, respectively, and the output equations are given by:

$$i_d^* = K_{pv}(V^* - V) + K_{iv}\gamma_d \tag{7.7}$$

$$i_q^* = K_{pf}(f^* - f) + K_{if}\gamma_q \tag{7.8}$$

Since the input to this controller can be divided into two terms: the reference and the feedback inputs, the linearised small-signal state-space equations can be written as:

$$\dot{[\triangle\gamma_{dq}]} = A_{vf}\,[\triangle\gamma_{dq}] + B_{vf_1}\,[\triangle V^*\ \triangle f^*]^T + B_{vf_2}\,[\triangle V\ \triangle f]^T \tag{7.9}$$

where

$$\triangle\gamma_{dq} = \begin{bmatrix} \triangle\gamma_d & \triangle\gamma_q \end{bmatrix}^T,\ A_{vf} = [0],\ B_{vf_1} = \begin{bmatrix} 1 & 0 \\ 0 & 1 \end{bmatrix},\ B_{vf_2} = \begin{bmatrix} -1 & 0 \\ 0 & -1 \end{bmatrix}$$

and

$$\left[\triangle i_{dq}^*\right] = C_{vf}\,[\triangle\gamma_{dq}] + D_{vf_1}\,[\triangle V^*\ \triangle f^*]^T + D_{vf_2}\,[\triangle V\ \triangle f]^T \tag{7.10}$$

where

$$\triangle i_{dq}^* = \begin{bmatrix} \triangle i_d^* & \triangle i_q^* \end{bmatrix}^T,\ C_{vf} = \begin{bmatrix} K_{iv} & 0 \\ 0 & K_{if} \end{bmatrix},\ D_{vf_1} = \begin{bmatrix} K_{pv} & 0 \\ 0 & K_{pf} \end{bmatrix},$$

$$D_{vf_2} = \begin{bmatrix} -K_{pv} & 0 \\ 0 & -K_{pf} \end{bmatrix}$$

7.2.2 PQ Control Mode

Figure 7.3 shows the block diagram of the PQ control mode. Typical of the Vf control mode, this controller is proposed for the second DG unit to control the injecting active and reactive power based on their reference values P^* and Q^*.

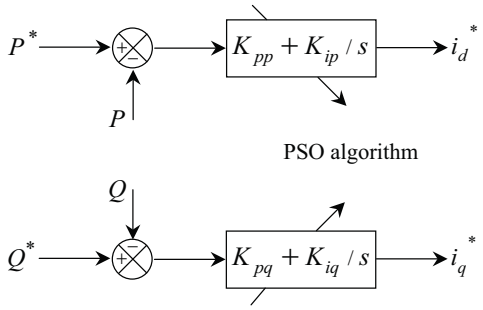

Figure 7.3: The block diagram of the proposed PQ control mode

The corresponding state-space equations can be expressed as:

$$\frac{d\varphi_d}{dt} = P^* - P, \qquad \frac{d\varphi_q}{dt} = Q^* - Q \tag{7.11}$$

where φ_d and φ_q are the state variables of the PI regulators of the active and reactive power control loops, respectively, and the output equations are given by:

$$i_d^* = K_{pp}(P^* - P) + K_{ip}\varphi_d \tag{7.12}$$

$$i_q^* = K_{pq}(Q^* - Q) + K_{iq}\varphi_q \tag{7.13}$$

Similar to the Vf control mode, the linearised small-signal state-space equations can be written as:

$$[\dot{\triangle\varphi_{dq}}] = A_{pq}\,[\triangle\varphi_{dq}] + B_{pq_1}\,[\triangle P^*\ \triangle Q^*]^T + B_{pq_2}\,[\triangle P\ \triangle Q]^T \tag{7.14}$$

where

$\triangle\varphi_{dq} = \begin{bmatrix} \triangle\varphi_d & \triangle\varphi_q \end{bmatrix}^T$, $A_{pq} = [0]$, $B_{pq_1} = \begin{bmatrix} 1 & 0 \\ 0 & 1 \end{bmatrix}$, $B_{pq_2} = \begin{bmatrix} -1 & 0 \\ 0 & -1 \end{bmatrix}$

and

$$\left[\triangle i_{dq}^{*}\right] = C_{pq}\left[\triangle \varphi_{dq}\right] + D_{pq_1}\left[\triangle P^{*}\ \triangle Q^{*}\right]^{T} + D_{pq_2}\left[\triangle P\ \triangle Q\right]^{T} \tag{7.15}$$

where

$$\triangle i_{dq}^{*} = \begin{bmatrix} \triangle i_d^{*} & \triangle i_q^{*} \end{bmatrix}^{T},\ C_{pq} = \begin{bmatrix} K_{ip} & 0 \\ 0 & K_{iq} \end{bmatrix},$$

$$D_{pq_1} = \begin{bmatrix} K_{pp} & 0 \\ 0 & K_{pq} \end{bmatrix},\ D_{pq_2} = \begin{bmatrix} -K_{pp} & 0 \\ 0 & -K_{pq} \end{bmatrix}$$

7.2.3 Current Controller

Figure 7.4 shows the block diagram of the current controller that is used for each DG unit. The linear current controller based on SVPWM and open loop voltage type is utilised with the inner current feedback loop. The objective of this controller is to ensure accurate tracking and short transients of the inverter output current. This controller is usually used in such a way that the voltage is applied to the inductive $R-L$ impedance, so that an impulse current in the inductor has a minimum error. Two PI regulators are used to eliminate current error, and both the inverter current loop and the grid voltage feed-forward loop are employed to improve the steady-state and dynamic performance [134].

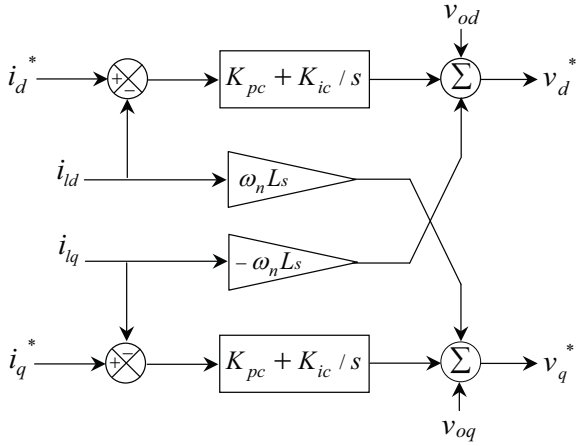

Figure 7.4: The block diagram of the current controller

In this work, the coupling inductance is not considered ($v_b = v_o$), so the corresponding state-space equations can be expressed as:

$$\frac{d\phi_d}{dt} = i_d^{*} - i_{ld}, \qquad \frac{d\phi_q}{dt} = i_q^{*} - i_{lq} \tag{7.16}$$

where ϕ_d and ϕ_q are the d and q axis state variables of the PI regulators of the current vectors, respectively, and the output equations are given by:

$$v_d^* = v_{od} - \omega_n L_s i_{lq} + K_{pc}(i_d^* - i_{ld}) + K_{ic}\phi_d \tag{7.17}$$

$$v_q^* = v_{oq} + \omega_n L_s i_{ld} + K_{pc}(i_q^* - i_{lq}) + K_{ic}\phi_q \tag{7.18}$$

The linearised small-signal state-space equations can be written as:

$$[\triangle\dot{\phi}_{dq}] = A_c\,[\triangle\phi_{dq}] + B_{c_1}\left[\triangle i_{dq}^*\right] + B_{c_2}\begin{bmatrix} \triangle i_{ldq} \\ \triangle v_{odq} \\ \triangle i_{odq} \end{bmatrix} \tag{7.19}$$

where

$\triangle\phi_{dq} = \begin{bmatrix} \triangle\phi_d & \triangle\phi_q \end{bmatrix}^T$, $A_c = [0]$, $B_{c_1} = \begin{bmatrix} 1 & 0 \\ 0 & 1 \end{bmatrix}$,

$B_{c_2} = \begin{bmatrix} -1 & 0 & 0 & 0 & 0 & 0 \\ 0 & -1 & 0 & 0 & 0 & 0 \end{bmatrix}$

and $\triangle i_{ldq}$, $\triangle v_{odq}$, $\triangle i_{odq}$ are the d and q axis current and voltage components shown in Figure 7.1, which can be defined as follows:

$\triangle i_{ldq} = \begin{bmatrix} \triangle i_{ld} & \triangle i_{lq} \end{bmatrix}^T$, $\triangle v_{odq} = \begin{bmatrix} \triangle v_{od} & \triangle v_{oq} \end{bmatrix}^T$, $\triangle i_{odq} = \begin{bmatrix} \triangle i_{od} & \triangle i_{oq} \end{bmatrix}^T$

$$\left[\triangle v_{dq}^*\right] = C_c\,[\triangle\phi_{dq}] + D_{c_1}\left[\triangle i_{dq}^*\right] + D_{c_2}\begin{bmatrix} \triangle i_{ldq} \\ \triangle v_{odq} \\ \triangle i_{odq} \end{bmatrix} \tag{7.20}$$

$C_c = \begin{bmatrix} K_{ic} & 0 \\ 0 & K_{ic} \end{bmatrix}$, $D_{c_1} = \begin{bmatrix} K_{pc} & 0 \\ 0 & K_{pc} \end{bmatrix}$,

$D_{c_2} = \begin{bmatrix} -K_{pc} & -\omega_n L_s & 1 & 0 & 0 & 0 \\ \omega_n L_s & -K_{pc} & 0 & 1 & 0 & 0 \end{bmatrix}$

7.2.4 Output LC Filter and Coupling Inductance

Assuming that the inverter drives perfect tracking ($v_i = v^*$), and for further investigation of using the coupling inductance, the small-signal state-space equations of the output LC

filter and the coupling inductance can be expressed as:

$$\frac{di_{ld}}{dt} = -\frac{R_f}{L_f} i_{ld} + \omega i_{lq} + \frac{1}{L_f} v_{id} - \frac{1}{L_f} v_{od} \tag{7.21}$$

$$\frac{di_{lq}}{dt} = -\frac{R_f}{L_f} i_{lq} - \omega i_{ld} + \frac{1}{L_f} v_{iq} - \frac{1}{L_f} v_{oq} \tag{7.22}$$

$$\frac{dv_{od}}{dt} = \omega v_{oq} + \frac{1}{C_f} i_{ld} - \frac{1}{C_f} i_{od} \tag{7.23}$$

$$\frac{dv_{oq}}{dt} = -\omega v_{od} + \frac{1}{C_f} i_{lq} - \frac{1}{C_f} i_{oq} \tag{7.24}$$

$$\frac{di_{od}}{dt} = -\frac{R_c}{L_c} i_{od} + \omega i_{oq} + \frac{1}{L_c} v_{od} - \frac{1}{L_c} v_{bd} \tag{7.25}$$

$$\frac{di_{oq}}{dt} = -\frac{R_c}{L_c} i_{oq} - \omega i_{od} + \frac{1}{L_c} v_{oq} - \frac{1}{L_c} v_{bq} \tag{7.26}$$

The linearised small-signal state-space equations can be written as:

$$\begin{bmatrix} \dot{\triangle i_{ldq}} \\ \triangle v_{odq} \\ \triangle i_{odq} \end{bmatrix} = A_{LCL} \begin{bmatrix} \triangle i_{ldq} \\ \triangle v_{odq} \\ \triangle i_{odq} \end{bmatrix} + B_{LCL1} \left[\triangle v_{idq}\right] + B_{LCL2} \left[\triangle v_{bdq}\right] \tag{7.27}$$

where

$$A_{LCL} = \begin{bmatrix} \frac{-R_f}{L_f} & \omega & \frac{-1}{L_f} & 0 & 0 & 0 \\ -\omega & \frac{-R_f}{L_f} & 0 & \frac{-1}{L_f} & 0 & 0 \\ \frac{1}{C_f} & 0 & 0 & \omega & \frac{-1}{C_f} & 0 \\ 0 & \frac{1}{C_f} & -\omega & 0 & 0 & \frac{-1}{C_f} \\ 0 & 0 & \frac{1}{L_c} & 0 & \frac{-R_c}{L_c} & \omega \\ 0 & 0 & 0 & \frac{1}{L_c} & -\omega & \frac{-R_c}{L_c} \end{bmatrix},$$

$$B_{LCL1} = \begin{bmatrix} \frac{1}{L_f} & 0 \\ 0 & \frac{1}{L_f} \\ 0 & 0 \\ 0 & 0 \\ 0 & 0 \\ 0 & 0 \end{bmatrix}, \quad B_{LCL2} = \begin{bmatrix} 0 & 0 \\ 0 & 0 \\ 0 & 0 \\ 0 & 0 \\ \frac{-1}{L_c} & 0 \\ 0 & \frac{-1}{L_c} \end{bmatrix}$$

For the reason that the inverter is modeled based on its own reference $d-q$ frame, the inverter output current $\triangle i_{odq}$ must be expressed in a common reference $D-Q$ frame using the transformation technique given by Equation (7.1) as follows:

$$[\triangle i_{oDQ}] = [T]\,[\triangle i_{odq}] \tag{7.28}$$

In contrast, the bus voltage (v_{bdq}) is the input signal to the inverter model which is represented in a common reference $D-Q$ frame, so the bus voltage can be converted into the inverter reference $d-q$ frame using the inverse transformation technique as follows:

$$[\triangle v_{bdq}] = [T]^{-1}\,[\triangle v_{bDQ}] \tag{7.29}$$

The overall state-space model of the controlled VSI system can be defined by combining the state-space equations of the power controller, current controller, and the output LC filter. For instance, the dynamic model of the inverter based Vf power control mode can be constructed from the state-space equations given by (7.9), (7.10), (7.19), (7.20), (7.27), (7.28) and (7.29) as follows:

$$[\triangle \dot{x}_{inv_1}] = A_{inv_1}\,[\triangle x_{inv_1}] + B_{inv_1}\,[\triangle v_{bDQ_1}] \tag{7.30}$$

$$[\triangle i_{oDQ_1}] = C_{inv_1}\,[\triangle x_{inv_1}] \tag{7.31}$$

where

$$[\triangle x_{inv_1}] = \begin{bmatrix} \triangle\gamma_{dq_1} & \triangle\phi_{dq_1} & \triangle i_{ldq_1} & \triangle v_{odq_1} & \triangle i_{odq_1} & \triangle V_1^* & \triangle f_1^* & \triangle V_1 & \triangle f_1 \end{bmatrix}^T$$

$$A_{inv_1} = \begin{bmatrix} B_{c_1}C_{vf} & 0 & B_{c_2} & 0 & 0 \\ B_{LCL_1}D_{c_1}C_{vf} & B_{LCL_1}C_c & A_{LCL} & 0 & 0 \\ & & +B_{LCL_1}D_{c_2} & & \\ & & +B_{LCL_2}T^{-1} & & \\ 0 & 0 & 0 & A_{vf_1} & 0 \\ 0 & 0 & 0 & 0 & A_{vf_2} \end{bmatrix}_{14\times 14}$$

$$A_{vf_1} = [B_{vf_1} + (B_{c_1}D_{vf_1}) + (B_{LCL_1}D_{c_1}D_{vf_1})]_{2\times 2}$$
$$A_{vf_2} = [B_{vf_2} + (B_{c_1}D_{vf_2}) + (B_{LCL_1}D_{c_1}D_{vf_2})]_{2\times 2}$$

$$B_{inv_1} = \begin{bmatrix} 0 & 0 & ... & B_{LCL_2}[T]^{-1} & 0 & 0 & 0 & 0 \end{bmatrix}^T_{2\times 14}$$
$$C_{inv_1} = \begin{bmatrix} 0 & 0 & ... & T & 0 & 0 & 0 & 0 \end{bmatrix}_{2\times 14}$$

For the microgrid that includes i DG units, the overall state-space model of the controlled VSI systems can be expressed as:

$$[\triangle \dot{x}_{inv}] = A_{inv}[\triangle x_{inv}] + B_{inv}[\triangle v_{bDQ}] \tag{7.32}$$

$$[\triangle i_{oDQ}] = C_{inv}[\triangle x_{inv}] \tag{7.33}$$

where

$$[\triangle x_{inv}] = \begin{bmatrix} \triangle x_{inv_1} & \triangle x_{inv_2} & \cdots & \triangle x_{inv_i} \end{bmatrix}^T$$

$$A_{inv} = \begin{bmatrix} A_{inv_1} & 0 & 0 & \cdot \\ 0 & A_{inv_2} & 0 & \cdot \\ \cdot & \cdot & \ddots & \cdot \\ \cdot & \cdot & \cdot & A_{inv_i} \end{bmatrix}, \quad B_{inv} = \begin{bmatrix} B_{inv_1} & 0 & 0 & \cdot \\ 0 & B_{inv_2} & 0 & \cdot \\ \cdot & \cdot & \ddots & \cdot \\ \cdot & \cdot & \cdot & B_{inv_i} \end{bmatrix}$$

$$[\triangle v_{bDQ}] = \begin{bmatrix} \triangle v_{bDQ_1} & \triangle v_{bDQ_2} & \cdots & \triangle v_{bDQ_i} \end{bmatrix}^T$$

$$C_{inv} = \begin{bmatrix} C_{inv_1} & 0 & 0 & \cdot \\ 0 & C_{inv_2} & 0 & \cdot \\ \cdot & \cdot & \ddots & \cdot \\ \cdot & \cdot & \cdot & C_{inv_i} \end{bmatrix}$$

To sum up, each inverter in a microgrid can be individually modeled, thus the above modelling approach provides a useful method to simplify constructing the complete model

of the microgrid that includes several DG units inverters.

7.3 State-Space Model of the Network and Load

The small-signal state-space model of the network and load are reported in [135]. Assuming that the number of loads is denoted by L and number of network nodes is denoted by N, then LN is the number of lines, and the corresponding state-space equation of the load can be written as:

$$[\triangle \dot{i}_{loadDQ}] = A_{load}\,[\triangle i_{loadDQ}] + B_{load}\,[\triangle v_{bDQ}] \tag{7.34}$$

In Equation (7.34), for the i^{th} load connected to the j^{th} node:

$$[\triangle i_{loadDQ}] = [\triangle i_{loadDQ1} \quad \triangle i_{loadDQ2} \ldots \triangle i_{loadDQL}]^T$$

$$A_{loadi} = \begin{bmatrix} \frac{-R_{loadi}}{L_{loadi}} & \omega \\ -\omega & \frac{-R_{loadi}}{L_{loadi}} \end{bmatrix},\ B_{loadi} = \begin{bmatrix} \frac{1}{L_{loadi}} & 0 \\ 0 & \frac{1}{L_{loadi}} \end{bmatrix}$$

Similarly, the state-space equation of the network can be expressed as:

$$[\triangle \dot{i}_{lineDQ}] = A_{net}\,[\triangle i_{lineDQ}] + B_{net}\,[\triangle v_{bDQ}] \tag{7.35}$$

In Equation (7.35), for the network with i^{th} lines:

$$[\triangle i_{netDQ}] = [\triangle i_{netDQ1} \quad \triangle i_{netDQ2} \ldots \triangle i_{netDQLN}]^T$$

$$A_{neti} = \begin{bmatrix} \frac{-R_{linei}}{L_{linei}} & \omega \\ -\omega & \frac{-R_{linei}}{L_{linei}} \end{bmatrix}, \quad i=1,2...LN$$

$$B_{neti} = \begin{bmatrix} \ldots & \frac{1}{L_{linei}} & 0 & \ldots & \frac{-1}{L_{linei}} & 0 & \ldots \\ \ldots & 0 & \frac{1}{L_{linei}} & \ldots & 0 & \frac{-1}{L_{linei}} & \ldots \end{bmatrix}$$

7.4 Overall Microgrid Model

Figure 7.5 shows the overall small-signal state-space model of the microgrid. The complete models of the inverter, network, and load can be combined to represent the microgrid model. The linearised equations given by (7.30), (7.34), and (7.35) show that the node

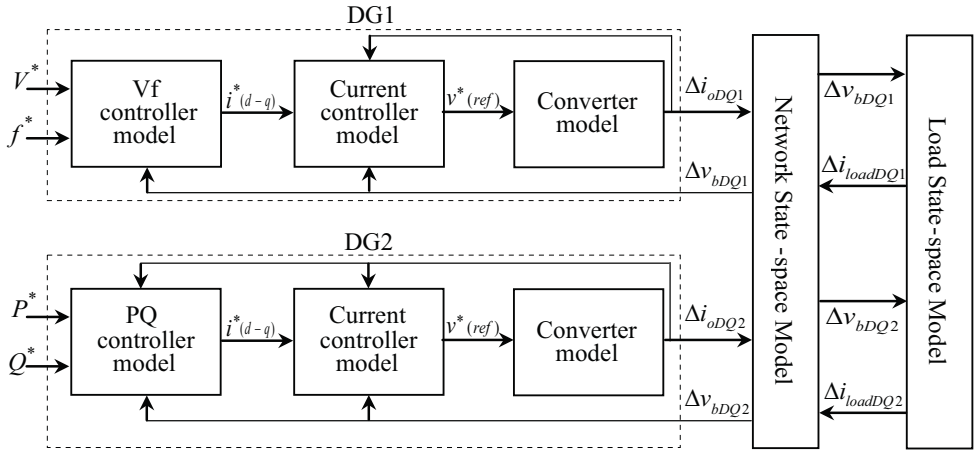

Figure 7.5: The overall small-signal state-space model of the microgrid

voltage is the input to each model. To ensure well defined node voltage, a virtual resistance of a large magnitude ($r_N \geqslant 1000\Omega$) is assumed between each network node and the ground [7]. The node voltage in terms of the inverter output current, load current, and the line current can be expressed as:

$$\triangle v_{bDQi} = r_N(\triangle i_{oDQi} - \triangle i_{loadDQi} + \triangle i_{netDQi}) \tag{7.36}$$

The node voltage of the microgrid model is given by:

$$[\triangle v_{bDQ}] = R_N(M_{inv}\,[\triangle i_{oDQ}] + M_{load}\,[\triangle i_{loadDQ}] + M_{net}\,[\triangle i_{netDQ}]) \tag{7.37}$$

where R_N is the diagonal matrix of size $(2N \times 2N)$ with elements equal to r_N. Assuming that I is the inverter, M_{inv} is a $(2N \times 2I)$ matrix that defines the inverter connection. For instance, if the I^{th} inverter is connected to the N^{th} node, the element $M_{inv(N,I)}$ is 1, and the rest of the elements of that row are 0. M_{load} is a $(2N \times 2L)$ matrix with -1 for the loads connected. Similarly, M_{net} is a $(2N \times 2LN)$ matrix with ± 1 elements taking into account the direction of the node current.

Using the linearised state-space equations (7.32), (7.34), and (7.35), the overall small-signal state-space model of the microgrid can be written as:

$$\begin{bmatrix} \dot{\triangle x_{inv}} \\ \triangle i_{lineDQ} \\ \triangle i_{loadDQ} \end{bmatrix} = A_{MG} \begin{bmatrix} \triangle x_{inv} \\ \triangle i_{lineDQ} \\ \triangle i_{loadDQ} \end{bmatrix} \tag{7.38}$$

where A_{MG} is the system state matrix which is given by (7.39). The stability analysis

can be investigated through the eigenvalues of the matrix A_{MG}

$$A_{MG} = \begin{bmatrix} A_{inv} + B_{inv}R_N M_{inv} C_{inv} & B_{inv}R_N M_{net} & B_{inv}R_N M_{load} \\ B_{net}R_N M_{inv} C_{inv} & A_{net} + B_{net}R_N M_{net} & B_{net}R_N M_{load} \\ B_{load}R_N M_{inv} C_{inv} & B_{load}R_N M_{net} & A_{load} + B_{load}R_N M_{load} \end{bmatrix} \quad (7.39)$$

7.5 Eigenvalue and Sensitivity Analysis

The eigenvalue analysis is the solution of the characteristic equation of the system state matrix. This solution produces eigenvalues (modes) that clarify the system stability around the operating point [132]. In conventional power systems, the eigenvalue analysis is extensively used to investigate the stability by identifying the oscillatory modes of the system components.

The sensitivity analysis is the method that measures the participation between state variables and the modes. The matrix of the participation factors can be defined once the eigenvalues are obtained. Using the right and left eigenvectors, the participation factors can be calculated as follows [136]:

$$p_{ki} = l_k^i r_k^i \quad (7.40)$$

where p_{ki} is the participation of the i^{th} mode in the k^{th} state, l_k^i and r_k^i are the left and right eigenvectors, respectively.

7.6 Modelling Results

As reported in Chapters 4 and 6, the model depicted in Figure 7.1 has been simulated for an inverter based DG unit and the parallel inverters based DG units in an autonomous microgrid operation, respectively. The simulation has been done using MATLAB/Simulink environment, and the results show that the proposed controller successfully achieve the control objectives. For these works, the small-signal dynamic model is developed in this chapter as in Equation (7.38), and then defined in a MATLAB/M-file script. Using the eigenvalue analysis, the stability has been examined through the location of the eigenvalues of the system state matrix A_{MG} in the complex plane. The purpose of this analysis is to

evaluate the performance of the microgrid around the given operating condition and under the proposed power controller. The sensitivity to the control parameters is also presented to identify the validity of the proposed controller. The following subsections describe the stability analysis in an autonomous microgrid operation mode as follows.

7.6.1 An Inverter Based DG unit

The parameters that represent the nominal operating condition of this system is shown in Table 7.1. In this case, the stability analysis has been investigated based on these parameters and for the following objectives as follows.

Table 7.1: Nominal System Parameters

Parameter	Value	Parameter	Value
DG unit	50 kW	$C_{dc-input}$	5000 µF
Frequency	50 Hz	Line resistance	0.4 Ω
R_f	1 Ω	Line inductance	2 mH
L_f	3 mH	K_{pc}	12.656
C_f	50 µF	K_{ic}	0.00215

7.6.1.1 Eigenvalue Analysis

As a solution of the system state matrix A_{MG} given in Equation (7.39), Table 7.2 shows the results of the eigenvalue analysis of the oscillatory modes. This analysis demonstrates that the model exhibits 9 eigen pairs: 6 complex conjugates and 3 real parts. The eigenvalues 1-14 represent the seven oscillatory modes of the controlled VSI system, all these modes are negative except 13 and 14 which are zero. That indicates the system has good dynamic properties under the given operating condition shown in Table 7.1 and the power control parameters which are found by the PSO algorithm and shown in Table 4.2. The negative real pairs (15,16) and (17,18) describe the oscillatory modes of the network line and load, respectively. In the simulation results, the load is considered to be active power for simplicity and set to 4.65 p.u. for the islanding mode, then reduced to 4.55 p.u. to emulate the load change condition. As shown in Figures 4.15 and 4.16, the power controller provides an excellent response of regulating the microgrid voltage and frequency. Thus, the eigenvalue analysis and the simulation results confirm that the proposed controller provides stable and reliable operation based on the PSO algorithm.

Table 7.2: Eigenvalue Analysis Results

Eigen values	Islanding mode		Load change	
	Real	Imaginary	Real	Imaginary
1,2	-899.5546087	±328.7569687	-899.4335534	±328.7635152
3,4	-40.29167979	±314.0002674	-32.67425223	±314.0000938
5,6	-227.8599673	±304.2016626	-231.9889082	±305.5816123
7,8	-189.6937473	±319.0404344	-184.0032894	±317.6541118
9,10	-45.51999665	±308.7666893	-45.51999665	±308.7666893
11,12	-3.34904e-06	±2.27168e-05	-3.34904e-06	±2.27168e-05
13,14	0	0	0	0
15,16	-41.86424517	0	-42.69199105	0
17,18	-129.0789640	0	-109.6873983	0

7.6.1.2 Sensitivity Analysis

A sensitivity analysis is a method that describes the dependency of the eigenvalues on system and controller parameters. Also, it can be used to identify the acceptable ranges of the control parameters. In this work, this analysis is considered in order to demonstrate the sensitivity to the proposed power controller parameters. Using Equation (7.40), the participation factors can be calculated for measuring the influence of the states on the modes of the proposed power controller. The criterion is that the states who heavily impact the modes have the maximum value in each row. As a result, Table 7.3 shows the dominant modes 15-18 who have noticeable impact on the states variables of the proposed power controller.

Table 7.3: Mode Participation Factors

States		Eigenvalues	
		15,16	17,18
Islanding	V	1.00	0.03
	f	0.02	0.92
Load change	V	0.96	0.00
	f	0.00	1.00

To confirm that these modes are largely sensitive to the state variables of the power controller, Figure 7.6 shows the trajectory of modes 15,16 as a function of the voltage control gain of the proposed power controller in the islanding mode. As shown in Table 7.3, these modes are largely sensitive to the state variables of the voltage control loop, thus Figure 7.6 confirms that changing K_{pv} in range of -0.9937 to -0.057 moves these modes to the right hand side that indicates low system stability, and the system is being unstable when the polarity of the K_{pv} value is changed. In like manner, while modes 17,18 heavily

impact the state variable of the frequency control loop, the variations of the K_{pf} in the range of 3.01086 to 0.065 displace these modes to the right hand plane as shown in Figure 7.7. Then, the system departs into the instability with the opposite value.

Similarly, during load change, the sensitivity analysis has been investigated for the same control objectives. Figures 7.8 and 7.9 show that changing the gains K_{pv} and K_{pf} also relocate the modes (15,16) and (17,18), respectively to the right hand side, and eventually lead to instability.

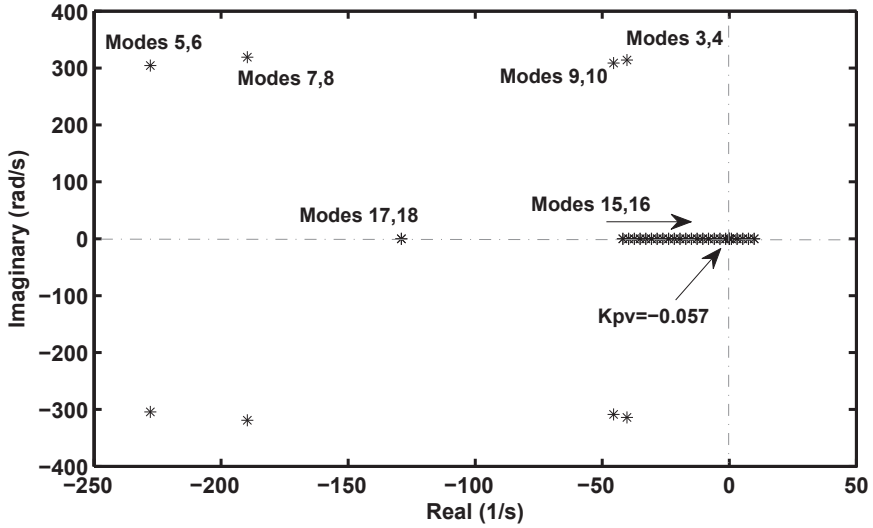

Figure 7.6: Locus of changing K_{pv} at the islanding mode

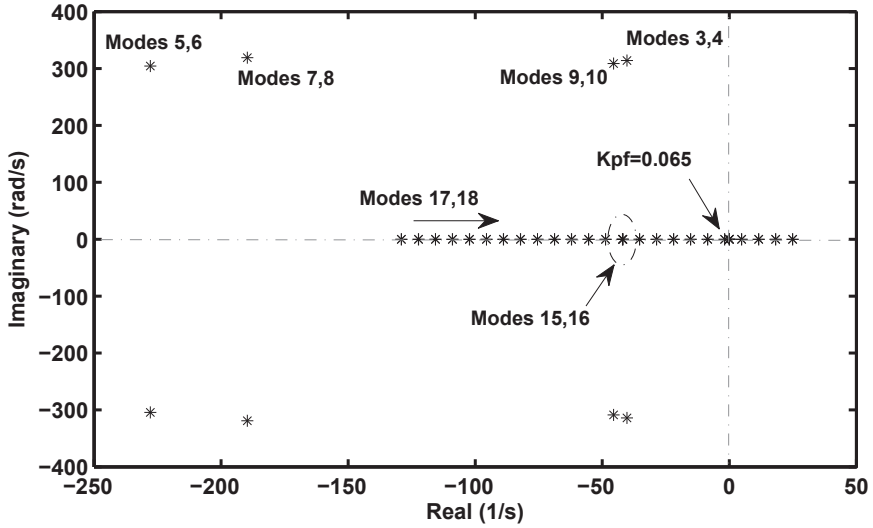

Figure 7.7: Locus of changing K_{pf} at the islanding mode

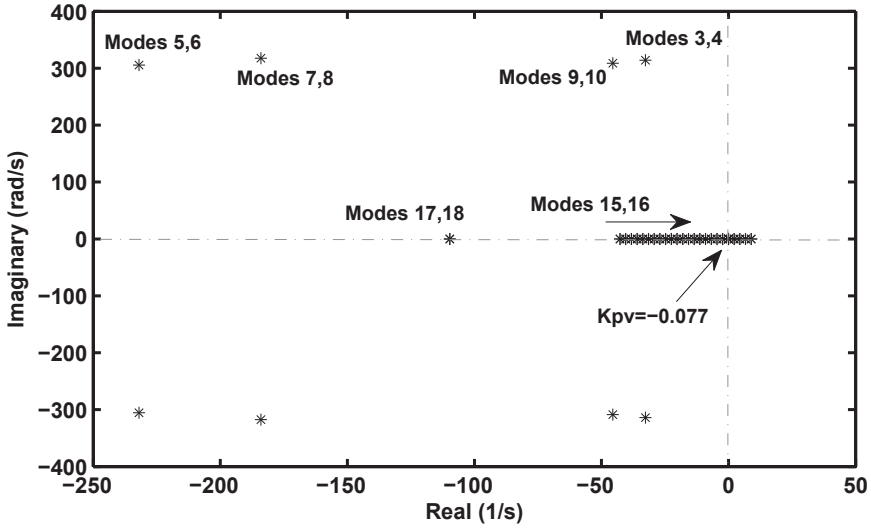

Figure 7.8: Locus of changing K_{pv} during load change

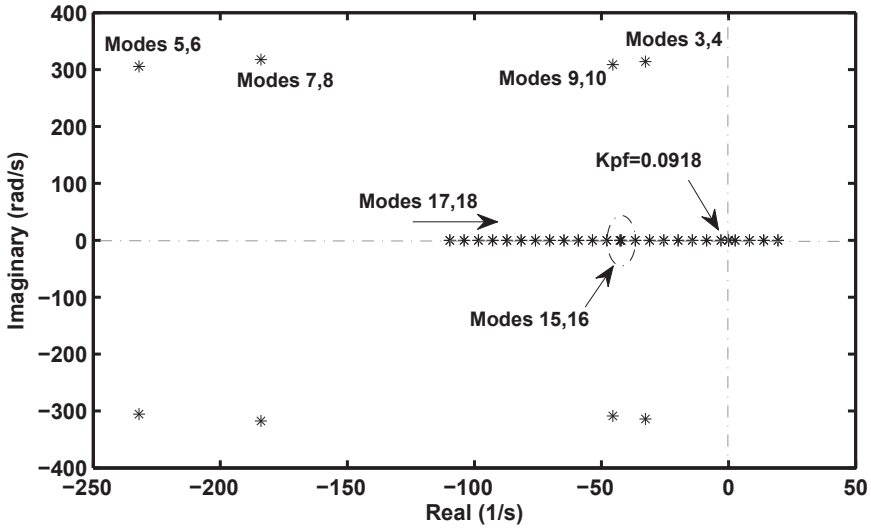

Figure 7.9: Locus of changing K_{pf} during load change

7.6.2 Parallel Inverters Based DG units

For two typical DG units, Table 7.4 shows the parameters that represent the nominal operating condition of the system. Similar to the analysis of an inverter based DG unit, the stability has been investigated based on these parameters and for the following objectives as follows.

Table 7.4: Nominal System Parameters

Parameter	Value	Parameter	Value
DG unit	50 kW	$C_{dc-input}$	5000 µF
Frequency	50 Hz	Line resistance	0.5 Ω
R_f	1 Ω	Line inductance	2 mH
L_f	3 mH	K_{pc}	12.656
C_f	50 µF	K_{ic}	0.00215

7.6.2.1 Eigenvalue Analysis

Table 7.5 shows the results of the eigenvalue analysis of the oscillatory modes. This analysis explains that the model exhibits 18 eigenvalue pairs: 9 pairs for each DG unit. In the islanding mode, while the Vf control mode is adopted by the two typical DG units which results in the same control parameters for each DG unit, the eigenvalue analysis reproduces the eigenvalues 1-18 for the second DG unit (19-36). In contrast, during the load change, different control strategies (Vf and PQ) are used by the DG units, which require non typical power control parameters, so modes 15-18 obtained for the first DG unit are different to modes 33-36 of the second DG unit.

For each DG unit, the eigenvalue analysis results in 6 complex conjugates and 3 real values. The eigenvalues 1-14 represent the seven oscillatory modes of the controlled VSI system of the first DG unit, all these modes are negative except 13 and 14, which are zero. Also, the negative real pairs (15,16) and (17,18) describe the oscillatory modes of the network line and load, respectively. The same sequence can be followed for the second DG unit. The overall results indicate that the system has good dynamic properties under the given operating condition and for the power control parameters which are found by the PSO algorithm.

7.6.2.2 Sensitivity Analysis

Using Equation (7.40), Table 7.6 shows the dominant modes 15-18 and 33-36 who have noticeable impact on the states variables of the proposed power controller. In the islanding mode, Figure 7.10 depicts the trajectory of modes 15,16 as a function of the voltage control

Table 7.5: Eigenvalues Analysis Results

	Eigen values	Islanding mode		Load change	
		Real	Imaginary	Real	Imaginary
DG 1	1,2	-891.7194	±329.0562	-894.0873	±328.9669
	3,4	-265.9247	±308.2475	-259.0511	±308.1169
	5,6	-3.15477	±314	-4.91496	±314
	7,8	-146.5525	±314.6954	-153.3870	± 314.9153
	9,10	-45.5199	± 308.7666	-45.5199	± 308.7666
	11,12	-3.34e-06	± 2.27e-05	-3.34e-06	±2.27e-05
	13,14	0	0	0	0
	15,16	-63.7946	0	-76.8579	0
	17,18	-176.4219	0	-143.9415	0
DG 2	19,20	-891.7194	±329.0562	-894.0873	±328.9669
	21,22	-265.9247	±308.2475	-259.0511	±308.1169
	23,24	-3.1547	±314	-4.91496	±314
	25,26	-146.5525	±314.6954	-153.3870	± 314.9153
	27,28	-45.5199	± 308.7666	-45.5199	± 308.7666
	29,30	-3.34e-06	± 2.27e-05	-3.34e-06	±2.27e-05
	31,32	0	0	0	0
	33,34	-63.7946	0	-83.4724	0
	35,36	-176.4219	0	-163.4658	0

gain of the first DG unit. As shown in Table 7.6, these modes are largely sensitive to the state variables of the voltage control loop. Figure 7.10 shows that changing K_{pv} in range of -1.501 to -0.0243 moves these modes to the right hand side that indicates low system stability, and the system is being unstable when the polarity of the K_{pv} value is changed. In the same way, while modes 17,18 heavily impact the state variables of the frequency control loop, the variations of the K_{pf} in the range of 4.107 to 0.229 displace these modes to the right hand plane as shown in Figure 7.11. Then, the system departs into the instability with the opposite value. For the second DG unit, same results are obtained, but for modes 33,34 and 35,36.

Similarly, during load change, the sensitivity analysis has been investigated for all control objectives. Figures 7.12, 7.13, 7.14, and 7.15 show that changing gains of the voltage, frequency, active and reactive power also relocate the modes (15,16), (17,18), (33,34), and (35,36) to the right hand side, and eventually lead to instability.

In conclusion, this analysis reveals the good system performance under the proposed control strategy. Also, appropriate ranges of the control parameters can be selected and prepared for the optimisation technique in order to ensure adequate stability margin for the system.

Table 7.6: Mode Participation Factors

States		Eigenvalues			
		15,16	17,18	33,34	35,36
Islanding	V_1	1.00	0.003	0.00	0.00
	f_1	0.001	0.97	0.00	0.00
	V_2	0.00	0.00	1	0.003
	f_2	0.00	0.00	0.001	0.97
Load change	V_1	0.94	0.001	0.00	0.00
	f_1	0.005	0.85	0.00	0.00
	P_2	0.00	0.00	1	0.003
	Q_2	0.00	0.00	0.001	0.75

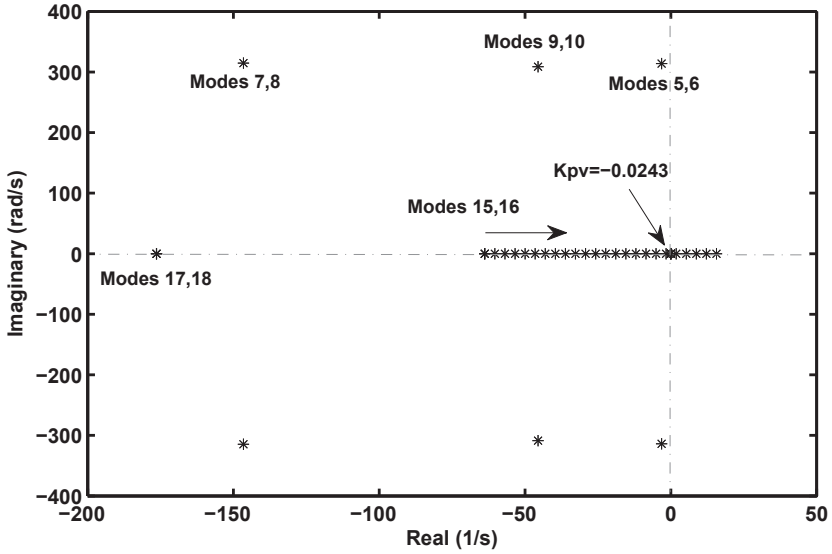

Figure 7.10: Locus of changing K_{pv} at the islanding mode

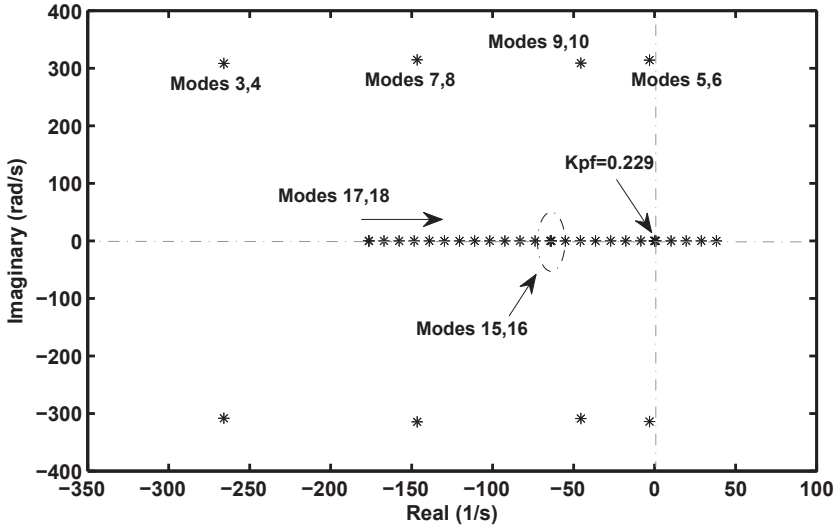

Figure 7.11: Locus of changing K_{pf} at the islanding mode

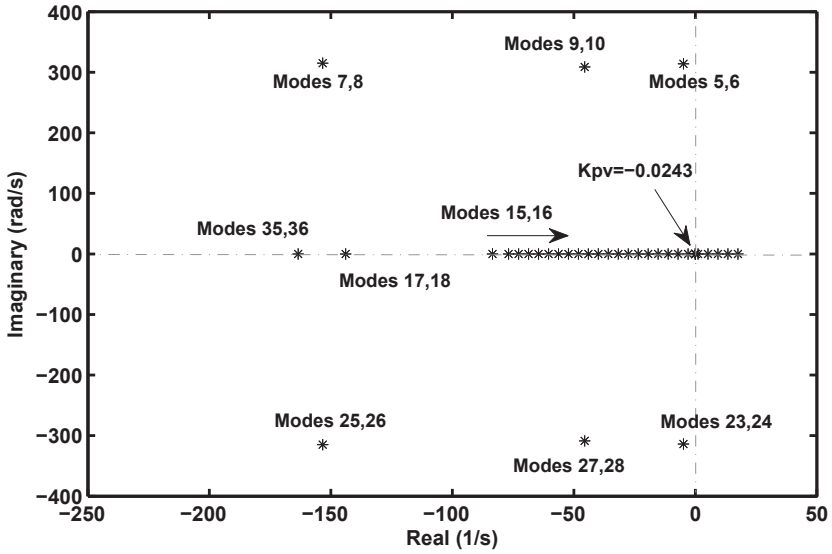

Figure 7.12: Locus of changing K_{pv} during load change

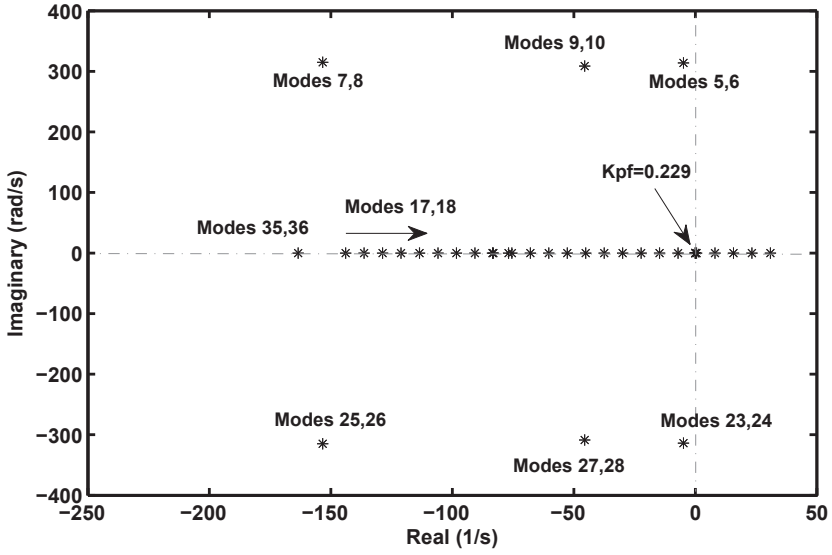

Figure 7.13: Locus of changing K_{pf} during load change

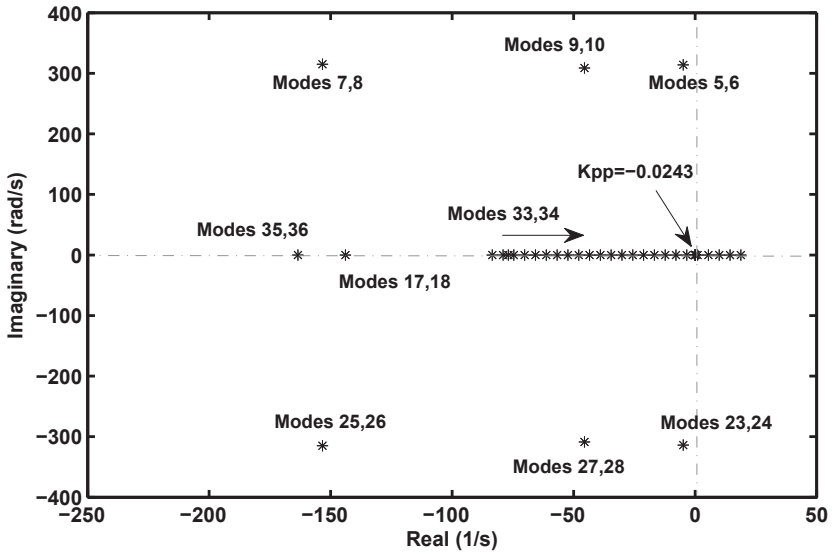

Figure 7.14: Locus of changing K_{pp} during load change

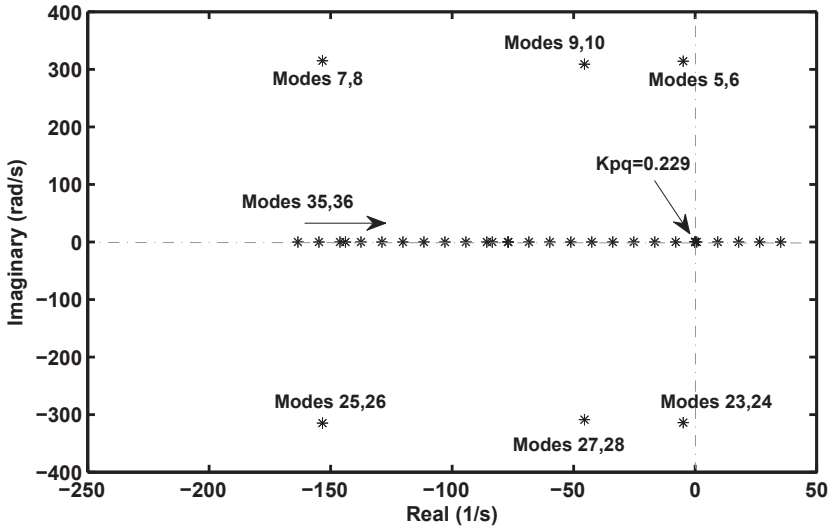

Figure 7.15: Locus of changing K_{pq} during load change

7.7 Conclusions

In this chapter, the small-signal state-space model has been developed for an autonomous microgrid operation mode. This model is used to examine the system stability by using the eigenvalue analysis in order to evaluate the system operation around the given operating point and under the proposed power controller. The modelling approach is developed in form that enables testing the stability for a number of the connected DG units in such a system. Therefore, the stability analysis of the microgrid operation that is proposed in Chapters 4 and 6 has been investigated for the cases of whether the microgrid is islanded or under load change condition. In this work, the system dynamic model is constructed based on the three main sub-models, namely: inverter, network, and load. The eigenvalue analysis is driven by the linearised system state matrix in order to investigate the system oscillatory modes and the sensitivity to the control parameters. The results of the eigenvalue analysis prove that the system offers reliable operation, and the sensitivity analysis confirms the validity of the proposed controller, which can be helpful to define the boundaries of the search process for the PSO algorithm.

Chapter 8

CONCLUSIONS

This thesis has investigated an optimal power control strategy for microgrids that relies on the PSO algorithm. The aim of this work is to maintain power quality when meeting the load for both microgrid operation modes: grid-connected and islanding. The following sections present the general conclusions and the scope for the future research.

8.1 General Conclusions

Based on the work described in the preceding chapters, the general conclusions of this thesis can be summarised in five main points.

- The PSO algorithm was implemented to solve the optimisation problem arising from the need to find optimum parameters for the proposed power controller. This algorithm is programmed to process the optimisation challenges based on the error in a real-time condition. It is also performed for each control objective individually. The performance of this algorithm provided precise results, and this approach should be adaptable to optimisation problems in many engineering applications.

- Control of the system voltage and frequency is achieved with an inverter based DG unit in an autonomous microgrid operation mode. This is done by proposing a voltage-frequency power controller based on a PSO algorithm that is used for real-time self-tuning. The fast dynamic response and an acceptable level of harmonic distortion are also obtained as two fundamental performance parameters of the system. The main goal was to improve the quality of the power supply that would otherwise be prone to sudden changes such as the transition from the grid-connected to the islanding operation mode or a load change. These changes can cause a voltage drop, severe deviation of the frequency, and long transient period. Therefore, it is

necessary to supply reliable power to maintain the system, in the face of such threats, to avoid the negative impacts for the end user, in particular for sensitive loads.

- The flow of the active and reactive power is regulated in grid-connected microgrid operation mode. This objective is achieved by proposing an active-reactive power controller based on the PSO algorithm that is employed for a real-time self-tuning. The load demand is equally shared between the microgrid and utility, in particular when the microgrid started in grid-connected operation mode or during a load change. Therefore, the Peak Shaving for the load demand is satisfactorily performed by reducing the imported power from the utility to the half. Consequently, this strategy can provide significant implications for the microgrid scenario, namely: decreasing the dependency on the bulk power system, increasing the market penetration of micro-sources, and reducing electric power costs.

- The regulation of the system voltage and frequency, associated with an appropriate power sharing mechanism between the DG units, was investigated for an autonomous microgrid. In other words, the voltage-frequency control mode was used for maintaining the system voltage and frequency within acceptable limits, whether the microgrid started in islanding operation mode or during a load change. The active-reactive power control mode is adopted only during the load change to keep injecting sustained output power from the connected DG units, except for one DG unit that stayed in voltage-frequency mode to control the system voltage and frequency. The main advantages of this strategy were to; supply reliable power to the load, ensure best utilisation of the connected DG units by exploiting their output power maximally, and properly distribute the abundant load demand among the DG units.

- The stability analysis was investigated for an autonomous microgrid. The small-signal state-space model for the parallel inverters was developed to represent the overall model for the microgrid. This model was constructed in form that allows examination of the stability of the microgrid which itself includes any number of connected DG units. The results show that the system is stable under the proposed power controller and the given operating point. The validity of the proposed power controller was also proved when the sensitivity to the control parameters were considered. The main benefit of developing the small-signal dynamic model was to verify the reliability of the system's operation. This analysis was very useful for measur-

ing the dependency, of the system's stability, on its state variables. Therefore, the sensitivity analysis provided a significant advantage, in being helpful for defining the boundaries of the search process for the PSO algorithm.

8.2 Future Work

The aforementioned conclusions led to several proposals for future research. These can be summarised in three main points.

- This thesis has successfully presented a modelling approach for the microgrid and an optimal power controller that used a PSO algorithm for solving the optimisation problems. The overall simulation results satisfied the aims of this work. This success should justify a scaling up of the simulation to a laboratory-based pilot microgrid incorporating the proposed power controller. The advantage of this setup is that it provides more validation of this research, and also creates a hardware prototype that can be used in practical applications.

- Sharing power between the microgrid and utility has been organised in grid-connected mode for the Peak Shaving facility. The proposed power control strategy provided equal load sharing whether the microgrid started in a utility mode or during a load change. This outcome justifies the development of a central energy management unit that can help share the load among the DG units for an economic power dispatch. In particular, this unit could be developed to share the load based on the analysis of the load demand, the availability of the power supply, and the time response.

- The PSO algorithm has been implemented for real-time self-tuning of the proposed power controller. This algorithm offered appropriate performance for finding the optimal control parameters required to reach the control objectives. The search process boundary was the main limitation and necessitated a sensitivity analysis through the linearised small-signal dynamic model. However, another automatic method could be developed based on the model's information to address this limitation. This approach could be interfaced with the applied PSO algorithm to provide online estimation for the search process boundaries.

References

[1] R. H. Lasseter, "Microgrids," in *Power Engineering Society Winter Meeting, 2002. IEEE*, vol. 1. IEEE, 2002, pp. 305–308.

[2] R. Strzelecki and G. Benysek, *Power electronics in smart electrical energy networks*. Verlag London: Springer, 2008.

[3] F. Katiraei and M. R. Iravani, "Power management strategies for a microgrid with multiple distributed generation units," *Power Systems, IEEE Transactions on*, vol. 21, no. 4, pp. 1821–1831, 2006.

[4] S. Chowdhury, S. Chowdhury, and P. Crossley, *Microgrids and active distribution networks*. Institution of Engineering and Technology, 2009.

[5] M. Pedrasa and T. Spooner, "A survey of techniques used to control microgrid generation and storage during island operation," in *Proceedings of the Australian Universities Power Engineering Conference*, 2006.

[6] Y. Abdelrady and I. Mohamed, *New Control Algorithms for The Distributed Generation Interface*. Waterloo: VDM Verleg, 2008.

[7] R. Majumder, B. Chaudhuri, A. Ghosh, G. Ledwich, and F. Zare, "Improvement of stability and load sharing in an autonomous microgrid using supplementary droop control loop," *Power Systems, IEEE Transactions on*, vol. 25, no. 2, pp. 796–808, 2010.

[8] I. Vechiu, O. Curea, A. Llaria, and H. Camblong, "Control of power converters for microgrids," *COMPEL: The International Journal for Computation and Mathematics in Electrical and Electronic Engineering*, vol. 30, no. 1, pp. 300–309, 2011.

[9] M. Suter, "Active filter for a microturbine," in *Telecommunications Energy Conference, 2001. INTELEC 2001. Twenty-Third International*. IET, 2001, pp. 162–165.

[10] M. Etezadi-Amoli and K. Choma, "Electrical performance characteristics of a new micro-turbine generator," in *Power Engineering Society Winter Meeting, 2001. IEEE*, vol. 2. IEEE, 2001, pp. 736–740.

[11] M. Davis, A. Gifford, and T. Krupa, "Microturbines-an economic and reliability evaluation for commercial, residential, and remote load applications," *Power Systems, IEEE Transactions on*, vol. 14, no. 4, pp. 1556–1562, 1999.

[12] M. Ellis, M. Von Spakovsky, and D. Nelson, "Fuel cell systems: efficient, flexible energy conversion for the 21st century," *Proceedings of the IEEE*, vol. 89, no. 12, pp. 1808–1818, 2001.

[13] M. Farooque and H. Maru, "Fuel cells-the clean and efficient power generators," *Proceedings of the IEEE*, vol. 89, no. 12, pp. 1819–1829, 2001.

[14] Y. Kim and S. Kim, "An electrical modeling and fuzzy logic control of a fuel cell generation system," *Energy Conversion, IEEE Transactions on*, vol. 14, no. 2, pp. 239–244, 1999.

[15] B. Ummels, M. Gibescu, E. Pelgrum, W. Kling, and A. Brand, "Impacts of wind power on thermal generation unit commitment and dispatch," *Energy Conversion, IEEE Transactions on*, vol. 22, no. 1, pp. 44–51, 2007.

[16] E. Muljadi, C. Butterfield, B. Parsons, and A. Ellis, "Effect of variable speed wind turbine generator on stability of a weak grid," *Energy Conversion, IEEE Transactions on*, vol. 22, no. 1, pp. 29–36, 2007.

[17] R. Billinton and W. Wangdee, "Reliability-based transmission reinforcement planning associated with large-scale wind farms," *Power Systems, IEEE Transactions on*, vol. 22, no. 1, pp. 34–41, 2007.

[18] T. Ackermann *et al.*, *Wind power in power systems*. Wiley Online Library, 2005, vol. 140.

[19] T. Thiringer, "Power quality measurements performed on a low-voltage grid equipped with two wind turbines," *Energy Conversion, IEEE Transactions on*, vol. 11, no. 3, pp. 601–606, 1996.

[20] J. Matevosyan and L. Soder, "Minimization of imbalance cost trading wind power on the short-term power market," *Power Systems, IEEE Transactions on*, vol. 21, no. 3, pp. 1396–1404, 2006.

[21] E. Kern Jr, E. Gulachenski, and G. Kern, "Cloud effects on distributed photovoltaic generation: Slow transients at the gardner, massachusetts photovoltaic experiment," *Energy Conversion, IEEE Transactions on*, vol. 4, no. 2, pp. 184–190, 1989.

[22] Y. Tan and D. Kirschen, "Impact on the power system of a large penetration of photovoltaic generation," in *Power Engineering Society General Meeting, 2007. IEEE*. IEEE, 2007, pp. 1–8.

[23] W. Xiao, W. Dunford, P. Palmer, and A. Capel, "Regulation of photovoltaic voltage," *Industrial Electronics, IEEE Transactions on*, vol. 54, no. 3, pp. 1365–1374, 2007.

[24] M. Green, "Recent developments and future prospects for third generation and other advanced cells," in *Photovoltaic Energy Conversion, Conference Record of the 2006 IEEE 4th World Conference on*, vol. 1. IEEE, 2006, pp. 15–19.

[25] P. Ribeiro, B. Johnson, M. Crow, A. Arsoy, and Y. Liu, "Energy storage systems for advanced power applications," *Proceedings of the IEEE*, vol. 89, no. 12, pp. 1744–1756, 2001.

[26] S. Daniel and N. AmmasaiGounden, "A novel hybrid isolated generating system based on pv fed inverter-assisted wind-driven induction generators," *Energy Conversion, IEEE Transactions on*, vol. 19, no. 2, pp. 416–422, 2004.

[27] Y. Mohamed, *New Control Algorithms for The Distributed Generation Interface: Plug-and-Play Integration and Robust Operation in Grid-Connected and Micro-Grid Modes*. Lightning Source Incorporated, 2009.

[28] "IEEE Standard for interconnecting distributed resources with electric power systems," *IEEE Std 1547-2003*, 2003.

[29] Z. Qingrong and C. Liuchen, "Study of advanced current control strategies for three-phase grid-connected pwm inverters for distributed generation," in *Control Applications, 2005. CCA 2005. Proceedings of 2005 IEEE Conference on*, pp. 1311–1316.

[30] K. Bong-Hwan, M. Byung-Duk, and Y. Jang-Hyoun, "An improved space-vector-based hysteresis current controller," *Industrial Electronics, IEEE Transactions on*, vol. 45, no. 5, pp. 752–760, 1998.

[31] L. Malesani and P. Tenti, "A novel hysteresis control method for current-controlled voltage-source pwm inverters with constant modulation frequency," *Industry Applications, IEEE Transactions on*, vol. 26, no. 1, pp. 88–92, 1990.

[32] T. Chun and M. Choi, "Development of adaptive hysteresis band current control strategy of pwm inverter with constant switching frequency," in *Applied Power Electronics Conference and Exposition, 1996. APEC'96. Conference Proceedings 1996., Eleventh Annual*, vol. 1. IEEE, 1996, pp. 194–199.

[33] L. Malesani, P. Tenti, E. Gaio, and R. Piovan, "Improved current control technique of vsi pwm inverters with constant modulation frequency and extended voltage range," *Industry Applications, IEEE Transactions on*, vol. 27, no. 2, pp. 365–369, 1991.

[34] M. P. Kazmierkowski and L. Malesani, "Current control techniques for three-phase voltage-source pwm converters: a survey," *Industrial Electronics, IEEE Transactions on*, vol. 45, no. 5, pp. 691–703, 1998.

[35] A. Schonung and H. Stemmler, "Static frequency changers with subharmonic control in conjunction with reversible variable speed ac drives," *Brown Boveri Rev*, vol. 51, no. 8/9, pp. 555–577, 1964.

[36] A. Nabae, S. Ogasawara, and H. Akagi, "A novel control scheme for current-controlled pwm inverters," *Industry Applications, IEEE Transactions on*, no. 4, pp. 697–701, 1986.

[37] Y. Wei, Z. Chengyong, L. Yi, and L. Gang, "A scheme of connecting microgird to ac grid via flexible power electronics interface," in *Power System Technology (POWERCON), 2010 International Conference on*, pp. 1–6.

[38] F. Gakis and S. Papathanassiou, "Simple control schemes for grid-connected three-phase voltage-source inverters of dg units," in *Proc. XVII International Conference on Electrical Machines, ICEM*, 2006, pp. 2–5.

[39] Z. Hui, Z. Hongwei, R. Jing, L. Weizeng, R. Shaohua, and G. Yongjun, "Three-phase grid-connected photovoltaic system with svpwm current controller," in *Power Electronics and Motion Control Conference, 2009. IPEMC '09. IEEE 6th International*, pp. 2161–2164.

[40] I. J. Gabe, V. F. Montagner, and H. Pinheiro, "Design and implementation of a robust current controller for vsi connected to the grid through an <emphasis emphasistype="italic">lcl</emphasis> filter," *Power Electronics, IEEE Transactions on*, vol. 24, no. 6, pp. 1444–1452, 2009.

[41] G. Perantzakis, F. Xepapas, S. Papathanassiou, and S. Manias, "A predictive current control technique for three-level npc voltage source inverters," in *Power Electronics Specialists Conference, 2005. PESC'05. IEEE 36th.* IEEE, 2005, pp. 1241–1246.

[42] Y. A. R. Mohamed and E. F. El-Saadany, "Adaptive discrete-time grid-voltage sensorless interfacing scheme for grid-connected dg-inverters based on neural-network identification and deadbeat current regulation," *Power Electronics, IEEE Transactions on*, vol. 23, no. 1, pp. 308–321, 2008.

[43] M. Jamshidi, *Systems of systems engineering: principles and applications.* CRC, 2008.

[44] S. Ahn, J. Park, I. Chung, S. Moon, S. Kang, and S. Nam, "Power-sharing method of multiple distributed generators considering control modes and configurations of a microgrid," *Power Delivery, IEEE Transactions on*, vol. 25, no. 3, pp. 2007–2016, 2010.

[45] U. Borup, F. Blaabjerg, and P. Enjeti, "Sharing of nonlinear load in parallel-connected three-phase converters," *Industry Applications, IEEE Transactions on*, vol. 37, no. 6, pp. 1817–1823, 2001.

[46] D. Wei, T. Xisheng, and Q. Zhiping, "Research on dynamic stability of hybrid wind/pv system based on micro-grid," in *Electrical Machines and Systems, 2008. ICEMS 2008. International Conference on*, pp. 2627–2632.

[47] C. Vilar Moreno, H. Amaris Duarte, and J. Usaola Garcia, "Propagation of flicker in electric power networks due to wind energy conversions systems," *Energy Conversion, IEEE Transactions on*, vol. 17, no. 2, pp. 267–272, 2002.

[48] A. Woyte, V. Van Thong, R. Belmans, and J. Nijs, "Voltage fluctuations on distribution level introduced by photovoltaic systems," *Energy Conversion, IEEE Transactions on*, vol. 21, no. 1, pp. 202–209, 2006.

[49] M. Marei, E. El-Saadany, and M. Salama, "A novel control algorithm for the dg interface to mitigate power quality problems," *Power Delivery, IEEE Transactions on*, vol. 19, no. 3, pp. 1384–1392, 2004.

[50] H. Fujita and H. Akagi, "Voltage-regulation performance of a shunt active filter intended for installation on a power distribution system," *Power Electronics, IEEE Transactions on*, vol. 22, no. 3, pp. 1046–1053, 2007.

[51] P. Lehn and M. Iravani, "Experimental evaluation of statcom closed loop dynamics," *Power Delivery, IEEE Transactions on*, vol. 13, no. 4, pp. 1378–1384, 1998.

[52] J. Lopes, C. Moreira, and A. Madureira, "Defining control strategies for microgrids islanded operation," *Power Systems, IEEE Transactions on*, vol. 21, no. 2, pp. 916–924, 2006.

[53] M. Aghaebrahimi, M. Amiri, and S. Zahiri, "An immune-based optimization method for distributed generation placement in order to optimize voltage profile," in *Sustainable Power Generation and Supply, 2009. SUPERGEN'09. International Conference on*. IEEE, 2009, pp. 1–7.

[54] M. A. Hassan and M. A. Abido, "Optimal design of microgrids in autonomous and grid-connected modes using particle swarm optimization," *Power Electronics, IEEE Transactions on*, vol. 26, no. 3, pp. 755–769, 2011.

[55] X. Yu and A. Khambadkone, "Combined active and reactive power control of power converter building block to facilitate the connection of micro-grid to electric power system," in *Energy Conversion Congress and Exposition, 2009. ECCE 2009. IEEE*. IEEE, 2009, pp. 1444–1450.

[56] F. Carastro, M. Sumner, and P. Zanchetta, "Shunt active filter for voltage and power improvements within a micro-grid," in *Power Electronics and Motion Control Conference, 2006. EPE-PEMC 2006. 12th International*. IEEE, 2006, pp. 1665–1670.

[57] M. Aliabadi, B. Behbahani, and A. Jalilvand, "Combination of ga and opf for allocation and active and reactive power optimization in distributed generation units," in *Power and Energy Conference, 2008. PECon 2008. IEEE 2nd International*. IEEE, 2008, pp. 1541–1544.

[58] Y. Xue, J. Deng, and S. Ma, "Power flow control of a distributed generation unit in micro-grid," in *Power Electronics and Motion Control Conference, 2009. IPEMC'09. IEEE 6th International*. IEEE, 2009, pp. 2122–2125.

[59] E. Sortomme and M. El-Sharkawi, "Optimal power flow for a system of microgrids with controllable loads and battery storage," in *Power Systems Conference and Exposition, 2009. PSCE'09. IEEE/PES*. IEEE, 2009, pp. 1–5.

[60] H. Wei, W. Ziping, N. Ming, Z. Jianhua, G. Yuanbo, and W. Chong, "Dynamic modelling and simulation of microturbine generation system for the parallel operation

of microgrid," in *Sustainable Power Generation and Supply, 2009. SUPERGEN'09. International Conference on.* IEEE, 2009, pp. 1–8.

[61] M. Reza, D. Sudarmadi, F. Viawan, W. Kling, and L. Van Der Sluis, "Dynamic stability of power systems with power electronic interfaced dg," in *Power Systems Conference and Exposition, 2006. PSCE'06. 2006 IEEE PES.* IEEE, 2006, pp. 1423–1428.

[62] F. Katiraei, M. Iravani, and P. Lehn, "Micro-grid autonomous operation during and subsequent to islanding process," *Power Delivery, IEEE Transactions on*, vol. 20, no. 1, pp. 248–257, 2005.

[63] J. Guerrero, L. de Vicuña, J. Matas, M. Castilla, and J. Miret, "A wireless controller to enhance dynamic performance of parallel inverters in distributed generation systems," *Power Electronics, IEEE Transactions on*, vol. 19, no. 5, pp. 1205–1213, 2004.

[64] F. Katiraei, M. Iravani, and P. Lehn, "Small-signal dynamic model of a micro-grid including conventional and electronically interfaced distributed resources," *Generation, Transmission & Distribution, IET*, vol. 1, no. 3, pp. 369–378, 2007.

[65] Z. Yu, J. Zhenhua, and Y. Xunwei, "Small-signal modeling and analysis of parallel-connected voltage source inverters," in *Power Electronics and Motion Control Conference, 2009. IPEMC '09. IEEE 6th International*, pp. 377–383.

[66] M. Marwali, J. Jung, and A. Keyhani, "Control of distributed generation systems-part ii: Load sharing control," *Power Electronics, IEEE Transactions on*, vol. 19, no. 6, pp. 1551–1561, 2004.

[67] M. López, L. de Vicuña, M. Castilla, P. Gayà, and O. López, "Current distribution control design for paralleled dc/dc converters using sliding-mode control," *Industrial Electronics, IEEE Transactions on*, vol. 51, no. 2, pp. 419–428, 2004.

[68] D. Vilathgamuwa, P. Loh, and Y. Li, "Protection of microgrids during utility voltage sags," *Industrial Electronics, IEEE Transactions on*, vol. 53, no. 5, pp. 1427–1436, 2006.

[69] M. Marwali, M. Dai, and A. Keyhani, "Robust stability analysis of voltage and current control for distributed generation systems," *Energy Conversion, IEEE Transactions on*, vol. 21, no. 2, pp. 516–526, 2006.

[70] M. Marwali, J. Jung, and A. Keyhani, "Stability analysis of load sharing control for distributed generation systems," *Energy Conversion, IEEE Transactions on*, vol. 22, no. 3, pp. 737–745, 2007.

[71] S. Kannan, S. M. R. Slochanal, and N. P. Padhy, "Application and comparison of metaheuristic techniques to generation expansion planning problem," *Power Systems, IEEE Transactions on*, vol. 20, no. 1, pp. 466–475, 2005.

[72] F. Wu, Y. Zheng, H. Yunhe, and N. Yixin, "Applications of ai techniques to generation planning and investment," in *Power Engineering Society General Meeting, 2004. IEEE*, pp. 936–940 Vol.1.

[73] A. Schrijver, *Theory of linear and integer programming.* John Wiley & Sons Inc, 1998.

[74] A. Farag, S. Al-Baiyat, and T. C. Cheng, "Economic load dispatch multiobjective optimization procedures using linear programming techniques," *Power Systems, IEEE Transactions on*, vol. 10, no. 2, pp. 731–738, 1995.

[75] R. A. Jabr, A. H. Coonick, and B. J. Cory, "A homogeneous linear programming algorithm for the security constrained economic dispatch problem," *Power Systems, IEEE Transactions on*, vol. 15, no. 3, pp. 930–936, 2000.

[76] J. K. Delson and S. M. Shahidehpour, "Linear programming applications to power system economics, planning and operations," *Power Systems, IEEE Transactions on*, vol. 7, no. 3, pp. 1155–1163, 1992.

[77] C. N. Kurucz, D. Brandt, and S. Sim, "A linear programming model for reducing system peak through customer load control programs," *Power Systems, IEEE Transactions on*, vol. 11, no. 4, pp. 1817–1824, 1996.

[78] H. M. Khodr, J. F. Gomez, L. Barnique, J. H. Vivas, P. Paiva, J. M. Yusta, and A. J. Urdaneta, "A linear programming methodology for the optimization of electric power-generation schemes," *Power Systems, IEEE Transactions on*, vol. 17, no. 3, pp. 864–869, 2002.

[79] K. H. Ng and G. B. Sheble, "Direct load control-a profit-based load management using linear programming," *Power Systems, IEEE Transactions on*, vol. 13, no. 2, pp. 688–694, 1998.

[80] B. Chattopadhyay, M. S. Sachdev, and T. S. Sidhu, "An on-line relay coordination algorithm for adaptive protection using linear programming technique," *Power Delivery, IEEE Transactions on*, vol. 11, no. 1, pp. 165–173, 1996.

[81] H. B. Elrefaie, M. R. Irving, and S. Zitouni, "A parallel processing algorithm for coordination of directional overcurrent relays in interconnected power systems," *Generation, Transmission and Distribution, IEE Proceedings-*, vol. 141, no. 5, pp. 514–520, 1994.

[82] D. Chattopadhyay, "A practical maintenance scheduling program mathematical model and case study," *Power Systems, IEEE Transactions on*, vol. 13, no. 4, pp. 1475–1480, 1998.

[83] A. A. El-Keib and H. Singh, "Fast linear programming state estimation using the dual formulation," *Power Systems, IEEE Transactions on*, vol. 7, no. 2, pp. 620–628, 1992.

[84] I. O. Habiballah and M. R. Irving, "Observability analysis for state estimation using linear programming," *Generation, Transmission and Distribution, IEE Proceedings-*, vol. 148, no. 2, pp. 142–145, 2001.

[85] A. L. Motto, J. M. Arroyo, and F. D. Galiana, "A mixed-integer lp procedure for the analysis of electric grid security under disruptive threat," *Power Systems, IEEE Transactions on*, vol. 20, no. 3, pp. 1357–1365, 2005.

[86] N. Alguacil, A. L. Motto, and A. J. Conejo, "Transmission expansion planning: a mixed-integer lp approach," *Power Systems, IEEE Transactions on*, vol. 18, no. 3, pp. 1070–1077, 2003.

[87] F. G. M. Lima, F. D. Galiana, I. Kockar, and J. Munoz, "Phase shifter placement in large-scale systems via mixed integer linear programming," *Power Systems, IEEE Transactions on*, vol. 18, no. 3, pp. 1029–1034, 2003.

[88] L. Bahiense, G. C. Oliveira, M. Pereira, and S. Granville, "A mixed integer disjunctive model for transmission network expansion," *Power Systems, IEEE Transactions on*, vol. 16, no. 3, pp. 560–565, 2001.

[89] M. A. Farrag and M. M. El-Metwally, "New method for transmission planning using mixed-integer programming," *Generation, Transmission and Distribution, IEE Proceedings C*, vol. 135, no. 4, pp. 319–323, 1988.

[90] F. Soudi and K. Tomsovic, "Optimized distribution protection using binary programming," *Power Delivery, IEEE Transactions on*, vol. 13, no. 1, pp. 218–224, 1998.

[91] A. J. Urdaneta, P. C. Paiva, H. Khodr, J. Dominguez-Navarro, and J. M. Yustam, "Integral planning of primary-secondary distribution systems using mixed integer linear programming," in *Power Engineering Society General Meeting, 2005. IEEE*, p. 2391 Vol. 3.

[92] S. Ashok and R. Banerjee, "An optimization mode for industrial load management," *Power Systems, IEEE Transactions on*, vol. 16, no. 4, pp. 879–884, 2001.

[93] J. Nocedal and S. Wright, *Numerical optimization*. Springer verlag, 1999.

[94] L. A. L. Zarate, C. A. Castro, J. L. M. Ramos, and E. R. Ramos, "Fast computation of voltage stability security margins using nonlinear programming techniques," *Power Systems, IEEE Transactions on*, vol. 21, no. 1, pp. 19–27, 2006.

[95] A. Schellenberg, W. Rosehart, and J. A. Aguado, "Cumulant-based stochastic nonlinear programming for variance constrained voltage stability analysis of power systems," *Power Systems, IEEE Transactions on*, vol. 21, no. 2, pp. 579–585, 2006.

[96] S. Bruno, E. De Tuglie, M. La Scala, and P. Scarpellini, "Dynamic security corrective control by upfcs," *Power Systems, IEEE Transactions on*, vol. 16, no. 3, pp. 490–497, 2001.

[97] E. De Tuglie, M. Dicorato, M. La Scala, and P. Scarpellini, "A static optimization approach to assess dynamic available transfer capability," *Power Systems, IEEE Transactions on*, vol. 15, no. 3, pp. 1069–1076, 2000.

[98] D. Pudjianto, S. Ahmed, and G. Strbac, "Allocation of var support using lp and nlp based optimal power flows," *Generation, Transmission and Distribution, IEE Proceedings-*, vol. 149, no. 4, pp. 377–383, 2002.

[99] A. Ramos, I. J. Perez-Arriaga, and J. Bogas, "A nonlinear programming approach to optimal static generation expansion planning," *Power Systems, IEEE Transactions on*, vol. 4, no. 3, pp. 1140–1146, 1989.

[100] D. E. Lidgate and B. H. Amir, "Optimal operational planning for a hydro-electric generation system," *Generation, Transmission and Distribution, IEE Proceedings C*, vol. 135, no. 3, pp. 169–181, 1988.

[101] G. B. Shrestha, B. K. Pokharel, L. Tek Tjing, and S. E. Fleten, "Medium term power planning with bilateral contracts," *Power Systems, IEEE Transactions on*, vol. 20, no. 2, pp. 627–633, 2005.

[102] A. H. Escobar, R. A. Gallego, and R. Romero, "Multistage and coordinated planning of the expansion of transmission systems," *Power Systems, IEEE Transactions on*, vol. 19, no. 2, pp. 735–744, 2004.

[103] E. E. Aponte and J. K. Nelson, "Time optimal load shedding for distributed power systems," *Power Systems, IEEE Transactions on*, vol. 21, no. 1, pp. 269–277, 2006.

[104] W. Hua, H. Sasaki, J. Kubokawa, and R. Yokoyama, "An interior point nonlinear programming for optimal power flow problems with a novel data structure," *Power Systems, IEEE Transactions on*, vol. 13, no. 3, pp. 870–877, 1998.

[105] W. Hau, H. Sasaki, J. Kubokawa, and R. Yokoyama, "Large scale hydrothermal optimal power flow problems based on interior point nonlinear programming," *Power Systems, IEEE Transactions on*, vol. 15, no. 1, pp. 396–403, 2000.

[106] H. Habibollahzadeh, G. X. Luo, and A. Semlyen, "Hydrothermal optimal power flow based on a combined linear and nonlinear programming methodology," *Power Systems, IEEE Transactions on*, vol. 4, no. 2, pp. 530–537, 1989.

[107] G. L. Torres and V. H. Quintana, "On a nonlinear multiple-centrality-corrections interior-point method for optimal power flow," *Power Systems, IEEE Transactions on*, vol. 16, no. 2, pp. 222–228, 2001.

[108] R. A. Gallego, A. J. Monticelli, and R. Romero, "Optimal capacitor placement in radial distribution networks," *Power Systems, IEEE Transactions on*, vol. 16, no. 4, pp. 630–637, 2001.

[109] S. Virmani, E. C. Adrian, K. Imhof, and S. Mukherjee, "Implementation of a lagrangian relaxation based unit commitment problem," *Power Systems, IEEE Transactions on*, vol. 4, no. 4, pp. 1373–1380, 1989.

[110] E. Diaz-Dorado and J. C. Pidre, "Optimal planning of unbalanced networks using dynamic programming optimization," *Power Systems, IEEE Transactions on*, vol. 19, no. 4, pp. 2077–2085, 2004.

[111] Z. Ouyang and S. M. Shahidehpour, "An intelligent dynamic programming for unit commitment application," *Power Systems, IEEE Transactions on*, vol. 6, no. 3, pp. 1203–1209, 1991.

[112] W. J. Hobbs, G. Hermon, S. Warner, and G. B. Shelbe, "An enhanced dynamic programming approach for unit commitment," *Power Systems, IEEE Transactions on*, vol. 3, no. 3, pp. 1201–1205, 1988.

[113] N. G. Boulaxis and M. P. Papadopoulos, "Optimal feeder routing in distribution system planning using dynamic programming technique and gis facilities," *Power Delivery, IEEE Transactions on*, vol. 17, no. 1, pp. 242–247, 2002.

[114] H. Kun Yuan, "Demand subscription services-an iterative dynamic programming for the substation suffering from capacity shortage," *Power Systems, IEEE Transactions on*, vol. 18, no. 2, pp. 947–953, 2003.

[115] E. Diaz-Dorado, E. Miguez, and J. Cidras, "Design of large rural low-voltage networks using dynamic programming optimization," *Power Systems, IEEE Transactions on*, vol. 16, no. 4, pp. 898–903, 2001.

[116] M. Mohammadi, S. Hosseinian, and G. Gharehpetian, "Ga-based optimal sizing of microgrid and dg units under pool and hybrid electricity markets," *International Journal of Electrical Power and Energy Systems*, vol. 35, no. 1, pp. 83 – 92, 2012.

[117] L. Arya, L. Titare, and D. Kothari, "Improved particle swarm optimization applied to reactive power reserve maximization," *International Journal of Electrical Power and Energy Systems*, vol. 32, no. 5, pp. 368 – 374, 2010.

[118] R. Hassan, B. Cohanim, O. De Weck, and G. Venter, "A comparison of particle swarm optimization and the genetic algorithm," in *Proceedings of the 1st AIAA Multidisciplinary Design Optimization Specialist Conference*, 2005.

[119] P. de Moura Oliveira, "Modern heuristics review for pid control," in *6th International PhD Workshop on Systems and Control: a Young Generation Viewpoint*, 2005, pp. 4–8.

[120] J. Kennedy, "Swarm intelligence," *Handbook of Nature-Inspired and Innovative Computing*, pp. 187–219, 2006.

[121] J. Robinson and Y. Rahmat-Samii, "Particle swarm optimization in electromagnetics," *Antennas and Propagation, IEEE Transactions on*, vol. 52, no. 2, pp. 397–407, 2004.

[122] R. Eberhart and J. Kennedy, "A new optimizer using particle swarm theory," in *Micro Machine and Human Science, 1995. MHS'95., Proceedings of the Sixth International Symposium on.* Ieee, 1995, pp. 39–43.

[123] Y. Shuyuan, W. Min, and j. Licheng, "A quantum particle swarm optimization," in *Evolutionary Computation, 2004. CEC2004. Congress on*, vol. 1, pp. 320–324 Vol.1.

[124] M. Millonas, "Swarms, phase transitions, and collective intelligence," Los Alamos National Lab., NM (United States), Tech. Rep., 1992.

[125] Yang and Xin-She, *Engineering optimization: An introduction with metaheuristic application.* Hoboken: John Wiley, 2010.

[126] Y. del Valle, G. K. Venayagamoorthy, S. Mohagheghi, J. C. Hernandez, and R. G. Harley, "Particle swarm optimization: Basic concepts, variants and applications in power systems," *Evolutionary Computation, IEEE Transactions on*, vol. 12, no. 2, pp. 171–195, 2008.

[127] N. Killingsworth and M. Krstic, "Auto-tuning of pid controllers via extremum seeking," in *American Control Conference, 2005. Proceedings of the 2005*, pp. 2251–2256 vol. 4.

[128] C. Il-Yop, L. Wenxin, D. A. Cartes, and K. Schoder, "Control parameter optimization for a microgrid system using particle swarm optimization," in *Sustainable Energy Technologies, 2008. ICSET 2008. IEEE International Conference on*, pp. 837–842.

[129] P. Dash, M. Padhee, and S. Barik, "Estimation of power quality indices in distributed generation systems during power islanding conditions," *International Journal of Electrical Power and Energy Systems*, vol. 36, no. 1, pp. 18 – 30, 2012.

[130] R. BiYing, T. XiangQian, T. Sha, and S. XiangDong, "Research on the control strategy of inverters in the micro-grid," in *Power and Energy Engineering Conference (APPEEC), 2010 Asia-Pacific*, pp. 1–4.

[131] J. A. P. Lopes, C. L. Moreira, A. G. Madureira, F. O. Resende, X. Wu, N. Jayawarna, Y. Zhang, N. Jenkins, F. Kanellos, and N. Hatziargyriou, "Control strategies for mi-

crogrids emergency operation," in *Future Power Systems, 2005 International Conference on*, pp. 6 pp.–6.

[132] L. L. Grigsby, *Power system stability and control*. Boca Raton: CRC Press, 2007, 2007006226 editor, Leonard Lee Grigsby. ill. ; 27 cm. Includes bibliographical references and index.

[133] N. Kroutikova, C. A. Hernandez-Aramburo, and T. C. Green, "State-space model of grid-connected inverters under current control mode," *Electric Power Applications, IET*, vol. 1, no. 3, pp. 329–338, 2007.

[134] W. Al-Saedi, S. W. Lachowicz, and D. Habibi, "An optimal current control strategy for a three-phase grid-connected photovoltaic system using particle swarm optimization," in *Power Engineering and Automation Conference (PEAM), 2011 IEEE*, vol. 1, pp. 286–290.

[135] N. Pogaku, M. Prodanovic, and T. C. Green, "Modeling, analysis and testing of autonomous operation of an inverter-based microgrid," *Power Electronics, IEEE Transactions on*, vol. 22, no. 2, pp. 613–625, 2007.

[136] S. Li, E. H. Abed, M. A. Hassouneh, Y. Huizhong, and M. S. Saad, "Mode in output participation factors for linear systems," in *American Control Conference (ACC), 2010*, pp. 956–961.

Appendix A

PARK AND CLARKE TRANSFORMATIONS

Park and Clarke transformations are mathematical transformations that use space vectors to simplify the three-phase quantities in electrical engineering. These can be employed in forward and inverse conversions as follows.

A.1 Forward and Inverse Park Transformation

The forward Park transformation converts a three-phase system (a, b, c) to a two-phase coordinate system (d, q). Figure A.1 shows the vector diagram of the space vector and projection of the space vector to the quadrature-phase components (d, q). The quadrature-phase vectors v_d and v_q are related to the actual three-phase vectors as follows.

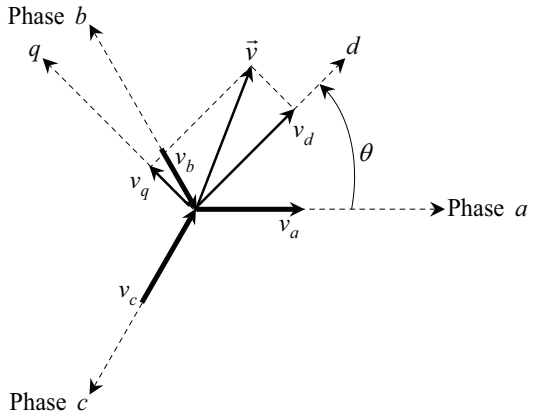

Figure A.1: Park Transformation

$$v_d = \frac{2}{3}\left[v_a.sin(\theta) + v_b.sin(\theta - \frac{2\pi}{3}) + v_c.sin(\theta + \frac{2\pi}{3})\right] \tag{A.1}$$

$$v_q = \frac{2}{3}\left[v_a.cos(\theta) + v_b.cos(\theta - \frac{2\pi}{3}) + v_c.cos(\theta + \frac{2\pi}{3})\right] \tag{A.2}$$

$$v_0 = \frac{1}{3}\left[v_a + v_b + v_c\right] \tag{A.3}$$

The inverse Park transformation converts the two-phase (d, q) to the (a, b, c) system.

$$v_a = [v_d.sin(\theta) + v_q.cos(\theta) + v_0] \tag{A.4}$$

$$v_b = \left[v_d.sin(\theta - \frac{2\pi}{3}) + v_q.cos(\theta - \frac{2\pi}{3}) + v_0\right] \tag{A.5}$$

$$v_c = \left[v_d.sin(\theta + \frac{2\pi}{3}) + v_q.cos(\theta + \frac{2\pi}{3}) + v_0\right] \tag{A.6}$$

A.2 Forward and Inverse Clarke Transformation

The forward Clarke transformation converts a three-phase system (a, b, c) to a two-phase coordinate system (α, β). Figure A.2 shows the vector diagram of the space vector and projection of the space vector to the quadrature-phase components (α, β). Assuming that the $a - axis$ and the $\alpha - axis$ are in the same direction, the quadrature-phase vectors v_α and v_β are related to the actual three-phase vectors as follows.

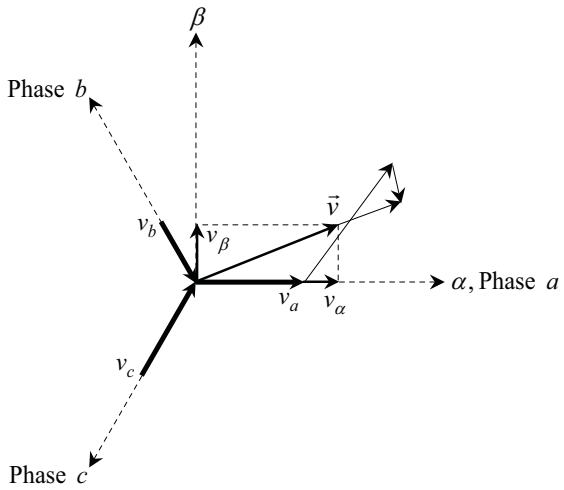

Figure A.2: Clarke Transformation

$$v_\alpha = v_a \tag{A.7}$$

$$v_\beta = \frac{1}{\sqrt{3}} v_a + \frac{2}{\sqrt{3}} v_b \tag{A.8}$$

The inverse Clarke transformation converts the two-phase (α, β) to the (a, b, c) system.

$$v_a = v_\alpha \tag{A.9}$$

$$v_b = -\frac{1}{2} v_\alpha + \frac{\sqrt{3}}{2} v_\beta \tag{A.10}$$

$$v_c = -\frac{1}{2} v_\alpha - \frac{\sqrt{3}}{2} v_\beta \tag{A.11}$$

Appendix B

SPACE VECTOR PWM

The Space Vector PWM (SVPWM) is one of the modern modulation techniques. While a classical sinusoidal modulation determines the phase duty cycle signal in form of the inner circle, the SVPWM technique extends this circle to the hexagon shape by injecting the signal third harmonic. Figure B.1 shows the eight voltage vectors (V_0 to V_7) which are used as switching patterns for the three-phase inverter. Also, Table B.1 summarises the output phase and line to line voltages of the three-phase inverter, which are yielded by the eight combinations of these patterns.

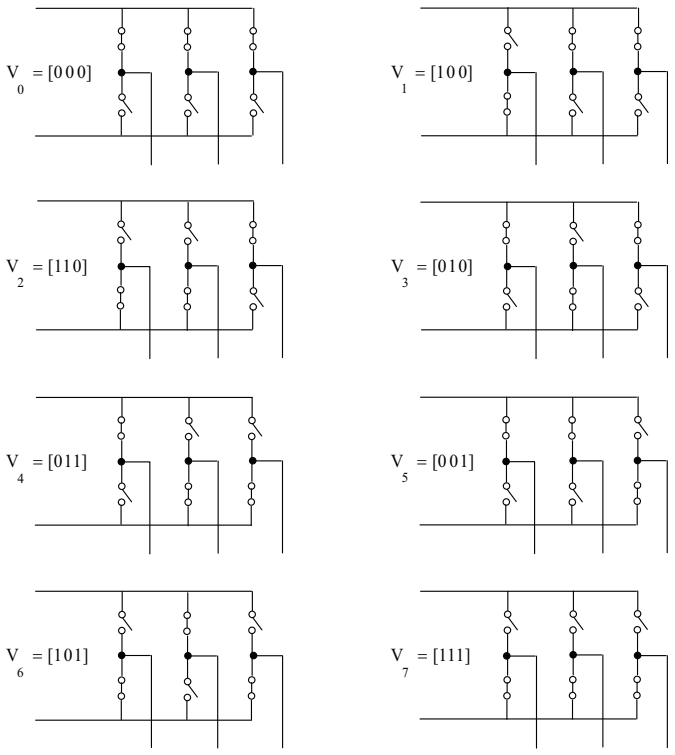

Figure B.1: The inverter voltage vectors

Table B.1: The Output Voltages of Three-Phase Inverter

Voltage vectors	Switching vectors			Line-neutral voltage			Line-line voltage		
	a	b	c	V_{an}	V_{bn}	V_{cn}	V_{ab}	V_{bc}	V_{ca}
V_0	0	0	0	0	0	0	0	0	0
V_1	1	0	0	2/3	-1/3	-1/3	1	0	-1
V_2	1	1	0	1/3	1/3	-2/3	0	1	-1
V_3	0	1	0	-1/3	2/3	-1/3	-1	1	0
V_4	0	1	1	-2/3	1/3	1/3	-1	0	1
V_5	0	0	1	-1/3	-1/3	2/3	0	-1	1
V_6	1	0	1	1/3	-2/3	1/3	1	-1	0
V_7	1	1	1	0	0	0	0	0	0

The principle of the SVPWM can be summarised as follows:

- Treats the sinusoidal voltage as a constant amplitude vector rotating at constant frequency.

- This PWM technique approximates the reference voltage V_{ref} by a combination of the eight switching patterns (V_0 to V_7).

- Coordinate Transformation (*abc* reference frame to the stationary $d-q$ frame): a three-phase voltage vector is transformed into a vector in the stationary $d-q$ coordinate frame which represents the spatial vector sum of the three-phase voltage.

- The vectors (V_1 to V_6) divide the plane into six sectors (each sector: 60 degrees).

- V_{ref} is generated by two adjacent non-zero vectors and two zero vectors.

The basic switching vectors and sectors shown in Figure B.2 are divided into two main phases. First, six active vectors (V_1 to V_6) located on the axis of the hexagon. The DC link voltage can be supplied to the load within these vectors which split the hexagon to the six sectors (1 to 6), each one with 60 degrees. Second, two zero vectors (V_0, V_7) placed at the origin of the hexagon and no voltage can be supplied to the load within these vectors.

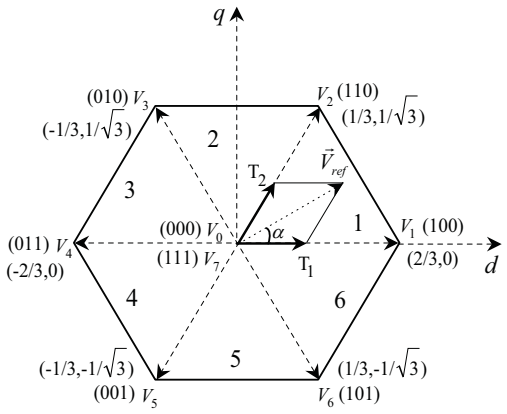

Figure B.2: Basic switching vectors and sectors

The SVPWM technique can provide high performance operation compared to the sine PWM. Based on Figure B.3, the main aspects of the SVPWM operation can be summarised as follows.

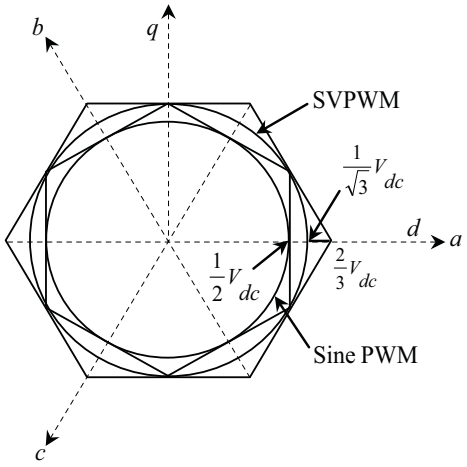

Figure B.3: Locus comparison of maximum linear control voltage in Sine PWM and SVPWM

- SVPWM generates less harmonic distortion in the output voltage or currents in comparison with sine PWM.
- SVPWM provides more efficient use of supply voltage in comparison with sine PWM.
- Sine PWM : Locus of the reference vector is the inside of a circle with radius of $1/2$ V_{dc}.
- SVPWM : Locus of the reference vector is the inside of a circle with radius of $1/\sqrt{3}$ V_{dc}.
- Voltage Utilization: Space Vector PWM = $2/\sqrt{3}$ times of Sine PWM.